Projected Changes in the Annual Cycle of Surface Temperature and Precipitation Due to Greenhouse Gas Increases

John G. Dwyer

Submitted in partial fulfillment of the

requirements for the degree

of Doctor of Philosophy

in the Graduate School of Arts and Sciences

COLUMBIA UNIVERSITY

2014

ABSTRACT

Projected Changes in the Annual Cycle of Surface Temperature and Precipitation Due to Greenhouse Gas Increases

John G. Dwyer

When forced with increasing greenhouse gases, global climate models project changes to the seasonality of several key climate variables. These include delays in the phase of surface temperature, precipitation, and vertical motion indicating maxima and minima occurring later in the year. The changes also include an increase in the amplitude (or annual range) of low-latitude surface temperature and tropical precipitation and a decrease in the amplitude of high-latitude surface temperature and vertical motion. The aim of this thesis is to detail these changes, understand the links between them and ultimately relate them to simple physical mechanisms.

At high latitudes, all of the global climate models of the CMIP3 intercomparison suite project a phase delay and amplitude decrease in surface temperature. Evidence is provided that the changes are mainly driven by sea ice loss: as sea ice

melts during the 21st century, the previously unexposed open ocean increases the effective heat capacity of the surface layer, slowing and damping the temperature response at the surface. In the tropics and subtropics, changes in phase and amplitude are smaller and less spatially uniform than near the poles, but they are still prevalent in the models. These regions experience a small phase delay, but an amplitude increase of the surface temperature cycle, a combination that is inconsistent with changes to the effective heat capacity of the system. Evidence suggests that changes in the tropics and subtropics are linked to changes in surface heat fluxes.

The next chapter investigates the nature of the projected phase delay and amplitude increase of precipitation using AGCM experiments forced by SST perturbations representing idealizations of the changes in annual mean, amplitude, and phase as simulated by CMIP5 models. A uniform SST warming is sufficient to force both an amplification and a delay of the annual cycle of precipitation. The amplification is due to an increase in the annual mean vertical water vapor gradient, while the delay is linked to a phase delay in the annual cycle of the circulation. A budget analysis of this simulation reveals a large degree of similarity with the CMIP5 results. In the second experiment, only the seasonal characteristics of SST are changed. For an amplified annual cycle of SST there is an amplified annual cycle of precipitation, while for a delayed SST there is a delayed annual cycle of precipitation. Assuming that SST changes can entirely explain the seasonal precipitation changes, the AGCM simulations suggest that the annual mean warming explains most of the amplitude increase and much of the phase delay in the CMIP5 models. However, imperfect agreement between the changes in the SST-forced AGCM simulations and the CMIP5 coupled simulations suggests that coupled effects may play a significant role.

Finally, the connections between changes in the seasonality of precipitation, temperature and circulation are studied in the tropics using models of varying complexity. These models include coupled model simulations with idealized forcing, a simple, semi-empirical model to describe the effect of land-ocean interactions, an aquaplanet model, and a dry, dynamical model. Each gives insights into the projected CMIP changes. Taken together they suggest that changes in the amplitude of vertical motions are consistent with a weakening of the annual mean circulation and can explain part of the changes in the amplitude of precipitation over both ocean and land, when combined with the thermodynamic effect described previously. By increasing the amplitude of the annual cycle of surface winds, the changes in circulation may also increase the amplitude of the surface temperature via the surface energy balance. The delay in the phase of circulation directly leads to a delay in the phase of precipitation, especially over ocean.

Contents

List of Tables

List of Figures

Acknowledgments

First and foremost, I want to express my gratitude to my two intellectually stimulating and compassionate mentors, Michela Biasutti and Adam Sobel. Through their example and with their support they have shaped me as a scientist in innumerable ways. I also wish to thank the many people at Columbia and beyond who have helped me along the way: Suzana Camargo, Lorenzo Polvani, Tiffany Shaw, Isla Simpson, Ron Miller, Arlene Fiore, Richard Seager, Ian Eisenman, George Kiladis, and many others. I thank Larry Rosen, Gus Correa, Naomi Henderson, and Haibo Liu for their computer support and data management. Last but not least, I would not be who I am today without the love, support, and encouragement of my wife Neon and my mother and two sisters (and Whiskey, my pup).

Dedicated to my father.

Chapter 1

Introduction

To understand the character of the climate system, climate scientists average data over long time periods of time to remove the vagaries of weather. For instance, multidecadal averages of global mean surface temperature and precipitation tell us about the Earth's energy balance and hydrological cycle. But the atmosphere is always in flux and embedded within these averages is a rich variability. Due to the Earth's rotation about and revolution around the sun, the temperature over most of the surface undergoes a tremendous range over the course of the day and throughout the year, even larger than the annual mean global temperature changes throughout much of the Earth's history. It is important to understand this cyclical variability in the climate of today as well as how it might change in the climate of tomorrow. My focus in this work is to describe, link, and understand projected changes in the annual cycle due to increases in anthropogenic greenhouse gases. I mainly focus on temperature and precipitation but also the tropical circulation to a lesser degree.

Ultimately the Earth's annual cycle is due to our planet's non-zero obliquity (axial tilt), which varies the amount of sunlight each hemisphere receives on its orbit about the sun. The time-varying nature can be well-described for much of the Earth by a sinusoid with a period of one year. The dominance of this near-sinusoidal forcing imprints many aspects of the Earth's surface and atmosphere with a sinusoid of the same frequency, though its amplitude (annual range) and phase (timing of the peak) depends on the variable. Consideration of the annual cycle is also important for fully understanding the annual mean climate. For instance, models that do not include an annual cycle of meridionally shifting heating when simulating the Hadley cell (the meridionally overturning circulation pattern in the tropical atmosphere (Hadley, 1735)) underestimate the strength of the annual mean Hadley cell (Lindzen and Hou, 1988; Fang and Tung, 1999; Dima and Wallace, 2003). Paleoclimate records show that annual mean precipitation increases when perihelion is coincident with the summer solstice despite no change in the annual mean solar heating (Merlis et al., 2012). Finally annual mean soil moisture and hydrological droughts cannot be fully explained without a seasonal cycle, due to non-linearities (Van Loon et al., 2014).

Understanding the climatological annual cycle of surface temperature was of interest to early climate scientists and geographers. They divided the mid-latitudes into different climate "zones," based on the amplitude of the annual cycle of surface temperature, with continental regions having a large annual range and maritime regions a small range (Ward, 1906). Other studies sought to describe the amplitude of the annual cycle of local surface temperature as a function of the fractional amounts of land and ocean within a fixed radius (Brooks, 1917), furthered by considering the direction of the prevailing wind to account for temperature advection (Brooks, 1918). Later work developed empirical formulas to describe the amplitude of the annual cycle of surface temperature based on nearby amounts of land and ocean (Gorczyński, 1920; Spitaler, 1922; Brunt, 1924; Simpson et al., 1924). Many of these studies focused on describing the annual range of temperature for Eurasian cities, and were later extended to describe the annual range of temperatures in the Atlantic Ocean (Hela, 1953). Concurrently, others described regional variability in terms of the phase lag of surface temperature from insolation, rather than the amplitude. These studies characterized continental regions as having a small phase lag from insolation and oceanic regions a large one (Prescott and Collins, 1951; Van den Dool and Können, 1981).

More recent work has combined both amplitude and phase to understand the regional variations of the annual cycle of surface temperature and the impact of insolation (Trenberth, 1983). Stine et al. (2009) described the local annual cycle in the mid-latitudes as a linear combination of two sinusoids, continental and oceanic, with a weighting factor proportional to the westward distance to the coast. Most recently McKinnon et al. (2013) used a Lagrangian trajectory model to quantify the annual cycle of surface temperature as the weighted amount of time that an ensemble of air parcels has spent over ocean or land. Combining this result with an energy balance model, the authors were able to explain 94% of the space-time variance of the annual cycle of surface temperature in the mid-latitudes.

Seasonality in the tropics is often described in terms of precipitation (wet and dry seasons), rather than the four seasons defined by temperature, because there is a relatively large annual range in precipitation and a relatively small range in surface temperature. Much of the large-scale tropical precipitation can be attributed to the Hadley Cell, which determines the structure of low-level convergence zones, such as the Intertropical Convergence Zone (ITCZ). The condensing moisture in the rising air of this narrow, horizontal band of surface convergence warms the atmosphere and precipitates. The location of the ITCZ is determined in part by hemispheric asymmetry of atmospheric energy, which can result from extratropical forcing according to both observations (Lea et al., 2003; Pahnke et al., 2007; Sachs et al., 2009) and models (Chiang and Bitz, 2005; Broccoli et al., 2006; Kang et al., 2008, 2009; Frierson and Hwang, 2011; Donohoe et al., 2014). The ITCZ also shifts on seasonal time scales, following the annual cycle, though it stays north of the equator throughout the year in most ocean basins. The other major source of precipitation on seasonal time scales is associated with monsoons, a seasonal phenomenon in which the prevailing winds reverse direction and advect moisture over land, inducing precipitation (Webster, 1987). Monsoons are a global phenomenon (Trenberth et al., 2000), but because they depend on asymmetries in tropical surface temperature, there is regional variability in their character.

A traditional aim of climate science was to characterize and understand the state of the atmosphere-ocean system and its natural variability. But due to anthropogenic increases in greenhouse gases the basic climate state of the Earth is changing. Some of these changes, like global mean surface temperature rise, accelerated Arctic warming, stratospheric cooling, increased tropical precipitation, poleward migration of the storm tracks, and tropical widening have already been observed (Solomon et al., 2007; Stocker et al., 2013). And more warming and other changes will occur even if greenhouse gas emissions stopped instantaneously because of the large lag in the climate system due to the ocean's high capacity to absorb heat.

Since the pre-industrial era, the Earth has warmed by 0.85°C (Solomon et al., 2007) and CO_2 has increased from 275 ppm to 400 ppm (Keeling, 1958; Machida et al., 1995). These and other changes have had an effect on the annual cycle of many biological systems. For example, they have led to earlier dates of leaf unfolding in Europe (Chmielewski and Rötzer, 2001), earlier appearance of butterflies in Britain (Roy and Sparks, 2000), an altered ocean food-chain due to certain plankton species developing earlier in the year (Edwards and Richardson, 2004), changes in hatching time for winter moths and oak tree buds (Visser and Holleman, 2001), and other mismatches in timing between species and their food sources (Visser and Both, 2005). Global warming has also affected hydroclimate, with earlier occurrences of warm temperatures, streamflows and snow melt in western North America (Regonda et al., 2005).

Because they are based on thresholds, many of these phenological changes are a result of annual mean warming, rather than changes in the annual cycle. But changes in the annual cycle of climate variables have also been observed, especially for surface temperature. The longest, most reliable records are in the mid-latitudes, in which various studies have identified a phase advance in surface temperature over land and a phase delay of surface temperature over ocean (Thomson, 1995; Thompson, 1995; Wallace and Osborn, 2002; Stine et al., 2009; Stine and Huybers, 2012). Various mechanisms have been proposed to explain aspects of these changes in seasonality. Thompson (1995) hypothesized that the phase advances over land were due to the temperature responding to the anomalistic year (the time it takes the Earth to make a full revolution around the sun with respect to perihelion) rather than the tropical year (the time it takes for the sun to return to its position at vernal equinox). Stine et al. (2009) suggested that a decrease in soil moisture could explain the phase advance over land, but this is at odds with the limited observational record (Robock et al., 2000). Another possibility, that increases in shortwave atmospheric absorption due to increases in greenhouse gas and aerosols is affecting the balance between insolation and surface temperature, is not replicated in global climate models (Wallace and Osborn, 2002; Stine et al., 2009). Most recently, Stine and Huybers (2012) proposed that 20th century trends in seasonality can be traced to changes in the atmospheric circulation, specifically those of the large scale patterns, like the Northern Annular Mode and Pacific-North American Pattern. Long-term trends over the late 20th century in these patterns may be responsible for advecting less heat between land and ocean, resulting in opposite changes of phase over land and ocean.

The effects of greenhouse gases on climate will continue to grow throughout the

21st century (Stocker et al., 2013). The best tool to understand the full nature of these changes is the global climate model (GCM), a three-dimensional, numerical model that couples the many components of the climate system (atmosphere, ocean, land, sea ice, etc.) and informs our understanding of climate variability and climate change. With increased computing power and more accurate physical parameterizations, GCMs have increased in resolution and complexity and improved their representation of the real climate. But even one of the first GCMs to include an annual cycle projected changes to the annual cycle of temperature, when forced with increased greenhouse gases. These changes were consistent with changes in today's models. That simulation, described in Manabe and Stouffer (1980), found an increase in annual, high-latitude surface temperature, with the largest increase occurring during winter, indicating a weaker annual cycle. The authors attributed this effect to sea ice loss: the ocean absorbs more sunlight in the summer due to a decrease in surface albedo, but the excess heat goes into melting ice and warming the mixed-layer ocean. The heating delays the build-up of early-winter sea ice, a time at which the air-sea temperature difference is very large. As a consequence of this reduced insulation, the ocean warms the surface layer during the winter. Using a more modern GCM, Mann and Park (1996) replicated this surface temperature amplitude increase and also found a delay in the timing of high latitude surface temperature, which they also attributed to sea ice loss. These changes are now being observed in satellite measurements of the Arctic (Screen and Simmonds, 2010).

Projected changes in the phase and amplitude of surface temperature are not only confined to high latitudes. Nearly all of the models in the World Climate Research Programme's (WCRP's) Coupled Model Intercomparison Project phase 3 (CMIP3) multimodel dataset (Meehl et al., 2007) project a phase delay in the seasonality of tropical SST (Biasutti and Sobel, 2009), though the phase delay weakens to around 1 day in the ensemble mean of the latest generation of climate models, known as CMIP5 (Taylor et al., 2011). But both CMIP3 and CMIP5 models project an amplitude increase of around 10% in the annual cycle of surface temperature (Sobel and Camargo, 2011). The authors suggest that the increase in the amplitude of the surface temperature is a result of an increase in the amplitude of surface wind speed – stronger winter easterlies and weaker summer easterlies in the subtropics – which are in turn a result of the tropical circulation weakening in strength (Knutson and Manabe, 1995; Held and Soden, 2006; Vecchi and Soden, 2007) and expanding in size (Lu et al., 2007; Seidel et al., 2008; Johanson and Fu, 2009).

The GCMs also project changes in the seasonality of other tropical variables. The vast majority of CMIP3 models project a phase delay in the seasonality of tropical precipitation, including the Sahel region of Africa (Biasutti and Sobel, 2009). There is also a delay over nearly all of the land monsoon regions, which was attributed to timing changes in tropospheric stability – enhanced stability in the spring and decreased stability in the fall (Seth et al., 2011). The precipitation delay in monsoon regions persists in the CMIP5 model (Seth et al., 2013). Like the amplitude of tropical temperature, the amplitude of tropical precipitation is projected to increase as simulated by the CMIP3 and CMIP5 models indicating greater summer precipitation relative to winter precipitation(Chou et al., 2007; Chou and Tu, 2008; Tan et al., 2008; Chou and Lan, 2011; Huang et al., 2013). This change has also been observed in satellite precipitation data, though not yet with statistical significance (Chou et al., 2013). The mechanism proposed for this behavior is an annual mean increase in water vapor resulting from global mean temperature rise. The ascending branch of the Hadley Cell then produces precipitation from this moisture increase. Because the ascending branch is located in the summer hemisphere, the increase in precipitation happens during the summer, when precipitation is already largest, resulting in an increase in the amplitude.

My goal in this work is to further our understanding of the GCM-projected changes in the annual cycle. What is the cause of the projected changes for surface temperature and precipitation? Are there other variables whose seasonal cycles are also projected to change? Are the heretofore described mechanisms adequate to explain all of these changes? I address these questions below.

In Chapter 2, which borrows heavily from Dwyer et al. (2012), I study the representation of the annual cycle of temperature at the surface and throughout the atmosphere in the CMIP3 models and compare it to a reanalysis dataset. At high latitudes, the models project an amplitude increase and a phase delay. I provide evidence that those changes are due to a reduction in sea ice extent and thickness, which leads to better coupling the atmosphere and ocean, resulting in a larger effective atmospheric heat capacity, which causes surface temperature to respond more weakly and sluggishly to insolation. I also analyze the projected changes in the annual cycle of surface temperature at low latitudes. There, the CMIP3 models project a phase delay and an amplitude increase. These changes cannot be primarily due to heat capacity since a phase delay and amplitude increase are not consistent with that mechanism. Using a simple energy balance model I show that these changes can be explained by changes in the annual cycle of total surface flux, which also shows a phase delay and amplitude increase.

Next, in Chapter 3 I analyze projected changes in the annual cycle of precipitation in the tropics (also described in Dwyer et al. (2014)). In order to gain a better understanding of the mechanisms involved in the increase of amplitude and the delay of phase of precipitation, I run two sets of idealized atmospheric simulations: one in which I increase the annual mean SST by 3 K everywhere and another in which I modify either the phase and/or the amplitude of the annual cycle of SST without changing the annual mean. Both the simulation with an increased annual mean temperature and a simulation with delayed phase and increased amplitude of SST result in an annual cycle of precipitation with an increased amplitude and delayed phase. However, an analysis of the moisture budget indicates a much greater similarity between the CMIP5 21st century changes and the uniform warming scenario than the scenario with seasonal modifications. I find that the amplitude increase of precipitation in both the CMIP5 models and the uniform warming simulation is a result of an increase in the annual mean, vertical water vapor gradient, though there is a negative contribution from an amplitude decrease in the annual cycle of vertical motions. Furthermore, I find that the phase delay of circulation is linked to a phase delay in the annual cycle of precipitation rather than being directly due to a thermodynamic process. The modified seasonality experiments show that the phase and amplitude of precipitation are tightly linked to the phase and amplitude of SST, respectively.

I continue to focus on tropical seasonality in Chapter 4 and link the seasonality changes in temperature, precipitation, and tropical circulation to one another by examining the results of model simulations of varying complexity. These models include CMIP5 simulations with idealized greenhouse gas forcings, a two-equation, semi-empirical model to describe land-ocean interaction, an aquaplanet (no land surface) with prescribed SST, and a dry, dynamical model with an annual cycle and realistic Hadley Cell. Each of these model simulations yields insights into the projected changes of tropical seasonality and links between different variables. The CMIP5 models with idealized forcings are instructive for understanding the timing of different mechanisms and the direction of causality between different effects. The semi-empirical model suggests how changes in seasonality over ocean may be affecting changes in seasonality over land and vice-versa. The aquaplanet shows that while land-ocean interactions may be affecting seasonality in the coupled models, they are not necessary to produce a phase delay in the annual cycle of ocean precipitation. Finally, the dry dynamical model suggests that an increase in atmospheric stability may be delaying the phase and increasing the amplitude of the annual cycle of vertical motions. I consider all of these results together along with previous work and discuss a framework that describes the interactions between the seasonality of these variables.

Chapter 2

Projected Changes in the Seasonal Cycle of Surface Temperature

2.1 Introduction

On annual and longer time scales the seasonal cycle is responsible for around 90% of the total surface temperature variance. In this study I focus on potential changes in the seasonality of the surface temperature due to expected increases in greenhouse gases. These are distinct from changes due to the mean temperature increase, even though the latter can also affect the seasonality of phenomena linked to specific climate thresholds, such as streamflow timing due to melting snow (Stewart et al., 2005) and plant flowering (Fitter and Fitter, 2002). Here I concentrate on changes to the phase and amplitude of the annual cycle in surface temperature (and to a lesser extent, temperature in the upper atmosphere), independent of the annual mean warming. Specifically, I am interested in the geographic pattern of the response in phase and amplitude to greenhouse gases and the mechanisms responsible for these changes.

In the models of the World Climate Research Programme's (WCRP's) Coupled

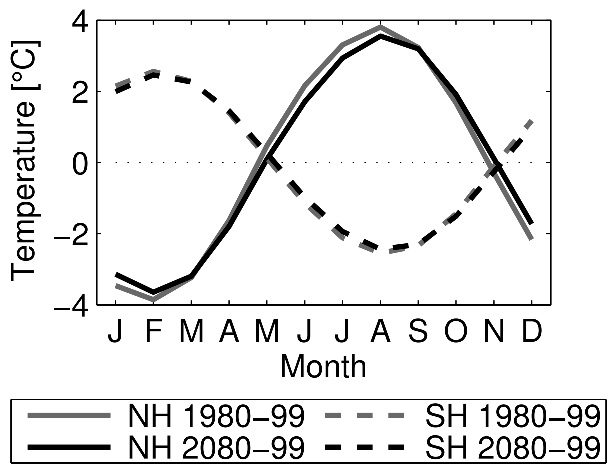

Figure 2.1: Hemispherically averaged, multimodel mean monthly surface air temperature anomaly over ocean in °C for the last two decades of the 20th (gray) and 21st (black) centuries. Both the NH (solid line) and SH (dashed line) have a phase delay and amplitude decrease.

Model Intercomparison Project phase 3 (CMIP3) multimodel dataset (Meehl et al., 2007), the main changes in the seasonality of surface temperature are a robust delay in phase and a robust decrease in amplitude, where I take robust to mean that the changes occur in all or nearly all of the models. This means that the models predict peak temperatures to occur later in the year and the difference between annual maximum and minimum temperatures to shrink. I illustrate these effects in Figure 2.1 by plotting the hemispheric, multimodel mean 2 m surface air temperature over ocean for the last two decades of the 20th and 21st centuries with the annual mean removed. By fitting the anomalies to sinusoids I can quantify the changes compared to the late 20th century: the temperature cycle in the late 21st century has a phase delay of 6 days in the NH and 3 days in the SH and an amplitude decrease of 6% in the NH and 3% in the SH.

As I will show in Section 2.4, the dominant component of the global mean response is a strong phase delay and amplitude reduction over high-latitude ocean. Manabe and Stouffer (1980), Manabe et al. (1992), and Mann and Park (1996) noticed this high-latitude signal in earlier generations of climate models and proposed that it was a consequence of an increase in effective heat capacity due to sea ice loss. Sufficiently thick sea ice insulates the atmosphere from the ocean and curtails heat storage in the climate system. As the ice thins and melts, the insulation weakens and disappears and the effective heat capacity of the surface increases. Due to this additional thermal inertia, the temperature responds more slowly and with a smaller amplitude than it would were the ice present.

I build on the earlier modeling studies by demonstrating the seasonality changes in the most recent generation of climate models, investigating the spatial patterns of seasonality changes, and providing evidence that sea ice is driving the high-latitude seasonality changes in the models. In order to verify this mechanism, I interpret the CMIP3 results in the context of a simple energy balance model for surface temperature. Using this and other tools I show that the high-latitude phase delay and amplitude reduction are consistent with an increased effective heat capacity and inconsistent with other potential mechanisms including changes in the seasonality of surface heat fluxes or heat transport. Furthermore, I link the effective heat capacity changes to sea ice loss quantitatively.

Previous observational studies in the NH midlatitudes have found a phase advance driven by changes over land and an amplitude reduction during the second half of the 20th century (Thomson, 1995; Mann and Park, 1996; Stine et al., 2009) and have questioned the ability of the CMIP3 models to reproduce the observed phase and amplitude variations. More recent work by the same authors suggest that the small seasonality changes over land might be due to natural variability in atmospheric circulation (Stine and Huybers, 2012), in which case one would not expect the multimodel mean to match such changes. Over the same period, Stine and Huybers (2012) found a nonstatistically significant phase delay and an amplitude reduction in the NH midlatitudinal oceans, and recent studies of surface temperature over the Arctic Ocean also found evidence of a phase delay and amplitude decrease due to strong late fall and early winter warming during the last 20–30 years (Serreze et al., 2009; Screen and Simmonds, 2010). The correspondence between Arctic sea ice loss over the last few decades (Stroeve et al., 2007) and local changes in seasonality suggests that a key mechanism for the simulated late 21st century seasonality changes is also present in nature.

In the tropics and subtropics there is a smaller, yet still robust, change in the temperature seasonality, different in nature from the high-latitude signal. There the CMIP3 models project a small phase delay and an amplitude increase, the latter being opposite in sign to the high-latitude amplitude response. Because the phase and amplitude changes are of the same sign, these low-latitude changes cannot be primarily driven by a change in effective heat capacity, as will be shown below. Instead, some other mechanism must be the primary cause. I provide evidence that changes in the seasonality of surface flux are linked to the low-latitude temperature phase delay and amplitude increase. The source of the low-latitude changes in fluxes is not clear, but it might be wind speed changes, which Sobel and Camargo (2011) argued were responsible for the amplitude increase. The seasonality changes in temperature, though small, could be related to seasonality changes in the onset and demise of the monsoons (Biasutti and Sobel, 2009; Seth et al., 2011), especially given the sensitivity of the ITCZ to the tropical SST distribution (for example, Chiang et al. (2002)).

The rest of the chapter is laid out as follows. In the next section I give background information on the data I analyze from CMIP3 and a reanalysis dataset and explain the methods I use to calculate the phase and amplitude of the annual cycle. In Section 2.3 I describe the climatological structure of the annual cycle at the surface and aloft as represented by both the CMIP3 multimodel mean and the reanalysis and demonstrate agreement between the two, as both capture the slow, weak surface temperature response to insolation over ocean and the fast, strong response over land. Moreover both datasets show that over sea ice, the temperature response is more land-like than ocean-like. In Section 2.4 I detail the changes to the annual cycle at the surface and aloft as projected by the models and discuss the differences at high and low latitudes. In Section 2.5 I look at both of these regions individually and demonstrate that the changes in sea ice account for much of the high-latitude temperature cycle change, while changes in the seasonality of surface flux explain the seasonal temperature changes. Finally, I summarize my findings in Section 2.6.

2.2 Data and Methods

Throughout this study I use the CMIP3 20th century historical simulations (20C3M) and 21st century A1B scenario simulations, where atmospheric CO_2 reaches 700 ppm by 2100 (Meehl et al., 2007). Monthly temperature data is sufficient to characterize the phase and amplitude of the annual cycle. I use only one realization of each model. All 24 models store temperature data at all levels, but only 20 models store sea ice data and 18 store total surface flux data. When data is missing, I take the multimodel mean to be the subset of models with available data. Surface temperature is defined as 2 m air temperature, which is tightly constrained by surface fluxes to be close to SST over open ocean, though not over sea ice (since SST is constrained to the freezing point of sea water). I compare the model results with the European Centre for Medium-Range Weather Forecasts (ECMWF) ERA-40 reanalysis data set (Uppala et al., 2005), which covers 1958–2001. The reanalysis assimilates satellite and terrestrial observations using a climate model. Where observations are relatively sparse, like the Arctic Ocean, comparison between the CMIP3 models and the reanalysis are not as informative as in other regions.

I calculate the phase of the seasonal cycle using two different techniques. The first uses empirical orthogonal functions (EOFs). In this approach I decompose the climatological mean, monthly data into spatial eigenfunctions of the covariance matrix and associated principal component time series (PCs) (Kutzbach, 1967). I obtain amplitude and phase information by fitting a sinusoid to the PC representing the annual cycle, which is always associated with the EOF capturing the highest fraction of the total variance, except within about 5° of the equator. The other method is Fourier transformation of the data to obtain the annual harmonic of each field of interest. Both methods are able to resolve phase and amplitude precisely from monthly data. Fourier transforms can be calculated pointwise, but they cannot obtain reliable phase information in the tropics because of the relatively small amplitude of the annual cycle there. EOFs are defined for the entirety of the domain of interest, but are dominated by regions of large annual variance. After spatially averaging area-weighted phases and amplitudes calculated with a Fourier transform, the results are nearly identical to those calculated using EOFs over the same domain.

Since my analysis is predicated on the temperature cycle's being accurately described by a sinusoid with a period of one year, I will only use locations for which its annual component explains at least 80% of the total variance. (I loosen this restriction to 70% when I plot the annual cycle of surface flux so that the two can be compared in the same regions). These are roughly the same regions for which insolation is dominated by the annual harmonic (Trenberth, 1983). Surface temperature and insolation each have over 95% of their total variance described by the annual cycle between 20° and 70°. At higher latitudes only around 85% of the insolation is due to the annual cycle due to the sunless winters and nightless summers. Over Antarctica, the temperature cycle has a large semi-annual component due to the "coreless winters" of relatively constant cold temperatures owing to the large landmass being in longwave radiative balance as well as to dynamical effects (Loon, 1967). In the Arctic, the temperature cycle is surprisingly annual, with over 95% of the total temperature variance described by the first harmonic. The strength of the annual harmonic of temperature in the Arctic can be partly attributed to the seasonal sea ice cycle, which is not discrete, but instead smoothly varies throughout the year with advancing and retreating ice margins, thickening and thinning sheet ice, melt pond formation and other effects (Eicken, 2008). In the tropics, the sun passes overhead two times per year and the second harmonic becomes prominent for both insolation and temperature: the variance explained by the annual cycle drops below 50% for the insolation and below 70% for temperature near the equator.

The Earth's axial and apsidal precession also changes the phase of the temperature cycle towards earlier seasons in the NH and later seasons in the SH (Stine and Huybers, 2012). Only four of the CMIP3 models have a different phase of insolation between the 20th and 21st centuries. I account for any such changes by measuring the temperature phase relative to the local insolation phase, so that any phase changes in the models are not due to celestial mechanisms.

2.3 Climatological Structure

Before analyzing the changes to the annual cycle, I look at the long-term mean of the phase and amplitude at the surface and aloft for both the multimodel mean and the reanalysis.

2.3.1 Surface

The seasonality of incoming diurnal mean solar radiation depends only upon latitude. The phase of annual insolation is a weak function of latitude, varying by only a few days between the tropics and poles, but the amplitude of annual insolation increases markedly with latitude from about 50 W m^{-2} at 10° to around 275 W m^{-2} at 90° (Trenberth, 1983). Since the temperature cycle is primarily governed by the solar cycle, the seasonality of temperature has a pattern that is qualitatively similar to that of insolation, but with substantial departures due to the local effective heat capacity of the surface layer.

Effective heat capacity of the surface is a function of both the material properties and dynamical behavior of the layer adjacent to the atmosphere. I refer to it as effective since it is neither the intensive heat capacity (per unit mass) of some material substance, nor the extensive heat capacity of a fixed mass of that substance. Rather, it is the heat capacity of the layer of material through which heat is transported sufficiently rapidly that it is influenced by the atmosphere on time scales of interest. The mixed-layer ocean has a relatively large heat capacity because turbulent mixing transports heat downward so that a thick layer of water is rapidly influenced by surface fluxes. This causes ocean surface temperature to respond sluggishly and with small amplitude to heat fluxes at the ocean surface. Temperature has a much faster and stronger response to insolation over land than over ocean because only a very thin layer of the land responds on annual time scales, since the primary soil heat transfer process is diffusion with a small diffusivity. The effective heat capacity of land depends to some extent on the type of soil and the moisture content, but a typical estimate would be roughly equivalent to a 2 m ocean mixed layer depth (Carson and Moses, 1963), though this does not account for the presence of rivers and lakes. For comparison, the heat capacity of an atmospheric air column is roughly equivalent to that of 4 m of ocean.

I plot the ERA-40 reanalysis and CMIP3 multimodel mean surface temperature phase lag from insolation averaged over 1958–2001 in Figure 2.2(a) and 2.2(b), respectively. The models show good fidelity to the reanalysis in their geographic structure. Phase delays are smaller over the continents, as temperature over land

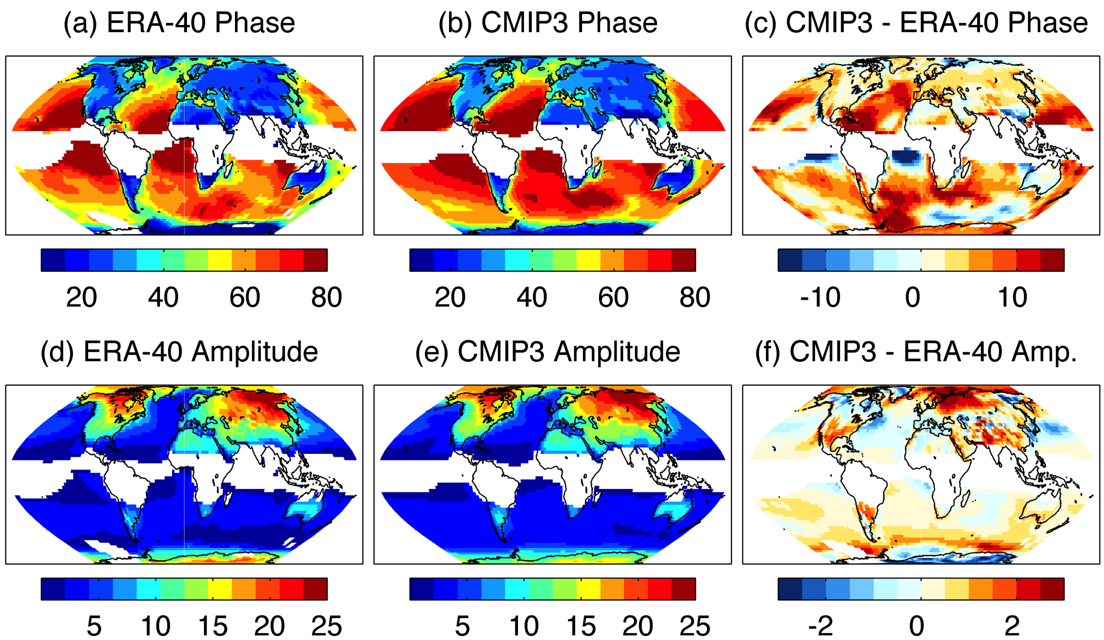

Figure 2.2: The 1958-2001 mean temperature phase from insolation (in days) for (a) the ERA-40 reanalysis and (b) the CMIP3 multimodel mean, with the difference between the two shown in (c). The mean amplitude (in °C) over the same period for (d) ERA-40, (e) CMIP3, and (f) their difference are plotted in the bottom row. Places where the annual cycle does not represent at least 80% of the total variance are not plotted.

responds more quickly than over ocean, and this effect is propagated downwind (the temperature phase in the NH midlatitudes can be well described by the westward distance from the coast (Stine et al., 2009)). The largest differences between models and the reanalysis are mainly over the midlatitude oceans where the models have a larger phase lag than those of ERA-40 (Figure 2.2(c)) for reasons unknown.

In regions of sea ice (e.g., the high-latitude Arctic and Southern oceans), the phase lag has a response in between those of land and ocean. Around the maximal winter extent ice margins, the temperature responds slowly, as over the ocean, while closer to the poles the temperature response is more akin to that over land for both the reanalysis and models. Since the observational record is limited in the high-latitude oceans, the reanalysis should not be viewed as a strong constraint on the

CMIP3 results there. This pattern is consistent with the insulating effect of sea ice becoming stronger in regions of more extensive and thicker ice coverage, and being responsible for the rapid polar temperature response due to a reduced effective heat capacity.

A similar pattern holds for the amplitude. Figure 2.2(d) and 2.2(e) show the temperature amplitude from the ERA-40 reanalysis and the CMIP3 multimodel mean, respectively. Both show that most of the surface has a relatively weak seasonal cycle with an amplitude under 5°C. The cycle is much stronger over land and sea ice. The difference between models and the ERA-40 reanalysis is plotted in Figure 2.2(f). Differences are mostly small, though the models have a larger amplitude in most places.

I provide more evidence that effective heat capacity sets the climatological surface temperature phase and amplitude and that the ice-covered ocean has a similar heat capacity to that of land in Figure 2.3. In both Figure 2.3(a) and (b) I plot the percentages of land and sea ice that comprise each zonal band as a function of latitude. In Figure 2.3(a) I plot zonal mean temperature phase, while in Figure 2.3(b) I plot zonal mean temperature amplitude divided by insolation amplitude. The phase is strongly anti-correlated with the fraction of land and sea ice ($r = -0.85$), while the amplitude is strongly correlated ($r = 0.83$), as expected from the different effective heat capacities of ocean and land or sea ice. If sea ice is not included, correlations of land fraction drop to $r = -0.64$ with phase and hold steady $r = 0.85$ with amplitude, suggesting that ice-covered ocean has a land-like effective heat capacity.

2.3.2 Aloft

The zonal mean temperature phase aloft as a function of latitude and pressure is plotted in Figure 2.4(a) and (b) for the ERA-40 reanalysis and the CMIP3 multimodel mean, respectively. While the two exhibit some differences, they have similar

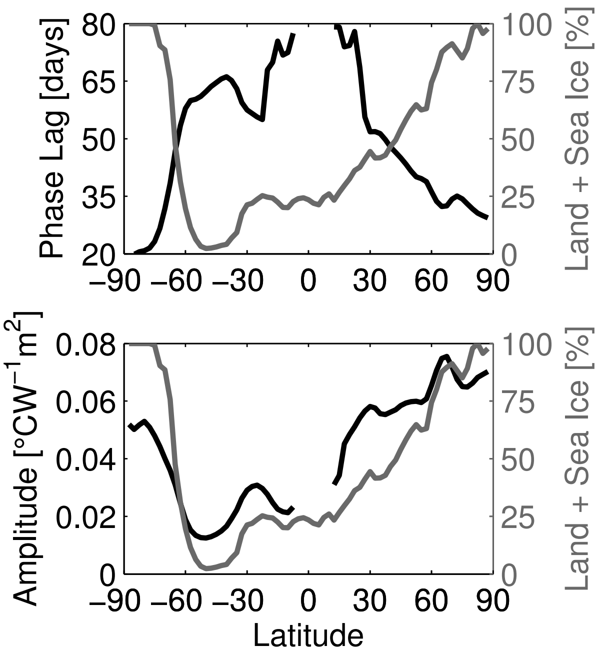

Figure 2.3: Zonal mean surface temperature phase lag from insolation (top, black) and amplitude divided by insolation amplitude (bottom, black). The percent of each latitude band made up of land or sea ice (top and bottom, gray) is also plotted. The data is for the CMIP3 multimodel mean from 1900-1960, but is representative of observations as well. Phase and amplitude both correlate strongly with the amount of land and sea ice ($r = -0.85$ and $r = 0.83$, respectively).

overall structures. For much of the troposphere, the phase lag stays roughly constant with height above the boundary layer, presumably reflecting vertical mixing from the surface. Figure 2.4(c) shows the difference in phase lag between models and the reanalysis. Most locations differ by less than 5 days.

Figure 2.4(d) and (e) show the corresponding plots for the amplitude. Both the reanalysis and models have a very different amplitude structure between the NH and SH. The high-latitude NH has an amplitude that falls off with height, while in the SH the amplitude is more vertically coherent and less variable overall. One difference between these two regions is the amount of land. Land comprises most of each latitude band poleward of 45°N while elsewhere it is mostly ocean (ignoring Antarctica) as in Figure 2.3. The reanalysis and models agree well on these features

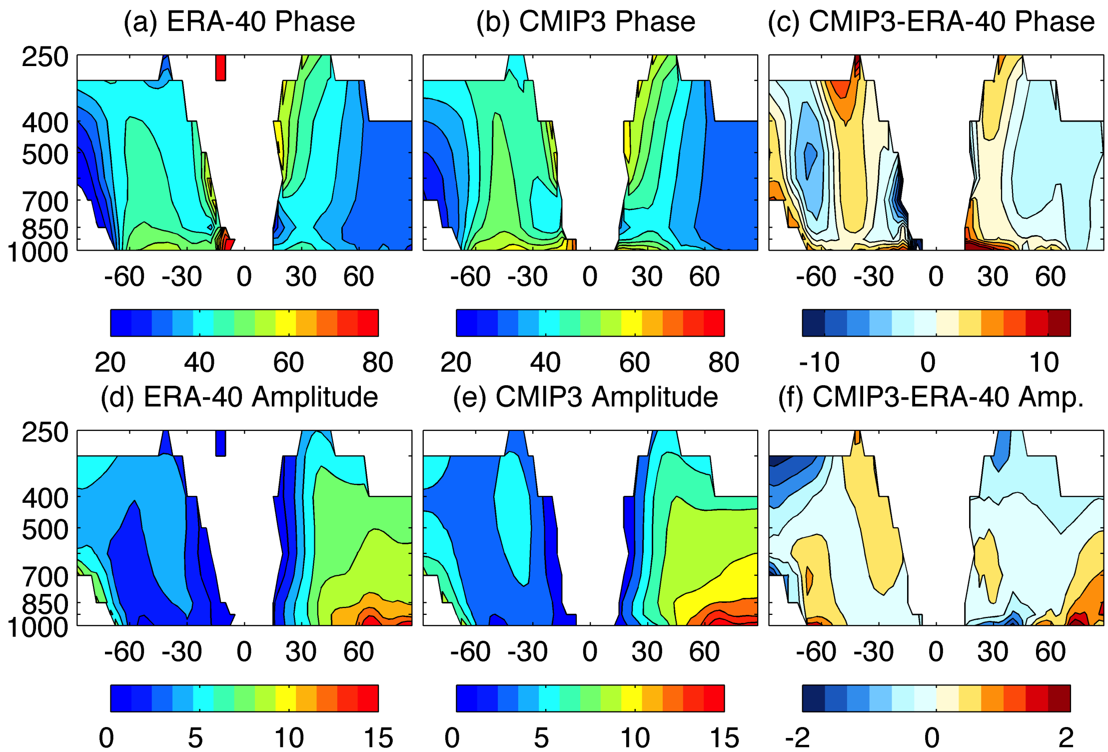

Figure 2.4: Climatological mean seasonality, as in Figure 2.2, except for zonally averaged tropospheric temperature aloft. The top row shows the phase for (a) ERA-40, (b) CMIP3, and (c) their difference. The bottom row shows the amplitude for (d) ERA-40, (e) CMIP3, and (f) their difference. In addition to ignoring locations where the annual cycle is weak, I do not plot the annual cycle in the stratosphere.

as shown in Figure 2.4(f).

2.4 Projected Changes

Beginning around the second half of the 20th century and continuing through the 21st century, the models simulate a roughly linear increase in the global mean surface temperature phase lag from insolation and a linear decrease in the amplitude. These global changes are present for each of the 24 Special Report on Emissions Scenarios (SRES) A1B CMIP3 simulations in the time-series of phase (Figure 2.5(a)) and amplitude (Figure 2.5(b)). The changes over land are smaller and less robust

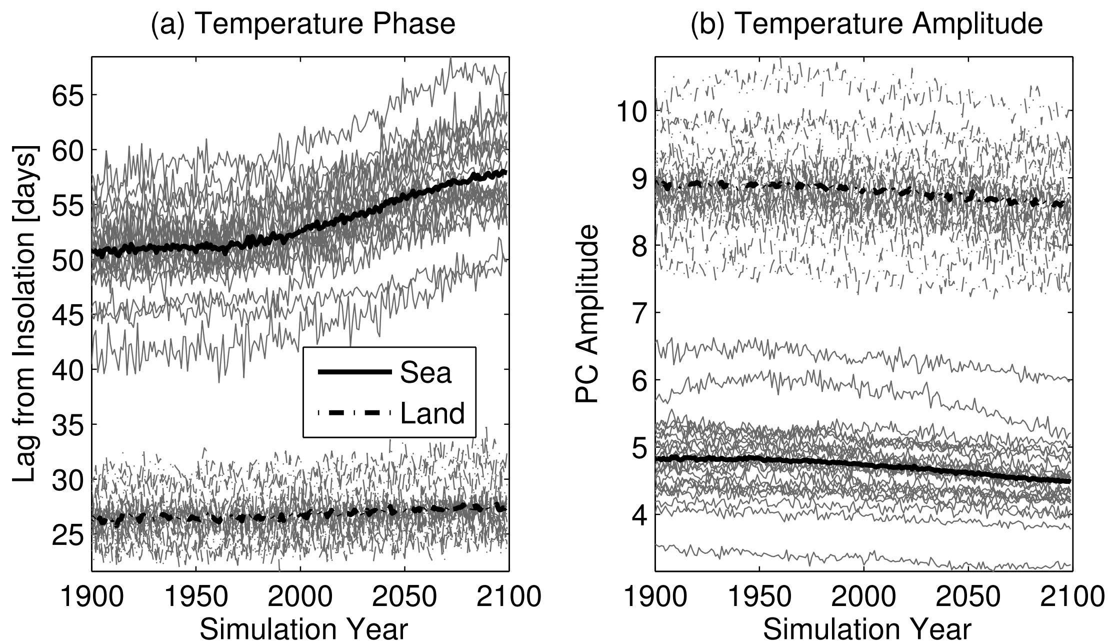

Figure 2.5: Time series of the global surface air temperature (a) lag from insolation and (b) amplitude calculated with EOFs for all 24 models in the 20C3M and A1B scenarios. The multimodel mean is in thick black and individual models are in gray. The solid and dash-dotted lines represent the phase and amplitude over ocean and land, respectively.

than those over ocean, consistent with the idea that sea ice loss is driving much of the change, as discussed in Section 2.5.1. Over ocean, the interannual variability is smaller than the change over the 21st century, for both phase and amplitude.

2.4.1 Surface

Where a change in effective heat capacity is the dominant mechanism altering the annual cycle of surface temperature, changes in phase and amplitude are constrained to be of the opposite sign. For example, if the effective heat capacity increases, the phase will shift to later in the year and the amplitude will decrease. On the other hand, in any region where there are changes in phase and amplitude which are not of opposite sign, changes in effective heat capacity are most likely

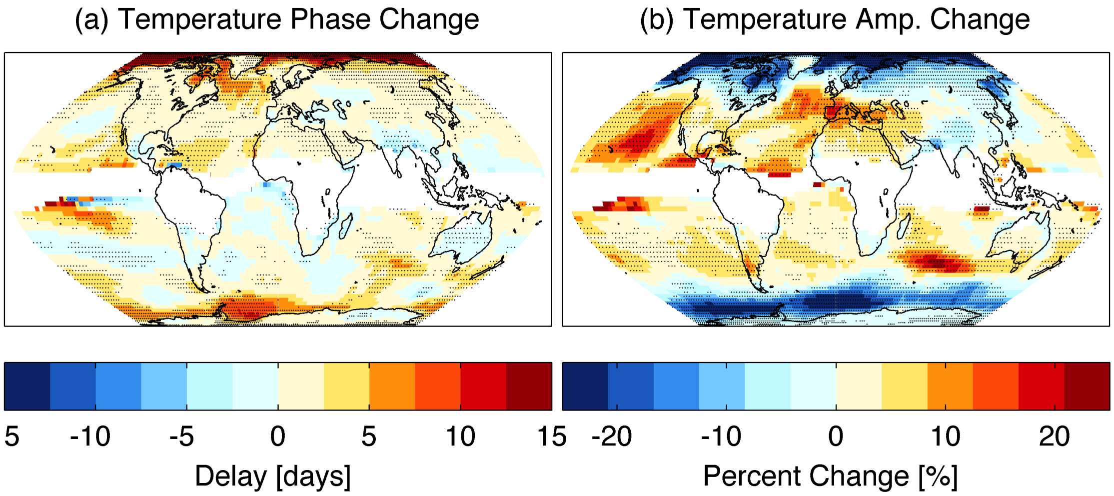

Figure 2.6: The CMIP3 multimodel mean annual surface temperature (a) phase and (b) amplitude change between 2080–99 and 1980–99. Stippling indicates that at least 75% of the models share the same sign as the mean change at that particular location.

not the primary driver.

The projected annual cycle changes in the 21st century are consistent with an effective heat capacity increase in regions of large climatological sea ice cover. Figure 2.6(a) and (b) show latitude-longitude maps of the multimodel mean projected temperature phase and amplitude changes between the last two decades of the 21st century and the last two decades of the 20th century. The largest changes are over high-latitude ocean with prominent sea ice, including the entire Arctic Ocean and the Weddell and Ross Seas of Antarctica. Changes in these regions are robust: at least 75% of models agree with the multimodel mean on the sign of these changes (as indicated by the stippling).

Near the poles, the phase delay and amplitude decrease are much larger over ocean than land. For example the delays in Greenland, Northern Canada, and the Antarctic coast are all smaller than the delays over ocean at the same latitude. The same holds true for amplitude, as I would expect from an effective heat capacity increase over ocean. The largest changes over high-latitude land are near the coast.

The phase delays in the tropics and subtropics are much smaller than those at high latitudes, and there are actually several regions of phase advance. There is no discernible land-sea contrast in the low and midlatitudes, suggesting that the homogenous delay is not solely due to ocean heat capacity. Contrary to the phase change pattern, amplitude changes in the subtropics show a clear large-scale change that is in the opposite direction from that in the high latitudes: there is an amplitude increase of around 5% equatorward of 45°, most pronounced over ocean regions. This amplitude increase is not as large as the polar amplitude decrease, even after weighting by area. Yet this increase is prevalent among the models, especially in the NH. In the deep tropics, where the semi-annual harmonic captures a large share of the total variance, the amplitude of the second harmonic also increases by 15–20%, with the largest changes in the Western Pacific Ocean (not shown). In between the low and high latitude responses (around 45°-60° in each hemisphere) is a transition zone where the amplitude change is small. In any individual model, the region of change is smaller, but averaging over all of the models enlarges the transition zone.

2.4.2 Aloft

The polar phase and amplitude changes are largest near the surface and weaken aloft, as shown in Figure 2.7(a) and (b). This is what I would expect for annual cycle changes controlled by surface characteristics, and supports the idea that the surface temperature phase delay and amplitude reduction at the high latitudes are caused by an increased effective surface heat capacity, as first suggested by Manabe and Stouffer (1980). In fact, Kumar et al. (2010) found a similar seasonal, spatial warming structure aloft in a model simulation with prescribed sea ice loss. The polar changes are likely limited to the lower atmosphere because of the lack of deep vertical mixing due to the strong local atmospheric stability, but I note that while

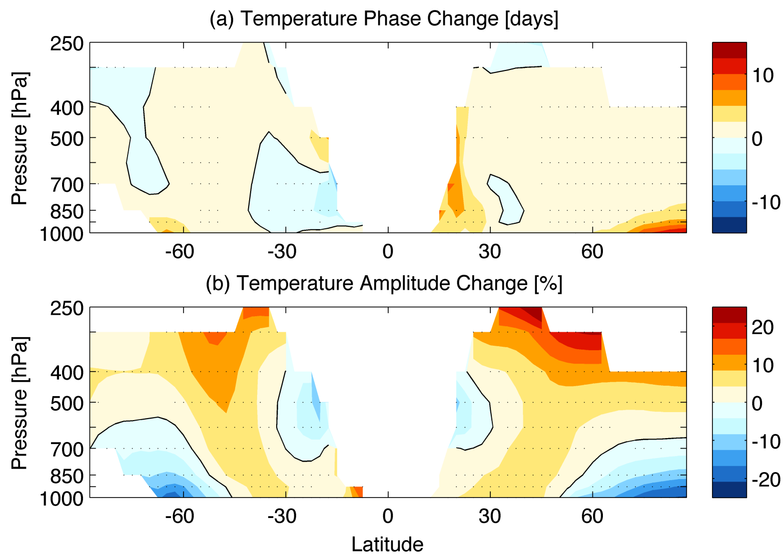

Figure 2.7: As in Figure 2.6, except for tropospheric seasonality changes for (a) phase and (b) amplitude.

the large surface phase delays are confined to the boundary layer and do not extend above 850 hPa, the amplitude reduction extends to around 600 hPa.

Away from the polar surface, most of the troposphere shows a small phase delay of one to two days in the temperature cycle, of the same sign and similar in strength to the mean phase changes at the surface in the midlatitudes. Even though this delay is small, it is present in most models throughout the high-latitude NH troposphere. In the subtropical midtroposphere, there are amplitude decreases in both hemispheres which appear to be independent from changes at the surface. Aside from these regions, the rest of the troposphere has an amplitude increase, which is stronger still in the midlatitude stratosphere (both in relative and absolute magnitude). Donohoe and Battisti (2013) argue that this amplitude increase is due to an increase in absorbed shortwave radiation by the atmosphere in the summer mainly because of increased water vapor. There is an impressive amount of symmetry in the amplitude changes, considering that the climatological amplitude is not particularly symmetric. The changes are also robust in most locations, except in regions where they reverse sign.

2.5 Mechanisms

To understand the high- and low-latitude seasonality changes in a more quantitative manner, I find it useful to analyze them in terms of a very simple model of the basic energy balance at the surface:

$$C\frac{\mathrm{d}T}{\mathrm{d}t} = F(t, T(t)), \tag{2.1}$$

where C is the effective heat capacity, T is the temperature, and F is the net heat flux flux into the surface. Even though C has a seasonal dependence due to changing mixed layer depths, sea ice, soil moisture and other effects, I treat it as a constant for each time period. This is both for the sake of simplicity and because the results of interest prove insensitive to the particulars of a seasonally varying heat capacity, once the annual mean value is specified. (This was verified by numerically solving the temperature equation with a sinusoidally varying $C(t)$ with different phases.)

To isolate the factors that can affect the seasonal temperature cycle, I partition the net flux as $F(t, T(t)) = Q(t) - \beta T$ where $Q(t)$ is the seasonal surface flux that is not linearly related to temperature (such as solar radiation) and β is a constant. Physically, $-\beta T$ represents longwave flux, turbulent heat fluxes, and meridional heat transports, to the extent that those damp the temperature response to $Q(t)$.

After Fourier transforming, I find the following relation for the annual harmonic ($\omega = 2\pi$ yr^{-1}) of T and Q:

$$\begin{aligned} i\omega C T &= Q - \beta T \\ T(\beta + i\omega C) &= Q, \end{aligned} \tag{2.2}$$

which yields the following phase and amplitude relations between T and Q:

$$\begin{aligned} \phi_T - \phi_Q &= \arctan \frac{\omega C}{\beta} \\ |T| &= \frac{|Q|}{\sqrt{\beta^2 + \omega^2 C^2}}. \end{aligned} \tag{2.3}$$

The temperature phase lag is set by the ratio of C to β. In the limiting case of small heat capacity, for which $\omega C/\beta \to 0$, the temperature is in phase with Q, while for very large heat capacity, $\omega C/\beta \to \infty$, and the temperature is in quadrature with Q. The relative amplitude of T to Q is inversely related to both C and β. To understand the effects of changes in C and β I linearize Equation 2.3 to find:

$$\begin{aligned} \Delta\phi_T - \Delta\phi_Q &= \frac{\omega C/\beta}{1 + (\omega C/\beta)^2} \left(\frac{\Delta C}{C} - \frac{\Delta \beta}{\beta} \right) \\ \frac{\Delta|T|}{|T|} - \frac{\Delta|Q|}{|Q|} &= \frac{-1}{1 + (\omega C/\beta)^2} \left(\left(\frac{\omega C}{\beta} \right)^2 \frac{\Delta C}{C} + \frac{\Delta \beta}{\beta} \right). \end{aligned} \tag{2.4}$$

Assuming small variations in β and ϕ_Q, an increase in heat capacity will cause a phase delay. Likewise, for small variations in β and $|Q|$, an increase in C will lead to a decreased amplitude. Thus heat capacity changes have opposite effects on phase and amplitude and that if phase and amplitude do not change in opposite ways, this implies that effective heat capacity changes are not the dominant effect. I can quantify this: since $(\omega C/\beta)^2$ is around 0.5 in the models, variations in C are dominant when $\Delta C/C \gg 2\Delta\beta/\beta$.

In the previous section I found that at high latitudes changes are qualitatively consistent with an increase in effective heat capacity in regions where sea ice decreases in extent, thins, or becomes less persistent throughout the year. Below, I make this connection in more quantitative detail.

In the tropics and subtropics, phase and amplitude both increase and must therefore be forced at least in part by something other than changes in effective heat capacity. Below I provide evidence that this may be a consequence of a fractional increase in β that is nearly an order of magnitude larger than the local fractional reduction in effective heat capacity.

2.5.1 High latitudes

Before demonstrating that the high-latitude phase delay and amplitude decrease of surface temperature are due to sea ice loss, I demonstrate that they are not directly due to changes in the surface flux cycle. For the flux to be responsible for the high-latitude seasonality changes to temperature, seasonal surface flux would need to delay and weaken. In fact, the reverse happens, as shown in Figure 2.8(a) and (b).

There is little change in the phase of surface flux at high latitudes. In fact, the phase actually advances over some high-latitude ocean regions, indicating that the high-latitude temperature phase delay is not driven by changes in the surface flux phase. The surface flux amplitude, on the other hand, does show robust changes in the high latitudes. These changes, however, are of the opposite sign to the temperature amplitude changes. Over high-latitude ocean in both hemispheres, the surface flux amplitude increases by around 50% in both hemispheres. The increase is confined to ocean and is in the same region as the reduction in the amplitude of surface temperature. Since the phase and amplitude changes of surface flux are of the opposite sign to the temperature changes, they cannot be responsible for the latter.

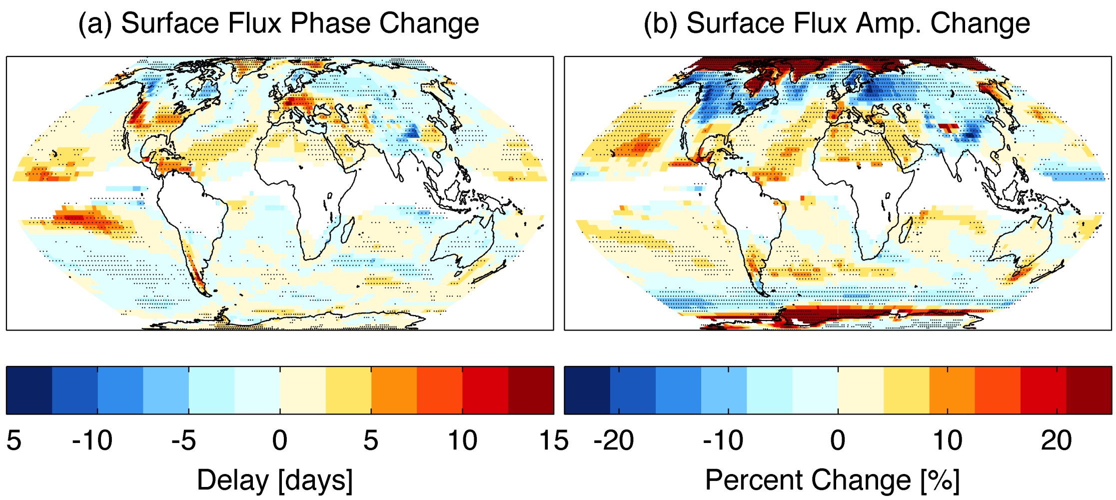

Figure 2.8: As in Figure 2.6, except for total surface flux change, not temperature change. Only locations where the annual cycle of surface flux represents at least 70% of the total variance are plotted.

The surface flux amplitude changes at high latitudes in Figure 2.8(b) are consistent with sea ice loss (Screen and Simmonds, 2010). Climatologically, the ice margin is not only the region of greatest upward turbulent heat flux during the winter, but also where the total surface flux amplitude is greatest. As the ice edge shifts poleward during the 21st century, the consequence to the surface flux is an increase in amplitude in the polar ocean and a decrease in amplitude in the sub-polar ocean (Deser et al., 2010). In the polar ocean, the albedo is also reduced, which increases the downward shortwave radiation at the surface during the summer, contributing to an increased surface flux amplitude at high latitudes.

In terms of the energy balance model, Figure 2.8(a) and (b) show the seasonality changes to $F = Q - \beta T$. The seasonality changes in $Q(t)$ are similar to those in $F(t)$ at high latitudes. Whether I take $Q(t)$ to be the net shortwave flux at the surface or at the top of the atmosphere, I find the same small phase advance and large amplitude increase in the high latitudes (not shown). Hence I can rule out seasonal changes of Q as responsible for driving the high-latitude seasonal temperature changes.

In the multimodel mean, the surface temperature has a phase delay and amplitude decrease at high latitudes, consistent with an effective heat capacity increase. I also look for this consistency on an individual model basis. For example, do models with large phase delays also tend to have large amplitude decreases? I address this question in Figure 2.9. On the y-axis I plot $\Delta\phi = \Delta\phi_T - \Delta\phi_Q$, the change in the phase of the surface temperature relative to the change in phase of seasonal surface flux, and on the x-axis I plot $\Delta A = \Delta(|T|/|Q|)$, the change in the ratio of amplitudes of surface temperature to seasonal surface flux. The phase and amplitude changes are averaged over the NH and SH oceanic polar caps for each model. I find correlations between the phase and amplitude changes for both polar caps: $r = -0.67$ in the NH and $r = -0.79$ in the SH. Results are similar if I plot $\Delta\phi_T$ against $\Delta|T|$, though the correlations strengthen to $r = -0.79$ in the NH and weaken to $r = 0.17$ in the SH. There is only one model where $\Delta\phi$ and ΔA have the same sign, and both phase and amplitude changes in that model are small.

Based on the energy balance model, I can calculate a theoretical relationship between phase and amplitude changes, assuming heat capacity changes while β stays fixed. Because Figure 2.9 shows a roughly linear relationship between the phase and amplitude changes, I use the linearized relationships of Equation 2.4 and obtain a theoretical slope of $-\beta\sqrt{1 + (\beta/\omega C)^2}$, though one might not expect a linear relationship because the changes are not small percentagewise (more than 25% for amplitude and 50% for phase, since a 15 day delay is half of the 30 day lag from insolation near the poles). I plot the multimodel mean of the theoretical slope with a dotted line in Figure 2.9. The theoretical slope (-0.08) is much flatter than the slope of the best fit line (-0.40) in the NH, while for the SH the slopes are more similar (-0.16 theoretically and -0.26 for the best-fit line). I do not completely understand why the theoretical and best-fit slopes differ so much in the NH. An

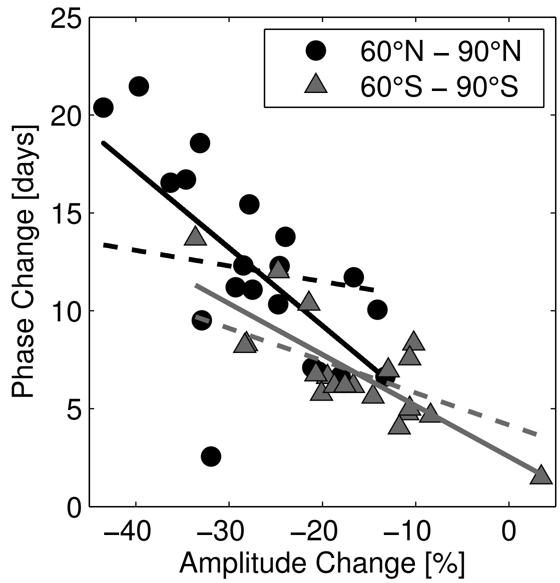

Figure 2.9: Scatter plot of phase ($\phi_T - \phi_Q$) and amplitude ($|T|/|Q|$) changes for the NH (black circles) and SH (gray triangles) oceanic polar caps of the CMIP3 models between the periods 1980–99 and 2080–99. Each pair of black and gray markers represents a single model. The solid lines are the least-squares best fit line and the dashed lines describe the theoretically predicted slopes as described in Section 2.5.1.

obvious possibility is that the very simple, zero-dimensional, two-parameter model is inadequate to capture the GCM behavior at this quantitative level; another is that the multimodel mean is not the most appropriate estimate of β to use to compute the theoretical slope. Nonetheless, a change in β alone would produce a positive correlation, and that the changes in phase and amplitude are negatively correlated qualitatively supports the hypothesis that heat capacity changes control the seasonality changes.

To further quantify the extent to which seasonality changes are due to C or β, I calculate the changes to effective heat capacity in the context of the energy balance model. Solving Equation 2.3 for C and β in terms of phase and amplitude gives the following:

$$
\begin{aligned}
C &= \frac{\sin\phi}{\omega A} \\
\beta &= \frac{\cos\phi}{A}.
\end{aligned}
\tag{2.5}
$$

Since I calculate A and ϕ directly via Fourier transform, Equation 2.5 gives expressions for the C and β changes for the CMIP3 models in the context of this simple temperature model.

In my calculations I take Q to be the net shortwave flux at the surface, but the results are nearly the same if I take it to be the net shortwave flux at the top of the atmosphere. For both the surface temperature and the net surface shortwave flux I calculate the average phase and amplitude over ocean poleward of 60° for each hemisphere for the last two decades of the 20th and 21st centuries. From these values I find C and β and plot the changes in Figure 2.10(a).

Changes to C show a robust increase across the multimodel ensemble in both hemispheres; nearly every single model predicts an increase in effective heat capacity. The multimodel mean increases are 82% and 43% for the NH and SH, respectively. Changes to β are smaller, but also positive for nearly all of the models. The multimodel mean increase is 16% for the NH and 9% for the SH. I interpret the β changes mathematically as an increased damping in the system, and physically as the turbulent and longwave fluxes and heat transports - in some combination - becoming more effective at returning the surface temperature to equilibrium. Which of the processes involved is most responsible for this change and how the change is ultimately forced by greenhouse gas increases is not yet clear and will require further study.

Despite the robust increase in β, the proportionally larger increase in C has the greater influence on the changes in the seasonality of temperature at high latitudes. From Equation 2.4, phase delays are proportional to $\Delta C/C - \Delta\beta/\beta$, indicating that if β did not change, the phase delay would be even larger. Amplitude changes are

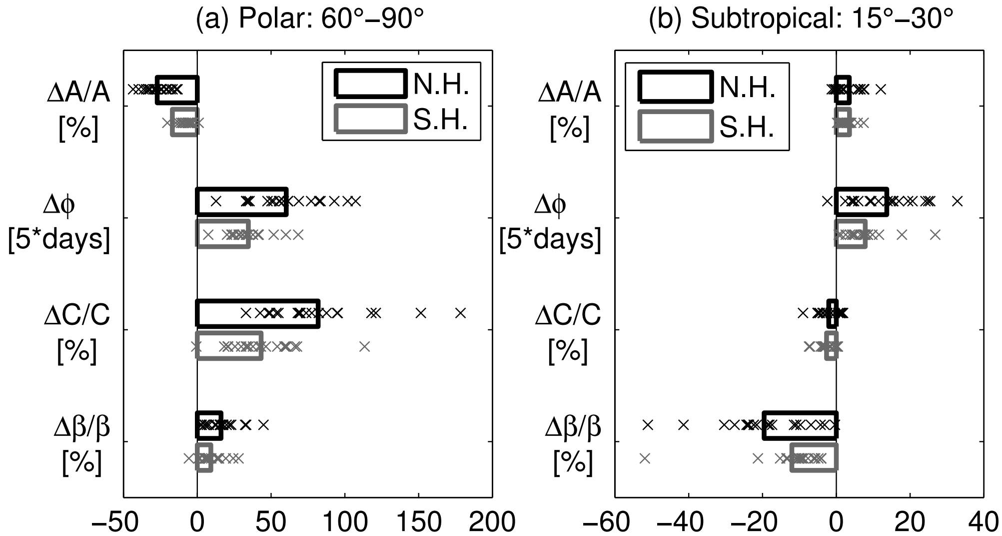

Figure 2.10: Changes in amplitude, phase, effective heat capacity, and β for the NH (black) and SH (gray) (a) high latitudes and (b) low latitudes over ocean for each CMIP3 model. The multimodel mean is represented by a bar and individual models by an $\times$. The amplitude and phase are found from a Fourier transform and the effective heat capacity and β are found from Equation 2.5. The changes in phase have been multiplied by 5 to use the same axis for all quantities. Note that the scale of (a) is 2.5 times that of (b).

proportional to $-\Delta\beta/\beta - (\omega C/\beta)^2 \Delta C/C$, where $(\omega C/\beta)^2$ is a proportionality factor averaging 0.4 for the NH and 0.7 for the SH in the 20th century. Since β and C both increase in the 21st century, both are responsible for a decreased amplitude. However, when I calculate the multimodel mean of $(\omega C/\beta)^2(\Delta C/C)(\Delta\beta/\beta)^{-1}$ I find that the contribution from the heat capacity change term is two to three times larger than that from the β term.

Sea ice loss was postulated to be the reason for high latitude changes in seasonality by earlier authors (Manabe and Stouffer, 1980; Manabe et al., 1992; Mann and Park, 1996). The explanation goes as follows: sea ice acts as a partition between the atmosphere and ocean by shutting off radiative transfer and turbulent heat fluxes between them. The only coupling is by conduction through the sea ice. As sea ice melts, the insulating effect wanes and the ocean and atmosphere can

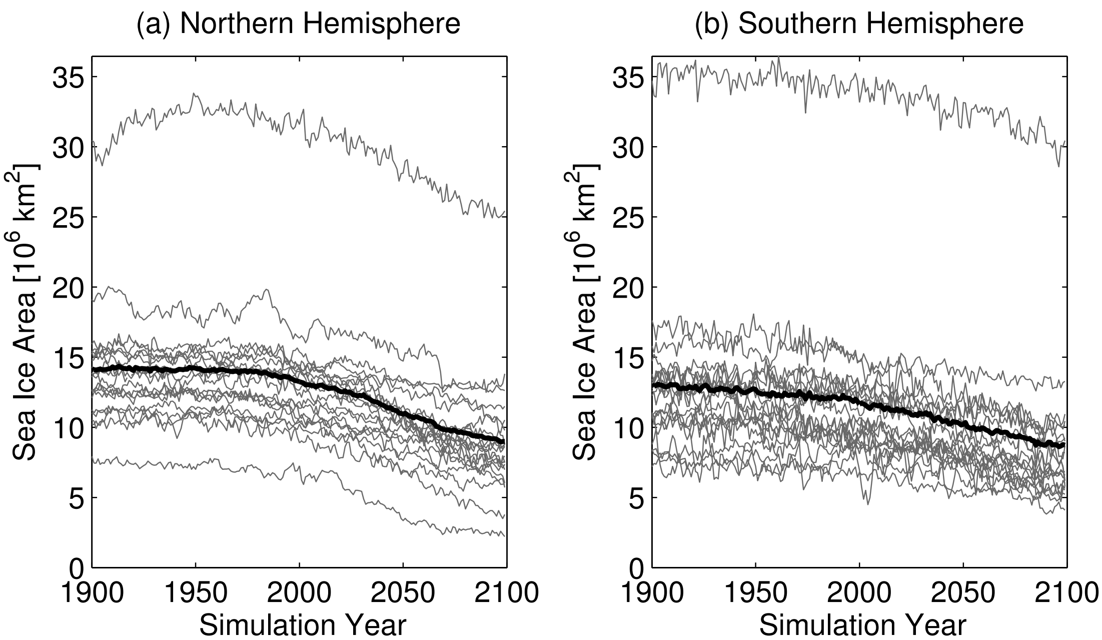

Figure 2.11: Time series of annually averaged sea ice area in the (a) NH and (b) SH polar caps (60°–90°) for the CMIP3 models. The thick black line is the multimodel mean.

more freely exchange heat, raising the effective heat capacity of the surface. Any external addition of heat, such as from solar radiation, will more easily be shared between the atmosphere and ocean if there is less sea ice. Sea ice loss is robust in the models: sea ice area diminishes in every model at a roughly linear rate during the 21st century (Figure 2.11). The NH suffers a larger ice loss than the SH, which may partly account for why the amplitude and phase changes are larger in the NH.

If all of the effective heat capacity increase were due to sea ice loss, then $\Delta C/C$ would be roughly proportional to the fractional change in open ocean area. I calculate the latter quantity for each model and in Figure 2.12 plot it against the fractional change in effective heat capacity for each model as calculated from Equation 2.5.

The two calculations of effective heat capacity correlate well with each other, indicating that sea ice loss is probably the dominant mechanism for the effective

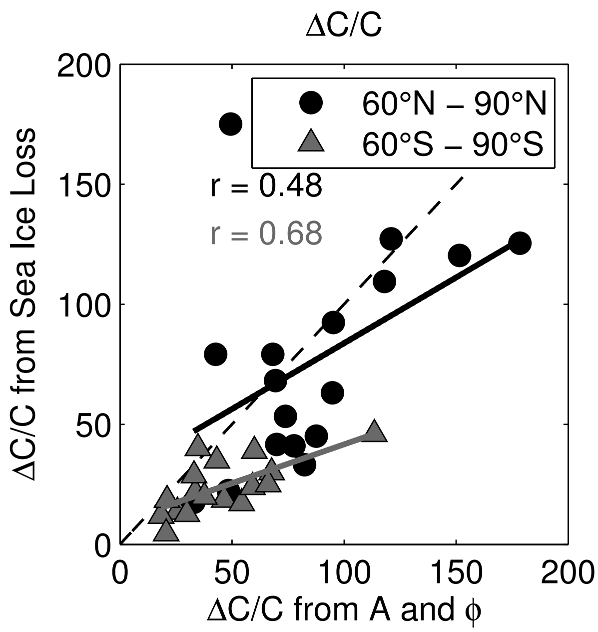

Figure 2.12: Scatter plot of fractional effective heat capacity changes in the CMIP3 models calculated from the increase in open ocean fraction on the y-axis and from the amplitude and phase on the x-axis for the NH (black circles) and SH (gray triangles) polar caps. Each marker represents an individual model and the line is the one-to-one line between the axes. Correlations are $r = 0.48$ for the NH and $r = 0.68$ for the SH. The slopes of the lines are 0.55 for the NH and 0.32 for the SH.

heat capacity change. While the correlations are strong, the models do exhibit a bias: the two effective heat capacity calculations are not randomly distributed about the one-to-one line, but instead the effective heat capacity change is larger when calculated from Equation 2.5. This could be due to the limitations of relating effective heat capacity increase to ice area alone. For example, simply measuring the open ocean increase does not take into account sea ice thinning, which would increase the effective heat capacity relative to a thick sea ice layer. Regardless, sea ice area loss appears to account for most of the effective heat capacity increase which is driving the delayed and weakened annual temperature cycle in the high latitudes.

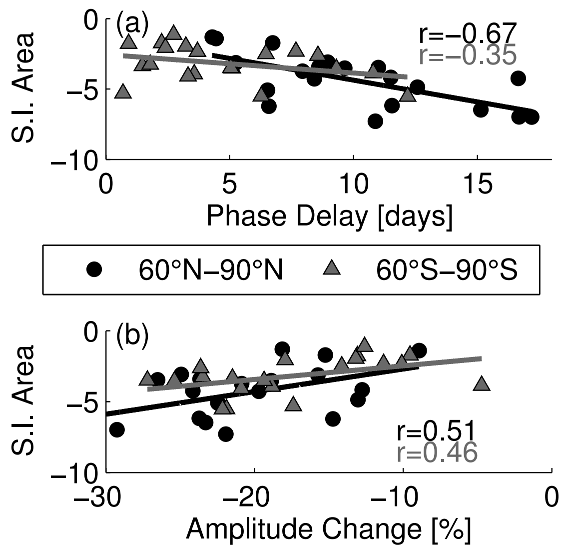

Figure 2.13: Correlations between sea ice area loss and (a) temperature phase delay and (b) temperature amplitude change for the polar NH (black circles) and polar SH (gray triangles) in the CMIP3 models between 2080–99 and 1980–99.

Another way to quantify the relationship between temperature annual cycle changes and sea ice changes is to correlate the two across models in the ensemble. I focus on high-latitude (poleward of 60°) annual cycle changes to air temperature over ocean in order to determine if models with large sea ice loss tend to have large phase delays and weak annual cycles. I find that correlations of temperature phase delay with annual sea ice area change are significant for the NH ($r = -0.67$), but not for the SH ($r = -0.35$) at the 95% level (Figure 2.13(a)). Correlations between amplitude change and sea ice area change are $r = 0.51$ for the NH and $r = 0.46$ for the SH and are significant for both hemispheres (Figure 2.13(b)). These correlations do not significantly change if I weight the area loss with a factor to account for the reduction of ice thickness.

2.5.2 Low Latitudes

While sea ice loss seems to explain the high-latitude phase and amplitude changes of the annual temperature cycle, it does not directly explain the changes at low latitudes. Equatorward of roughly 45° the models simulate a slight phase delay and an increased amplitude. One possible explanation for this behavior is that the high-latitude seasonality changes are transported equatorward, for example, by midlatitude eddies. There are two reasons this is unlikely. For one, the amplitude increases at low latitudes, while it decreases near the poles. The other reason is that models that have large delays in the high latitudes do not tend to have large delays in the subtropics. The only region-to-region phase correlations that appear significant are between the extratropics and subtropics in the Northern Hemisphere ($r = 0.59$). But the amplitude correlations are small between these two regions ($r = 0.17$), suggesting that the delay in the low latitudes is not simply communicated from higher latitudes.

An alternate explanation is that the temperature seasonality changes are a result of surface flux seasonality changes. While the phase and amplitude of surface flux changes are opposite in sign to those of the temperature changes at high latitudes, this is not the case at low latitudes as shown in Figure 2.8. The phase of both surface temperature and surface flux show a small delay - less than 5 days - from 45°S–45°N. The amplitude changes of temperature and surface flux are even more similar. From 45°S–45°N both temperature and surface flux amplitude show broad increases of around 5%.

There is also a strong spatial correlation between the temperature and flux changes. Phase delays occur in the same places such as the Eastern Pacific and the NH subtropical Atlantic. The temperature and flux also both have especially large amplitude increases in the Eastern Pacific and Eastern Atlantic. I create a measure of spatial correlation in Figure 2.14 by plotting the multimodel mean seasonality

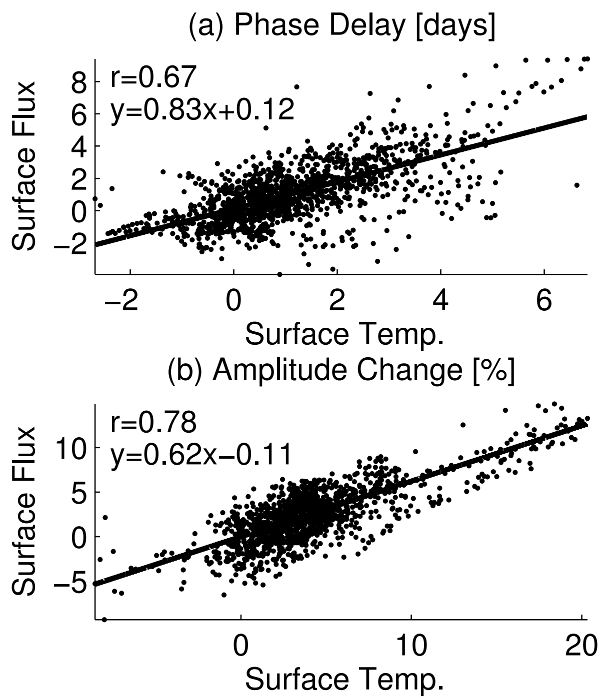

Figure 2.14: Scatter plot of 21st century seasonality changes of surface flux versus surface temperature for (a) phase and (b) amplitude for subtropical ocean grid boxes. There is an area-weighted correlation between these two variables for both phase and amplitude, indicating that, for example, subtropical locations that have large surface flux delays tend to have large surface temperature delays. The data is restricted to 15°–30° in both hemispheres and does not include locations where the annual harmonic of each variable does not dominate its total variance. The solid line represents the area-weighted least-squares regression.

changes for temperature and flux against one another for all subtropical ocean grid boxes between 15°–30° in both hemispheres, excluding locations where the annual cycle is small. There are strong correlations of $r = 0.67$ for the phases and $r = 0.78$ for the amplitudes, indicating that the surface flux changes are spatially correlated with the surface temperature changes.

These changes can be understood in the context of the energy balance model. While the seasonal cycle of total flux, F, delays and strengthens in the subtropics in Figure 2.8, the same cannot be said of the temperature-independent component of the flux, Q. There is almost no change in the phase or amplitude of the net shortwave radiation at the surface (not shown). Since $F = Q - \beta T$, this suggests that changes in β are responsible for the changes in total surface flux.

To find the explicit changes to C and β, I use the same procedure as for the high latitudes by calculating C and β from A and ϕ with Equation 2.5 and plot these results in Figure 2.10(b). The phase delay is around 2.8 days in the NH and 1.6 days in the SH, while the amplitude increase is around 3–4% for both the NH and SH. While small, these changes are robust in the models: the vast majority have the same sign as the mean change. Unlike in the high latitudes, I find a small decrease in the subtropical heat capacity around 2–3% in both hemispheres. This might be a consequence of a reduction in tropical ocean mixed layer depth (Philip and Oldenborgh, 2006). The larger changes are in β, which decreases by 20% in the NH and 12% in the SH. Since $\Delta\phi \propto \Delta C/C - \Delta\beta/\beta$, I can attribute the subtropical phase delay primarily to the β decrease. Likewise, since $\Delta A/A \propto -\Delta\beta/\beta - (\omega C/\beta)^2 \Delta C/C$, and $\omega C/\beta < 1$, the amplitude increase is also primarily due to the β decrease.

The reduction in β indicates that 21st century temperature in the subtropics becomes more weakly damped. Physically, a weakened β means that the combination of turbulent and latent fluxes and heat transports become less effective at returning the surface temperature to equilibrium. A reduced β does not necessarily imply a weakened surface flux amplitude because the total surface flux $F = Q - \beta T$ also depends on the phase relationship between T and Q. For the low latitudes, the surface flux amplitude increases despite the reduction in β. Sobel and Camargo (2011) presented evidence that the surface flux amplitude increases are driven by changes in the seasonal cycle of surface winds, with subtropical winds increasing in the winter hemisphere and decreasing in the summer hemisphere. At a fixed subtropical location, these changes in wind speed change sign over the year and thus will not be described well by a simple change in an otherwise constant coefficient β. Further, because surface air humidity (the other state variable that enters bulk formulae for the surface latent heat flux, besides wind speed and SST) can adjust so quickly to other factors, it may be appropriate to view these wind speed changes as an external forcing on the surface fluxes, rather than a change in a damping coefficient in an SST equation. These considerations suggest that the simple model I have proposed to interpret the high-latitude seasonality changes projected by the models may be inadequate to capture the low-latitude changes. Further work is required to determine the exact roles of the surface wind and other factors in the surface energy budget. It is clear, however, that there is a link between the net surface heat flux and the seasonal temperature cycle at low latitudes, unlike at high latitudes where the effective heat capacity governs the changes in seasonality.

2.6 Conclusions

In this study I analyzed the changes to the seasonality of surface temperature in response to an increase in greenhouse gases during the 21st century as represented by CMIP3 models. I found large, robust, global changes to the annual cycle of surface temperature: a phase delay and an amplitude reduction. By analyzing these changes geographically, I found that the phase delay and amplitude decrease are strongest at high latitudes and drive the global response. These polar changes are consistent with an effective heat capacity increase of the surface layer due to sea ice loss. At low latitudes there is a small phase delay and an amplitude increase, which I linked to changes in the seasonality of the surface heat flux.

CMIP3 climate models accurately represent the typical phase and amplitude of the annual cycle aloft and at the surface as represented by the ERA-40 reanalysis. While the two are not completely independent, since the reanalysis incorporates a climate model, the agreement is encouraging. Geographic variations in models and the reanalysis are spatially consistent and can be traced to different surface effective heat capacities: temperature over ocean responds slowly and weakly, while temperature over land and sea ice responds rapidly and strongly.

At high latitudes the temperature cycle delays and weakens in response to greenhouse gases in the CMIP3 models. I provided evidence that sea ice loss is driving these changes. By fitting CMIP3 data to a parameterized surface energy balance model, I found that an increase in effective heat capacity primarily accounts for the phase delay and amplitude decrease at high latitudes. I also demonstrated that the increase in effective heat capacity for each model was consistent with the increase in open-ocean fraction, indicating that sea ice loss is driving the effective heat capacity and seasonality changes at high latitudes. I provided further evidence of this mechanism by showing strong correlations between sea ice loss and phase and amplitude changes among the models at the high latitudes in each hemisphere.

The projected delayed and weakened temperature cycle in the high-latitudinal NH is a manifestation of Arctic Amplification, the accelerated annual mean warming in the Arctic Ocean relative to the rest of the globe predicted by all CMIP3 A1B 21st century climate simulations. Arctic Amplification has a seasonal component to it as well, with models predicting little warming in summer and substantial warming during the late fall and early winter (Serreze and Francis, 2006). This warming structure is consistent with the changes in the annual harmonic of phase and amplitude. While the models predict the surface annual cycle changes to grow over the course of the 21st century, recent studies have already found early signs of changes in the Arctic Ocean. Among four different data sets, Serreze et al. (2009) and Screen and Simmonds (2010) found evidence of a delayed and weakened temperature cycle in the Arctic Ocean, consistent with rapid sea ice loss over this time period and providing support for future changes expected by the CMIP3 models.

I suggest that the high-latitude seasonal temperature changes are credible. Not only are they prevalent among the models, but they are also linked to a clearly identifiable physical process in the models: sea ice loss. While there has been some disagreement between models and observations of temperature phase changes over midlatitude NH land during the 20th century (Stine et al., 2009), substantial sea ice loss is already occurring in the Arctic. Furthermore, trends of an Arctic temperature phase delay and amplitude decrease have been observed during the last 30 years.

Changes in the temperature cycle at low latitudes are different in nature than those at high latitudes. While still robust, they have a small phase delay and a small amplitude increase, inconsistent with an increase in effective heat capacity. However, the changes in both phase and amplitude are consistent with a delayed and strengthened surface flux cycle that I traced to a decrease in damping of surface temperature by turbulent and longwave heat fluxes in the energy balance model. I also found a strong spatial correlation between seasonality changes in surface flux and surface temperature in the subtropics. Sobel and Camargo (2011) describe a link between changes in the amplitude of the seasonal cycle in SST and those in surface wind speed and describe the latter partly as a consequence of the expansion of the Hadley cell and further discussed in Chapter 4. Phase changes in tropical precipitation (Biasutti and Sobel, 2009) are not strongly tied to the seasonality changes in SST as discussed in the following chapter.

Chapter 3

The Effect of Greenhouse-Gas-Induced Changes in SST on the Annual Cycle of Zonal Mean Tropical Precipitation

3.1 Introduction

The annual cycle of tropical precipitation, primarily characterized by the monsoons and the meridional movement of the ITCZ, is responsible for much of the variance in global precipitation. Even relatively small changes in the annual cycle of tropical precipitation may have large impacts, both globally and locally. For example, they can affect the timing and quantity of latent heat release and energy transport, which can also affect the general circulation. Changes in monsoonal timing have large regional implications due to the dependence of many agricultural and pastoral communities on rainfall.

Nearly all of the models in the World Climate Research Programme's (WCRP's)

Coupled Model Intercomparison Project phase 3 (CMIP3) multimodel dataset (Meehl et al., 2007) project consistent changes to the annual cycle of tropical SST and precipitation in simulations with increased greenhouse gases: a phase delay and an amplification (Chou et al., 2007; Tan et al., 2008; Biasutti and Sobel, 2009; Sobel and Camargo, 2011; Seth et al., 2011; Dwyer et al., 2012). CMIP5 (Taylor et al., 2011) models show changes of the same sign, as I discuss in Section 3.3 and as documented elsewhere (Biasutti, 2013; Seth et al., 2013; Huang et al., 2013). These CMIP3 and CMIP5 studies suggest a variety of causes to explain the projected changes in the annual cycle, including: high-latitude phase delays due to reduced sea ice affecting the tropics; changes in the strength and extent of the Hadley Cell affecting the amplitude of precipitation and SST via changes in the surface wind speed on turbulent surface fluxes; an increase in low-level water vapor vertically advected by the Hadley Cell leading to an increase in the amplitude of precipitation; changes in the timing and strength of the annual cycle of surface heat fluxes affecting the annual cycle of surface temperature; increased vertical stability later in the year due to enhanced warming aloft delaying the timing of tropical precipitation; and a reduction of soil moisture early in the year in monsoon regions delaying monsoonal precipitation. Most of this work focuses on the projected amplitude changes, especially for precipitation. Projected phase changes have received less attention and are not as well understood.

I am interested in what modifies the annual cycles of both precipitation and surface temperature in the greenhouse-gas forced, fully coupled models. In this chapter I address a more limited question: given a change in the annual mean or annual cycle of SST, what is the response of the annual cycle of precipitation and to what extent can this explain changes in the coupled models? Using an atmospheric general circulation model (AGCM) forced with SST provides a simple framework to evaluate this question, but there are drawbacks to this approach. In particular, prescribing SST eliminates feedbacks between the ocean and atmosphere that are present in both the real climate and coupled models (Fu and Wang, 2004; Kitoh and Arakawa, 1999). Despite this, given the observed SST and radiative forcings, AGCMs capture the annual precipitation anomalies over land and for the tropics over all, though there is some discrepancy over ocean (Liu et al., 2012). Similar studies where the annual cycle of SST was modified or suppressed have been carried out to study the effect of SST on the Asian summer monsoon (Shukla and Fennessy, 1994), the equatorial Atlantic and Pacific (Li and Philander, 1997), precipitation in the Amazon basin (Fu et al., 2001), and precipitation in the tropical Atlantic (Biasutti et al., 2003, 2004).

As I will show later, the AGCM experiments reproduce many aspects of the change in seasonality seen in the coupled models. This suggests that the same mechanism might be operating in the greenhouse gas forced, coupled models. (Here I use the term seasonality to denote the annual cycle only and not higher frequency harmonics). While this study cannot rule out alternative mechanisms for the seasonality changes of precipitation in the coupled models, it demonstrates that changes to the annual mean and annual cycle of SST are each sufficient to affect the annual cycle of precipitation simulated in the coupled models.

Ultimately, greenhouse gases are responsible for the changes to both SST and precipitation in the coupled models. While these results suggest that precipitation is responding to changes to SST, the mechanism by which greenhouse gases affect the seasonality of SST is not yet clear. The previous chapter suggested a link to the surface fluxes (specifically latent heat flux), which may be due to changes in the Hadley Circulation (Sobel and Camargo, 2011).

In the following section I describe the methods, AGCM, experimental design, and sensitivity of the results to my methods. Next in Section 3.3 I describe the annual mean and seasonal changes to SST and precipitation in the CMIP5 models, which motivates the modeling studies. In Section 3.4 and 3.5 I describe and interpret the results of my simulations in which I uniformly increased the SST and changed the seasonality of SST, respectively. In Section 3.6 I discuss how to interpret the coupled results in light of the uncoupled, idealized simulations. I conclude in Section 3.7 and summarize my results.

3.2 Methods and Experimental Design

I reproduce the CMIP3 results of an amplitude increase and a phase delay for SST and precipitation in the tropics (25°S–25°N) with 35 CMIP5 models for which monthly precipitation and surface temperature data for both the historical simulation and rcp8.5 scenario are available. Rcp8.5 is a high greenhouse gas emission scenario with a year 2100 radiative forcing of around 8.5 W m^{-2} relative to pre-industrial conditions (Taylor et al., 2011). A full list of models included in this study is given in Table 3.1.

For the simulations, I use the atmospheric component (CAM4) of the National Center for Atmospheric Research (NCAR) Community Climate Systems Model, version 4 (CCSM4) (Gent et al., 2011) at the standard resolution (1.9°×2.5°). To create a control simulation, I run the model for 40 years with climatological SST determined from the Hadley Center and NOAA for the 1982–2001 observation period (Hurrell et al., 2008). The perturbed simulations were run for at least 10 years, sufficiently long to characterize the annual cycle of precipitation. The only change I made in the perturbed simulations was to either alter the mean or the annual cycle of SST. Land temperatures were free to adjust on their own and the atmospheric chemical composition was the same between simulations.

I use two methods to calculate the seasonal characteristics of temperature and precipitation. The first is to Fourier transform data to directly obtain the phase and amplitude of the annual harmonic; this decomposition can be performed pointwise.

Model	Group, Country
ACCESS1-3	CSIRO-BOM, Australia
BCC-CSM1-1	BCC, China
BCC-CSM1-1-m	BCC, China
BNU-ESM	GCESS, China
CanESM2	CCCma, Canada
CCSM4	NCAR, USA
CESM1-BGC	NSF-DOE-NCAR, USA
CESM1-CAM5	NSF-DOE-NCAR, USA
CESM1-WACCM	NSF-DOE-NCAR, USA
CMCC-CM	CMCC, Italy
CMCC-CMS	CMCC, Italy
CNRM-CM5	CNRM-CERFACS, France
CSIRO-Mk3-6-0	CSIRO-QCCCE, Australia
FGOALS-g2	LASG-CESS, China
FGOALS-s2	LASG-IAP, China
FIO-ESM	FIO, China
GFDL-CM3	NOAA-GFDL, USA
GFDL-ESM2G	NOAA-GFDL, USA
GFDL-ESM2M	NOAA-GFDL, USA
GISS-E2-R	NASA GISS, USA
GISS-E2-H	NASA GISS, USA
HadGEM2-CC	MOHC, UK
HadGEM2-ES	MOHC, UK
INM-CM4	INM, Russia
IPSL-CM5A-LR	IPSL, France
IPSL-CM5A-MR	IPSL, France
IPSL-CM5B-LR	IPSL, France
MIROC-ESM	MIROC, Japan
MIROC-ESM-CHEM	MIROC, Japan
MIROC5	MIROC, Japan
MPI-ESM-LR	MPI-M, Germany
MPI-ESM-MR	MPI-M, Germany
MRI-CGCM3	MRI, Japan
NorESM1-M	NCC, Norway
NorESM1-ME	NCC, Norway

Table 3.1: The 35 CMIP5 models used in this study.

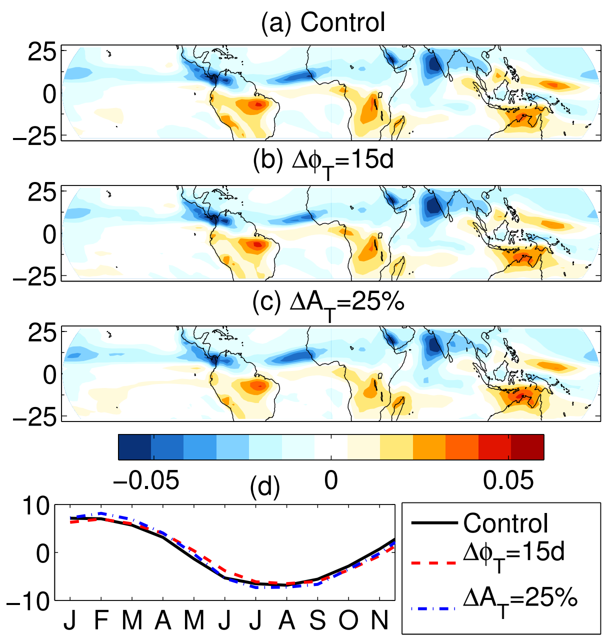

Figure 3.1: The first EOF of tropical precipitation, representing the annual cycle, for the control simulation (a), a simulation forced with a 15 day phase delay of SST (b), and a simulation forced with a 25% amplitude increase of SST (c). I also plot the PC1s associated with each EOF in (d).

The second method is Empirical Orthogonal Function (EOF) analysis, which extracts patterns of coherent variability in the data (Kutzbach, 1967). The dominant spatial pattern (EOF1) explains 85% of the variability in tropical SST and 70% in tropical precipitation. By fitting a sinusoid to the principal component (PC) associated with the annual cycle, PC1, I obtain the amplitude and phase (Biasutti and Sobel, 2009; Dwyer et al., 2012). Any change to PC1 of precipitation can be interpreted as a change in the timing or strength of the ITCZ movement or monsoonal precipitation (Figure 3.1(a)), assuming that EOF1 changes little, an assumption I address below.

To create the SST forcing for the uniform warming (UW) experiment, I simply adjust the climatological SST by a fixed amount (3 K) for every month and at every spatial grid point. For the seasonality experiment, I modify the phase and amplitude of the SST forcing by first calculating the phase and amplitude of the annual harmonic of the control SST at each grid point using a Fourier transform and then either shifting the phase or amplifying the amplitude of the first harmonic before performing an inverse Fourier transform.

Alternatively, I could change the seasonality of all harmonics, instead of only the first. I test this effect by comparing two forced simulations differing only in the number of harmonics that are shifted. The difference between the two simulations is small for SST, precipitation and other climate variables. I also tested the effect of changing the seasonality of sea ice in addition to SST. This led to large near-surface air temperature differences at high latitudes, but only small changes in precipitation at low latitudes.

In order to interpret the changes to PC1 as a shift or amplification of the timing of tropical precipitation, I require that the leading EOF pattern of each experiment be similar to that of the control. In the simulations I perform, the EOF patterns are very similar. Figures 3.1(b) and (c) show the EOF1 pattern of precipitation for a phase delay of 15 days and an amplitude increase of 25%, respectively. The effect of the phase of SST on the EOF1 pattern of precipitation is small everywhere. Changing the amplitude of SST has a slightly larger effect on the EOF1 pattern of precipitation – it becomes stronger in some regions and weaker in others. Because the EOF1 patterns are normalized to the same global variance, an increased amplitude of precipitation will be expressed through the amplitude of PC1, not EOF1. I also verify my results by projecting the precipitation data for each forced run onto EOF1 of the control run and find only small differences from the standard method of projecting the precipitation data onto its own EOF1, leaving the conclusions unchanged.

3.3 CMIP5 Results

In response to increased greenhouse gases in the rcp8.5 scenario, most CMIP5 models project not only annual mean increases to tropical temperature and precipitation, but also consistent changes to the seasonality of these quantities. I summarize the tropical CMIP5 changes for ocean and land in Table 3.2. All models predict increases in the annual mean of SST and oceanic precipitation with multimodel mean changes of 2.9 K and 0.2 mm day^{-1}, respectively. There is less agreement among models on the sign of the annual mean change in terrestrial precipitation, which has a multimodel mean increase of 0.1 mm day^{-1}. However, the amplitude increase and phase delay of precipitation are more robust over land than ocean – nearly all models agree on the sign of the changes to the seasonality of land precipitation. (I calculate changes in the annual cycle over land by limiting the EOF in spatial extent. This produces an EOF structure nearly identical to that of Figure 3.1(a), but with all of the power concentrated in land regions. A similar procedure is applied for the ocean.) In the multimodel mean, phase delays are larger over land (3.5 days) than ocean (2.7 days), though the amplitude increases are larger over ocean (15.5%) than land (8.2%). Seasonal changes of SST are weaker than those for precipitation, though most models show an amplitude increase and phase delay.

Figure 3.2 shows the multimodel mean pattern of changes in SST and precipitation. Annual mean surface temperature increases throughout the tropics, especially on land, with the greatest ocean warming occurring on or near the equator (Figure 3.2(a)). Increases in precipitation in the tropical oceans (Figure 3.2(b)) mainly occur in regions with large climatological precipitation (Held and Soden, 2006; Chou and Neelin, 2004), as well as regions that have large increases in SST (Xie et al., 2010; Huang et al., 2013).

The amplitude of surface temperature (Figure 3.2(c)) broadly increases throughout much of the tropics, aside from the Western Pacific. This is in agreement with

	SST		Ocean Precip.		Land Precip.	
Δ Annual Mean	2.9 ± 0.1	(35)	0.2 ± 0.0	(35)	0.1 ± 0.0	(27)
Δ Amplitude [%]	4.2 ± 0.5	(33)	15.5 ± 1.1	(34)	8.2 ± 0.9	(35)
Δ Phase [days]	1.1 ± 0.2	(29)	2.7 ± 0.6	(27)	3.5 ± 0.4	(34)

Table 3.2: Multimodel mean changes in the annual mean, phase, and amplitude over ocean and land in the tropics (25°S–25°N) for the CMIP5 models between 2080–2099 relative to 1980–1999. Seasonal changes were calculated using an EOF analysis confined to either ocean or land. Confidence intervals indicate one standard error of the multimodel mean change and numbers in parentheses indicate the number of models projecting changes of the same sign as the mean for each quantity out of a total of 35 models. Units for the annual mean changes are K for SST and mm day^{-1} for precipitation, amplitude changes are given as a percentage and phase delays are in days.

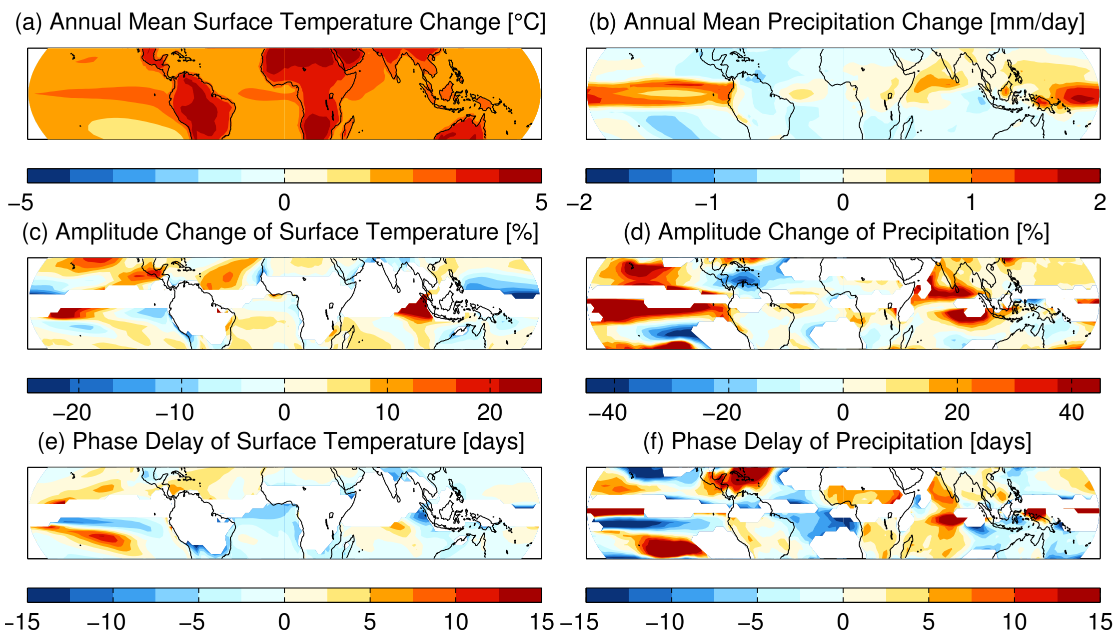

Figure 3.2: The CMIP5 rcp8.5 multimodel mean change between 2080-2099 and 1980-1999 for annual mean temperature (a) and precipitation (b), amplitude change of the annual cycle of temperature (c) and precipitation (d), and phase delay of the annual cycle of temperature (e) and precipitation (f). Any location where the first harmonic makes up less than 80% or 50% of the total variance for temperature and precipitation, respectively, is not shaded. Additionally, for (d) and (f) I only shade grid points that have at least an annual mean precipitation of 1 mm day^{-1}.

the tropical-wide amplitude increase of PC1 (Table 3.2), calculated by performing an EOF analysis over tropical SST (25°S–25°N). Changes in the amplitude of the annual cycle of precipitation, plotted in Figure 3.2(d), are positive along much of the equator, especially in the Western Pacific and Indian Ocean, where the increase in amplitude is above 50%. These changes share some commonalities with the pattern of amplitude changes of SST in Figure 3.2(c) (spatial correlation of 0.36) and to the annual mean SST change in Figure 3.2(a) to a lesser extent (spatial correlation of 0.22). Many land monsoon regions also show increases in the amplitude of the annual cycle of precipitation, indicating an increase of summer precipitation relative to winter precipitation (Biasutti and Sobel, 2009; Seth et al., 2011; Sobel and Camargo, 2011; Seth et al., 2013). The intensification of the annual cycle of precipitation is mostly due to an increase during summer, with a smaller contribution from a reduction during winter (not shown).

The phase of surface temperature (Figure 3.2(e)) delays for much of the NH tropical ocean off the equator, as well as in the Eastern Pacific and Indian Ocean in the SH. While there are some regions of phase advance, the PC1 of tropical SST has a weak phase delay. Precipitation (Figure 3.2(f)) is noisier, with strong regions of phase delay in the Caribbean Sea, Indian Ocean, and Central Pacific and regions of phase advance in the tropical Atlantic and Eastern Pacific. Projected changes of the timing of precipitation in these regions have a larger magnitude than the tropical mean and may have important, local consequences. Overall the PC1 of tropical, oceanic precipitation shows a phase delay (Table 3.2).

I demonstrate the scatter between models in Figure 3.3 which shows the seasonality changes of the zonal mean SST and precipitation for the individual models and the multimodel mean. Amplitude changes of SST (Figure 3.3(a)) are more tightly grouped than those of precipitation (Figure 3.3(b)), though the changes in precipitation are larger. The same is true for the phase delays (Figures 3.3(c) and (d)).

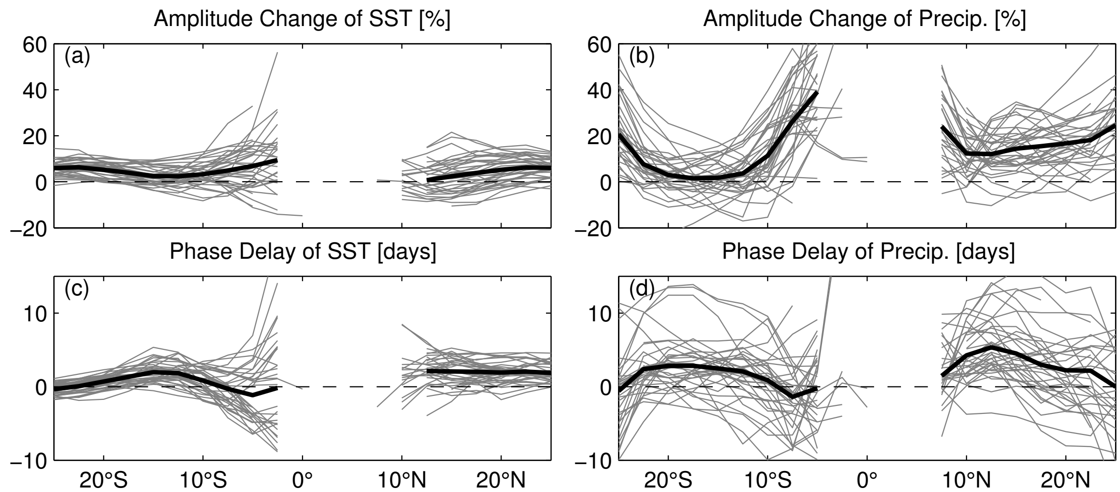

Figure 3.3: Zonal mean changes for the CMIP5 models between 2080–2099 and 1980–1999 for (a) the amplitude of SST, (b) the amplitude of precipitation, (c) the phase of SST, and (d) the phase of precipitation. The thick black line indicates the multimodel mean, and the thin gray lines the individual models. Values were calculated by first zonally averaging (over ocean for SST and over ocean and land for precipitation) and then calculating seasonal characteristics. Seasonal changes are only plotted where the annual harmonic is responsible for at least 85% of the total variance.

To investigate the nature of the seasonal precipitation changes in response to greenhouse gases, I analyze the moisture budget, following and extending previous work (Chou et al., 2007; Tan et al., 2008; Chou and Lan, 2011; Huang et al., 2013). The moisture equation in flux form is

$$\left\langle \vec{\nabla} \cdot (\vec{u}q) \right\rangle = E - P - \left\langle \frac{\partial q}{\partial t} \right\rangle, \tag{3.1}$$

where $\vec{u}$ is the horizontal velocity, q is the specific humidity multiplied by the latent heat of vaporization, E is the evaporation, and P is the precipitation given in units of W m^{-2} (1 mm day^{-1} $\approx$ 28 W m^{-2}). Angle brackets indicate a mass-weighted vertical integration from the surface to the tropopause:

$$\langle A \rangle = \frac{1}{g} \int_{p_{sfc}}^{p_{trop}} A \mathrm{d}p, \tag{3.2}$$

where I use p_{sfc} = 1000 hPa and p_{trop} = 250 hPa for simplicity. Assuming that

$\omega = 0$ at the surface and the tropopause, then $\left\langle \vec{\nabla} \cdot (\vec{u}q) \right\rangle = \left\langle \omega \frac{\partial q}{\partial p} \right\rangle + \left\langle \vec{u} \cdot \vec{\nabla} q \right\rangle$, and the moisture budget can be written as:

$$P = E + \left\langle -\vec{u} \cdot \vec{\nabla} q \right\rangle + \left\langle -\omega \frac{\partial q}{\partial p} \right\rangle - \left\langle \frac{\partial q}{\partial t} \right\rangle . \tag{3.3}$$

I apply this decomposition to monthly data for the historical simulation for 1980–1999 and plot the annual mean, amplitude, and phase of each component in Figure 3.4. In the annual mean, the dominant balance averaged over the tropics is between P and E with a smaller contribution from $\left\langle -\omega \frac{\partial q}{\partial p} \right\rangle$, which becomes substantial in the deep tropics between 10°S and 10°N (Figure 3.4(a)). The sum of the budget terms overestimates P by about 15% when averaged over the tropics, but shows better agreement in the deep tropics. Sub-monthly transients and surface effects likely account for most of this difference (Seager and Henderson, 2013).

I also calculate the annual cycle of the budget. By zonally averaging each term in Equation 3.3 and then calculating the temporal Fourier transform, I obtain the amplitude and phase of the first harmonic of each term in Equation 3.3. I also calculate the phase and amplitude for the sum of the terms on the right hand side of the equation since this is not simply the sum of the phases or the sum of the amplitudes of each term (see Section 3.8). Analyzing the annual cycle of the budget allows for a visualization of the annual cycle with two variables (amplitude and phase) rather than 12 monthly values, and for a concise determination of which term best explains precipitation on seasonal time scales.

I plot the amplitudes of the terms in the moisture budget in Figure 3.4(b). Thick lines are used for each term where the annual harmonic is responsible for at least 85% of the total variance, mostly outside of the deep tropics. The amplitude of precipitation is similar in latitudinal structure to the amplitude of the sum of the terms on the right hand side of the budget but smaller. Because the amplitude of the sum of the terms is very similar to the amplitude of $\left\langle -\omega \frac{\partial q}{\partial p} \right\rangle$, I conclude that the primary balance of A_P is with $A_{\left\langle -\omega \frac{\partial q}{\partial p} \right\rangle}$ – the amplitude of vertical moisture

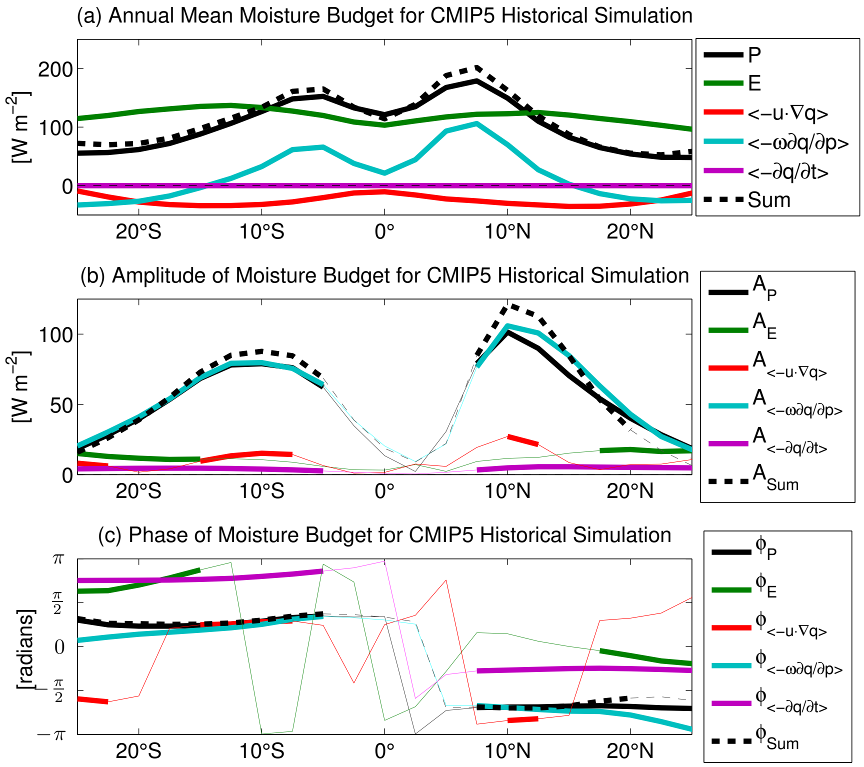

Figure 3.4: Annual mean (a), amplitude (b), and phase (c) of the terms in the moisture budget (Equation 3.3) for the multimodel mean of the CMIP5 simulations. The solid, thick, black line is precipitation and the dashed, thick, black line is the sum of the other terms in the moisture budget. In (c), phases of $\pi/2$ and $-\pi/2$ correspond to maxima in April and October, respectively. Thick lines indicate where the annual harmonic is responsible for at least 85% of the total variance.

advection. These two terms are also in phase throughout the tropics as demonstrated in Figure 3.4(c), indicating that the annual cycles of P and $\left\langle -\omega \frac{\partial q}{\partial p} \right\rangle$ are in balance. The phases of the budget terms (Figure 3.4(c)) also shows that ϕ_P is well described by the phase of the sum of the budget terms, except where the amplitude of the annual cycle is nearly zero. For the CMIP5 models this occurs around 2°N and poleward of around 20°N.

I investigate how A_P, ϕ_P, and other terms change in the rcp8.5 scenario by taking the Fourier transform of Equation 3.3 and solving for A_P and ϕ_P, while neglecting the moisture storage terms as these are of the same order as the residual of the budget. Assuming that the changes for each term between the rcp8.5 and control simulations (averaged over 2080–2099 and 1980–1999, respectively) are sufficiently small, I can write ΔA_P and $\Delta\phi_P$ as linear combinations of perturbations to the amplitudes and phases of each term in Equation 3.3 (see Section 3.8). The contribution of each perturbation term to either ΔA_P or $\Delta\phi_P$ is the product of the perturbation term and a factor that depends on the relative amplitude and phases of the budget terms.

I plot the contribution from each term in Figure 3.5(a). Here the thick lines represent where the changes in the amplitude of the annual cycle of precipitation were statistical different from zero at the 95% level (in this case everywhere), and the $\times$ markers at the bottom of the figure represent where the annual cycle of both precipitation and the sum of the moisture budget terms each capture at least 85% of the total variance. I focus on these regions in the analysis. The solid, black line is the actual amplitude change in precipitation, and the dashed, black line is the sum of the contributions from the perturbations to each term, which will resemble ΔA_P if the decomposition is accurate. ΔA_P is positive throughout the tropics, and is largest near the climatological maxima at 7.5°S and 7.5°N. The sum of perturbations matches ΔA_P well except at 7.5°S and 15°N. The primary contribution to the sum comes from $\Delta A_{\langle -\omega\partial q/\partial p\rangle}$, the changes in the amplitude of the annual cycle of vertical moisture advection – unsurprising since this term dominates the budget in the control simulation (Figure 3.4(b)). Similarly for phase, $\Delta\phi_P$ is well described by the sum of the contributions from the individual terms in the tropics, though $\Delta\phi_P$ is slightly larger than the sum in the NH (Figure 3.5(b)). As before, the thick lines represent where changes in the phase are statistically significant. In the deep tropics, the annual cycle is weak so changes in the phase are neither well-defined nor statistically significant. The largest contribution to balancing $\Delta\phi_P$ comes from $\Delta\phi_{\left\langle -\omega\frac{\partial q}{\partial p}\right\rangle}$, though ΔA_E also plays a role, especially in the SH and around 20°N.

Because of the strong balance in the annual cycle budget between P and $\left\langle -\omega \frac{\partial q}{\partial p} \right\rangle$, it is unsurprising that the changes in the amplitude of precipitation are best explained by similar changes in $A_{\left\langle -\omega \frac{\partial q}{\partial p} \right\rangle}$. To gain insight into what aspect of $\left\langle -\omega \frac{\partial q}{\partial p} \right\rangle$ is changing in the rcp8.5 simulation I can decompose changes in $A_{\left\langle -\omega \frac{\partial q}{\partial p} \right\rangle}$ and $\phi_{\left\langle -\omega \frac{\partial q}{\partial p} \right\rangle}$ into contributions from six different terms: changes in the annual mean, amplitude, and phase of ω and $\partial q / \partial p$ (See Section 3.9 for the full procedure).

First I consider the decomposition of $\Delta A_{\left\langle -\omega \frac{\partial q}{\partial p} \right\rangle}$ and plot the results in Figure 3.5(c). The sum of the decomposition is very similar to $\Delta A_{\left\langle -\omega \frac{\partial q}{\partial p} \right\rangle}$, even where the annual cycle is weak, validating my procedure and the neglect of small terms. For most of the tropics, the dominant contribution is from $\partial \Delta \overline{q} / \partial p$ – an increase in the annual mean vertical gradient of water vapor. This effect is a thermodynamic consequence of the increase in temperature. Because the relative humidity stays roughly constant, the rise in mean temperature increases the moisture (i.e., specific humidity) throughout the troposphere, but especially in the lower atmosphere due to the Clausius-Clapeyron relation. The seasonally varying, ascending branch of the Hadley Cell then converts the enhanced vertical moisture gradient into additional precipitation (Held and Soden, 2006). Because vertical motion in the deep tropics is upward in the summer, the increase in $\partial \overline{q} / \partial p$ results in an increase in A_P.

The other term that significantly affects $\Delta A_{\left\langle -\omega \frac{\partial q}{\partial p} \right\rangle}$ is that due to the change in the amplitude of the circulation. This term contributes negatively to A_P for much of the tropics and partially compensates for the increase of $\partial \Delta \overline{q} / \partial p$. The negative contribution is associated with a reduction in the amplitude of the annual cycle of vertical motion due to some combination of reduced upward motion in summer and reduced subsidence in winter – indicative of a slowdown in the tropical, meridional circulation throughout the annual cycle.

Previous studies have found similar results for changes due to increased green-

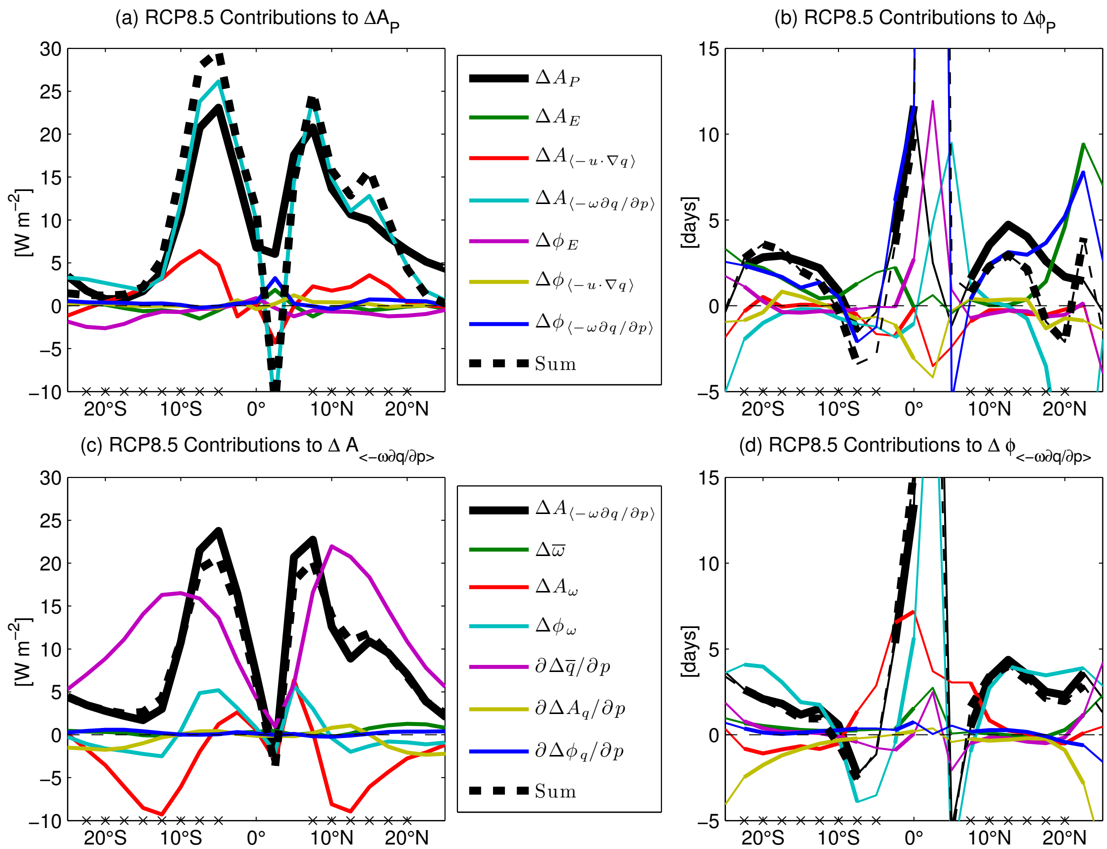

Figure 3.5: Contributions of terms to ΔA_P (a) in the rcp8.5 CMIP5 simulation as well as ΔA_P itself (solid, thick, black line). The contribution of each term is the change in amplitude or phase multiplied by an appropriate factor (see Section 3.8). The sum of the contributions is given by the dashed, thick, black line. As in (a), but for $\Delta\phi_P$ (b). I further decompose $\Delta A_{\langle -\omega \frac{\partial q}{\partial p}\rangle}$ (c) and $\Delta\phi_{\langle -\omega \frac{\partial q}{\partial p}\rangle}$ (d) into changes related to the annual mean, amplitude, and phase of ω and $\partial q/\partial p$. Data is plotted with a thinner line for latitudes at which the changes in the amplitude (a,c) or phase (b,d) are not statistically significant from zero at the 95% level. Latitudes for which the annual harmonics of both precipitation and the sum of the moisture budget terms makes up at least 85% of the total variance are marked with an $\times$.

house gases in the coupled models (Chou et al., 2007; Tan et al., 2008; Chou and Lan, 2011; Huang et al., 2013). In particular, Tan et al. (2008) compared the changes in various terms of the moisture budget in summer and winter months. While they did not decompose changes in $\left\langle -\omega \frac{\partial q}{\partial p} \right\rangle$ into annual mean and seasonal deviations, they found that changes in $\left\langle -\omega \frac{\partial \Delta q}{\partial p} \right\rangle$ drove an increase in summer precipitation in the coupled models with some compensation from $\left\langle -\Delta\omega \frac{\partial q}{\partial p} \right\rangle$. I confirm these results in the CMIP5 models and extend previous studies by analyzing the phase response.

I decompose $\Delta\phi_{\left\langle -\omega \frac{\partial q}{\partial p} \right\rangle}$ into a linear combination of terms, as I did with amplitude, and plot the results in Figure 3.5(d). While $\Delta\phi_{\left\langle -\omega \frac{\partial q}{\partial p} \right\rangle}$ is not solely responsible for the changes in $\Delta\phi_P$, it is the largest contributor to $\Delta\phi_P$. Over the tropics, $\Delta\phi_{\left\langle -\omega \frac{\partial q}{\partial p} \right\rangle}$ is mostly positive and mainly balanced by a phase delay of ω. This result rules out a thermodynamic explanation in terms of the Clausius-Clapeyron relation for the phase delay of precipitation, and indicates the importance of changes in the timing of circulation. The causes of the circulation changes are not yet known.

3.4 Uniform Warming Experiment

To better understand the coupled response I turn to uncoupled simulations in which I can manipulate the SST. I begin by comparing the control, CAM4 AGCM simulation to that of the historical CMIP5 simulations. In the annual mean, the various terms of the moisture budget of the control simulation (Figure 3.6(a)) are similar to their counterparts in the CMIP5 models, except for stronger precipitation and vertical moisture advection in the deep tropics. There is also a larger interhemispheric asymmetry of precipitation and vertical moisture advection in the AGCM compared to the CMIP5 models, perhaps because of an erroneous, double ITCZ in the coupled models (Lin, 2007). The amplitude of the annual cycle in the control simulation (Figure 3.6(b)) is weaker than that in the CMIP5 multimodel mean.

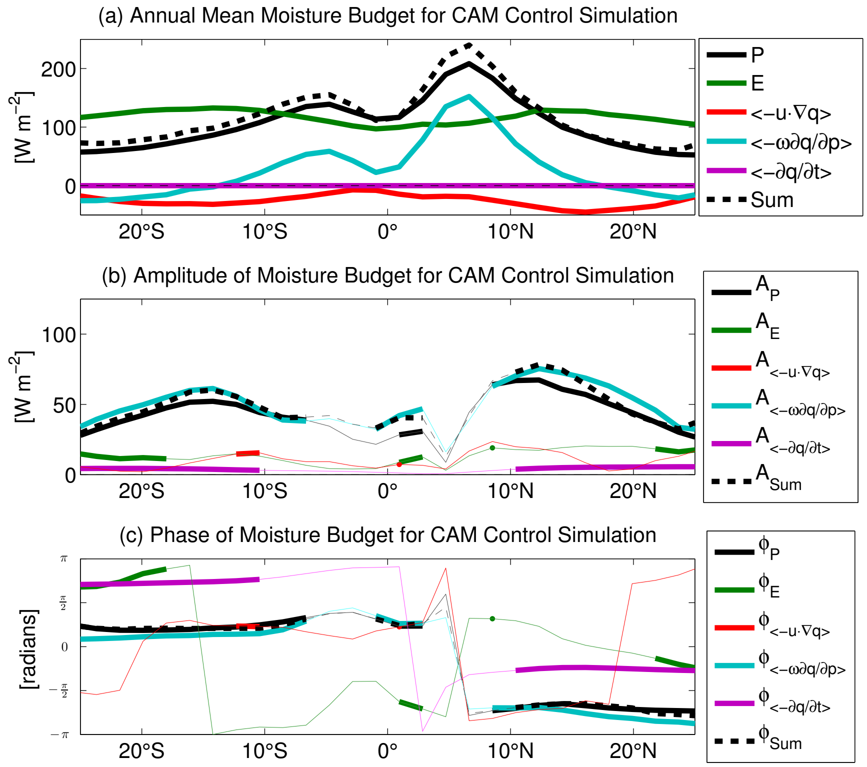

Figure 3.6: As in Figure 3.4, but for the AGCM control simulation for the annual mean (a), amplitude (b), and phase (c) of precipitation.

Although there are two maxima in the amplitude of precipitation, they are weaker and less well-defined than for the CMIP5 models. For both the annual mean and amplitude as well as for the phase (Figure 3.6(c), the sum of the decomposition of budget terms describes the precipitation well, including near the equator and poleward of 20°N, where it failed for the CMIP5 models. A comparison of the control simulations of CAM4 and CCSM4 (the coupled version of the AGCM model and included in the CMIP5 runs) shows nearly the same differences as those between CAM4 and the CMIP5 multimodel mean.

When the uncoupled model is forced with the climatological SST from the historical and rcp8.5 CCSM4 coupled simulations it captures the sign, and approximate magnitude and latitudinal structure of the changes in the seasonality of precipitation and other budget terms as produced by the coupled model (not shown). Differences between the two simulations are likely due to some combination of differences in the atmospheric composition, in the background climate state, the damping effect of coupling on surface fluxes (Chiang and Sobel, 2002; Wu and Kirtman, 2005, 2007; Emanuel and Sobel, 2013), sampling error, and that the CCSM4 is a transient simulation. While these differences prevent precise, quantitative agreement between the coupled and uncoupled GCMs, the overall similarity of the results indicates that the uncoupled model is a useful tool for understanding the changes in the annual cycle in the coupled model.

Next I investigate the effects that a spatially uniform, mean temperature increase has on the seasonal characteristics of precipitation in the UW experiment. I increase the SST by 3 K (Cess et al., 1990), a value almost identical to the increase of 2.9 K in the annual mean, tropical mean SST in the CMIP5 models between the end of the 21st and 20th centuries. As a result of the SST warming, annual mean precipitation increases throughout the tropics and according to the EOF method, the annual cycle of precipitation is amplified by 18.1% and its phase is delayed relative to the control simulation by 5.1 days.

I plot the latitudinal structure of the changes in the amplitude of the annual cycle of precipitation and related budget terms in the UW experiment in Figure 3.7(a). The amplitude of precipitation increases throughout the tropics, with the strongest increase around 15°N. The sum of budget terms, dominated by $\Delta A_{\langle -\omega \frac{\partial q}{\partial p} \rangle}$, agrees with A_P where the annual cycle is strong, though it overestimates the maximum.

The phase changes of precipitation agree well with the sum of the contributions, except poleward of 20° (Figure 3.7(b)) and show a delay at the equator and poleward of 12° in both hemispheres. This delay is statistically significant from zero in the NH, but not in much of the deep tropics or SH as indicated by the thin lines. When calculated via the EOF method over ocean or land in the entire trop-

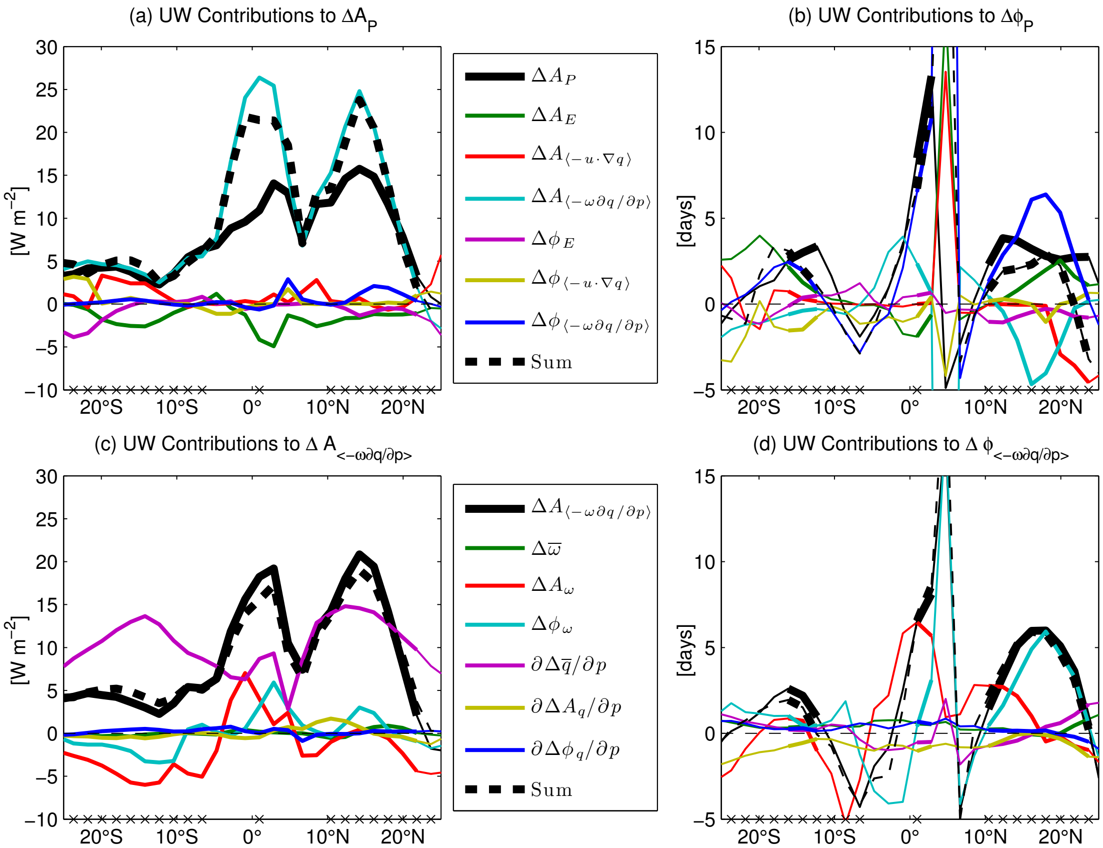

Figure 3.7: As in Figure 3.5, but for the UW simulation. Contributions to (a) ΔA_P, (b) $\Delta\phi_P$, (c) $\Delta A_{\langle -\omega\frac{\partial q}{\partial p}\rangle}$, and (d) $\Delta\phi_{\langle -\omega\frac{\partial q}{\partial p}\rangle}$.

ics, precipitation has a clear, statistically significant phase delay, but is a noisier quantity at individual latitude bands. Still, the latitudinal structure is similar to that of the coupled models (compare to Figure 3.5(b)). As with the CMIP5 models, $\Delta\phi_{\langle -\omega\frac{\partial q}{\partial p}\rangle}$ plays a large role and ΔA_E also contributes. Note that $\Delta A_{\langle -\omega\frac{\partial q}{\partial p}\rangle}$ provides a negative contribution in both hemispheres, especially around 15°N.

Next I decompose the changes in $\Delta A_{\langle -\omega\frac{\partial q}{\partial p}\rangle}$, since this is the primary balance with ΔA_P (Figure 3.7(c)). As with the rcp8.5 CMIP5 models, the primary balance is with $\partial\Delta\overline{q}/\partial p$. The annual mean increase in moisture gradient contributes to the seasonal amplification of precipitation in the same way as in the coupled models. Unlike in the rcp8.5 case, though, the latitudinal structure of these changes is not as symmetric about the equator. Similarly, a decrease in the amplitude of the circulation compensates for some of the increase in $\partial\Delta\overline{q}/\partial p$, but with a weaker and less symmetrical latitudinal structure about the equator than in the rcp8.5 case.

Returning to the budget for the phase changes, I decompose $\Delta\phi_{\langle -\omega\frac{\partial q}{\partial p}\rangle}$ into a linear combination of terms (Figure 3.7(d)). Here the decomposition works very well as the linear combination of decomposed terms is nearly identical to $\Delta\phi_{\langle -\omega\frac{\partial q}{\partial p}\rangle}$. The primary contribution comes from a delay in the phase of circulation, especially in the NH, with a smaller contribution coming from a change in the amplitude of circulation. These changes outweigh a negative contribution to the phase delay of precipitation from $\Delta A_{\langle -\omega\frac{\partial q}{\partial p}\rangle}$, which is mainly the result of the annual mean increase in moisture gradient.

Despite the differences between coupled models with realistic 21st century forcings (including greenhouse gas changes and aerosols) and an AGCM with a uniform SST increase, there is much similarity in their seasonal precipitation responses. Both show an amplification and phase delay in the annual cycle of precipitation in the tropics with similar latitudinal structure. Moreover, the terms that contribute to these seasonal changes are very similar between these simulations, indicating that the same processes may be at work. To summarize, an annual mean, uniform warming in SST causes an amplification of the annual cycle of precipitation mostly through the annual mean change in water vapor combined with the climatological seasonal circulation; it also causes a phase delay that is related to a phase delay in the circulation.

3.5 Modified Seasonality Experiment

In the second set of experiments, I investigate the effect that changing only the seasonal characteristics of SST has on the annual cycle of precipitation. I run seven simulations with amplitude as in the control run and phase shifts varying

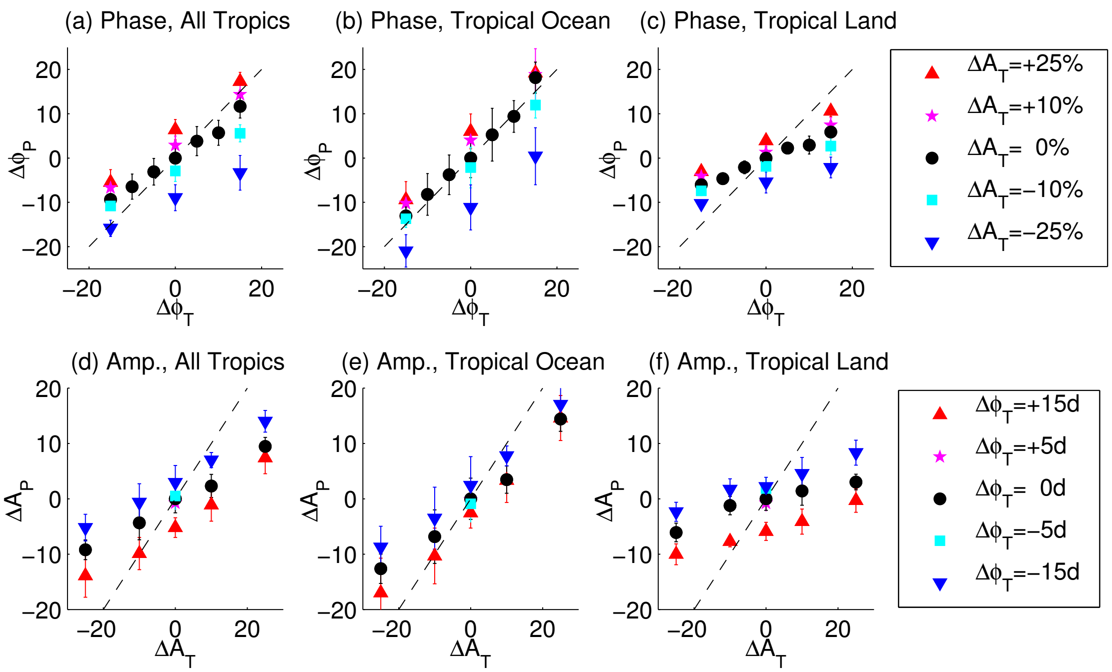

Figure 3.8: Results of AGCM simulations with the seasonality of precipitation as a function of imposed seasonality of SST. I plot the phase of precipitation against the phase of SST for the entire tropics (a), tropical ocean (b), and tropical land (c), with the colors representing the imposed amplitude of SST for each simulation. Similarly, I plot the amplitude of precipitation against the amplitude of SST for the entire tropics (d), tropical ocean (e), and tropical land (f), with colors representing the imposed phase of SST. Error bars represent one standard error.

from a 15 day advance to a 15 day delay (see Section 3.2 for details) and plot the resulting changes in the phase of precipitation as black circles in Figure 3.8(a). The results show that a delayed SST causes delayed precipitation and advanced SST causes advanced precipitation. Moreover, the relationship between the phases of SST and precipitation is linear. This is the case even when the phase perturbations are imposed on simulations with a different amplitude of the annual cycle of SST (colored markers in Figure 3.8(a)).

For all sets of simulations with identical changes in the amplitude of SST, the change in the phase of precipitation is weaker than the imposed change in the phase of SST (the slope of the linear relationship is less than one). This low sensitivity appears to be due to the presence of land. The phase of precipitation in Figure 3.8(a) is calculated from a PC associated with an EOF structure that includes both land and ocean (Figure 3.1). If I perform an EOF analysis with a domain limited to the ocean and calculate the seasonality of precipitation from its PC, the slope is nearly one, as in Figure 3.8(b). Likewise, when I limit the EOF analysis to precipitation over land (Figure 3.8(c)) I find a slope that is close to zero. This is consistent with Biasutti et al. (2003) and Biasutti et al. (2004), who found that the seasonality of precipitation primarily follows SST over ocean, but insolation over land.

As was the case for phase, the change in amplitude of the annual cycle of precipitation is linearly related with a positive slope to the change in amplitude of the annual cycle of SST. Figure 3.8(d) shows the relationship holds for any set of simulations with the same phase of SST and varying amplitudes of SST, though again, the slope is less than one. In this case, limiting the EOF to ocean (Figure 3.8(e)) results in a slightly stronger sensitivity, but with a slope still less than one. I would expect a sensitivity of one if the relationship between SST and tropical, oceanic precipitation were linear. In reality and in GCMs, the relationship between SST and precipitation is more complicated, as precipitation is suppressed in a convectively stable environment.

When I constrain the EOF to land (Figure 3.8(f)), the slope is still greater than zero, but very small. Part of the reason for the shallow slope is because precipitation is positive definite. Near zero winter precipitation is the case in many land-monsoon regions, such as the Sahel, South Asia, Australia, and South Africa. In these regions, anything more than a 10% increase in the amplitude of the annual cycle of precipitation would require an increase in the annual mean or changes in higher harmonics to prevent winter precipitation from becoming negative in the AGCM.

In addition to the direct forcing of phase on phase and amplitude on amplitude, there are cross-effects: the phase of SST affects the amplitude of precipitation and the amplitude of SST changes the phase of precipitation, as illustrated by the spread of the colored markers in Figure 3.8. If I limit the EOF analysis to oceanic precipitation only (Figure 3.8(b) and (e)), the effect remains with about the same magnitude as for the case with global precipitation (Figure 3.8(a) and (d)). The effect is not an artifact of EOF analysis - it also exists when I perform the analysis with a Fourier transform of the data. If oceanic, tropical precipitation were entirely dependent on SST alone, I would not expect these cross-effects.

I interpret these effects as primarily due to the presence of land. Limiting the EOF to ocean does not eliminate the cross-effects because tropical convection can organize on large scales that cover both ocean and land for phenomena like monsoons, inextricably linking the two domains. In this sense, oceanic precipitation is a function of both SST and insolation, the latter of which peaks earlier in the year.

The cross-effects can be understood mathematically by thinking of tropical precipitation P as a linear combination of insolation (I) and SST (T): $P = \sigma I + \tau T$, where σ and τ give the relative strengths of I and T and ensure correct units. By writing this equation in seasonal form as $A_P e^{-i\phi_P} = \sigma A_I + \tau A_T e^{-i\phi_T}$ (where A and ϕ are the amplitude and phase lag from insolation of the annual cycle for the subscripted quantities) and solving for the seasonality of precipitation I find:

$$A_P = \sqrt{\sigma^2 A_I^2 + \tau^2 A_T^2 + 2\sigma\tau A_I A_T \cos\phi_T)} \tag{3.4}$$

$$\phi_P = \arctan\left(\frac{\tau A_T \sin\phi_T}{\tau A_T \cos\phi_T + \sigma A_I}\right). \tag{3.5}$$

Assuming small changes to the phase and amplitude of SST, I can write the resulting changes to the phase and amplitude of precipitation as:

$$\Delta A_P = \Delta A_T \left(\frac{\tau^2 A_T + \tau\sigma A_I \cos\phi_T}{A_P} \right) + \Delta\phi_T \left(\frac{-\tau\sigma A_I A_T \sin\phi_T}{A_P} \right) \quad (3.6)$$

$$\Delta\phi_P = \Delta A_T \left(\frac{\tau\sigma A_I \sin\phi_T}{A_P^2} \right) + \Delta\phi_T \left(\frac{\tau\sigma A_I A_T \cos\phi_T + \tau^2 A_T^2}{A_P^2} \right). \quad (3.7)$$

Since all of the amplitudes and phases are positive and $\phi_T \approx 73$ days for tropically averaged SST, this model gives the expected result that delayed and amplified SST produces delayed and amplified precipitation. The model also predicts the presence of cross-effects with the right signs: a delayed SST leads to a weakened annual cycle of precipitation and an amplified SST leads to a delayed annual cycle of precipitation. The magnitude of these effects depend not only on the various unforced amplitudes and phases, but also on the relative importance of SST and insolation at forcing precipitation.

I also confirm that this is the case by running aquaplanet simulations, which have no land – only an ocean with an imposed seasonally varying SST – and no zonal asymmetries in the boundary conditions. As expected, in the aquaplanet simulations the direct effects are still present: delayed and amplified SST yields delayed and amplified precipitation, respectively. However, the cross-effects are smaller and no longer statistically significant at the 95% level. The effect that the amplitude of SST has on the phase of precipitation is reduced by 60% in the aquaplanet simulations and the effect that the phase of SST has on the amplitude of precipitation is reduced by 85%. Insolation still varies throughout the year, and has a phase-locked annual cycle of shortwave absorption in the atmosphere that may account for the remainder of the cross-effects. But when the effects of land and other zonal asymmetries are totally removed, the cross-effects diminish considerably.

I also repeat the budget analysis that I performed for the CMIP5 and UW simulations for a simulation with a 5-day SST phase delay and a 10% SST amplitude increase (p5a10) and plot the results in Figure 3.9. The chosen values of phase delay and amplitude increase to SST are exaggerated compared to the CMIP5 multimodel mean changes in order to obtain clearer results. In this simulation ΔA_P increases throughout the tropics, but to a lesser degree than in the rcp8.5 and UW simulations. The increase is statistically significant, except in the deep tropics. The sum of the contributions generally agrees with the actual change in ΔA_P, but overestimates the changes near the peaks. As in the other simulations, the primary contribution comes from $\Delta A_{\langle -\omega \frac{\partial q}{\partial p} \rangle}$. The change in the phase of precipitation is positive over the tropics, indicating a delay. Like the UW simulation, it is balanced by $\Delta \phi_{\langle -\omega \frac{\partial q}{\partial p} \rangle}$ (Figure 3.9(b)), but here with greater statistical significance.

When I decompose the changes to $\Delta A_{\langle -\omega \frac{\partial q}{\partial p} \rangle}$ (Figure 3.9(c)), I find that the sole contribution arises from a change in the amplitude of the circulation. In the rcp8.5 and UW simulations, by comparison, most of the change was due to the annual mean increase in moisture gradient, with a negative contribution from a change in the amplitude of circulation. Phase changes in $\left\langle -\omega \frac{\partial q}{\partial p} \right\rangle$ (Figure 3.9(d)), are also balanced by changes in the circulation - in this case mostly from a change in the phase of the circulation and somewhat from a change in the amplitude of ω. In this simulation, the direct effect of the moisture change is unimportant for understanding the changes in the seasonality of precipitation. Instead the seasonal changes of SST are communicated to the precipitation via the circulation.

3.6 Comparison Between AGCM Experiments and CMIP5

To better understand the nature of the seasonal changes in precipitation in the CMIP5 models, I construct a simple, empirical model from the results of the AGCM simulations. For example, since the CMIP5 multimodel mean and the UW simula-

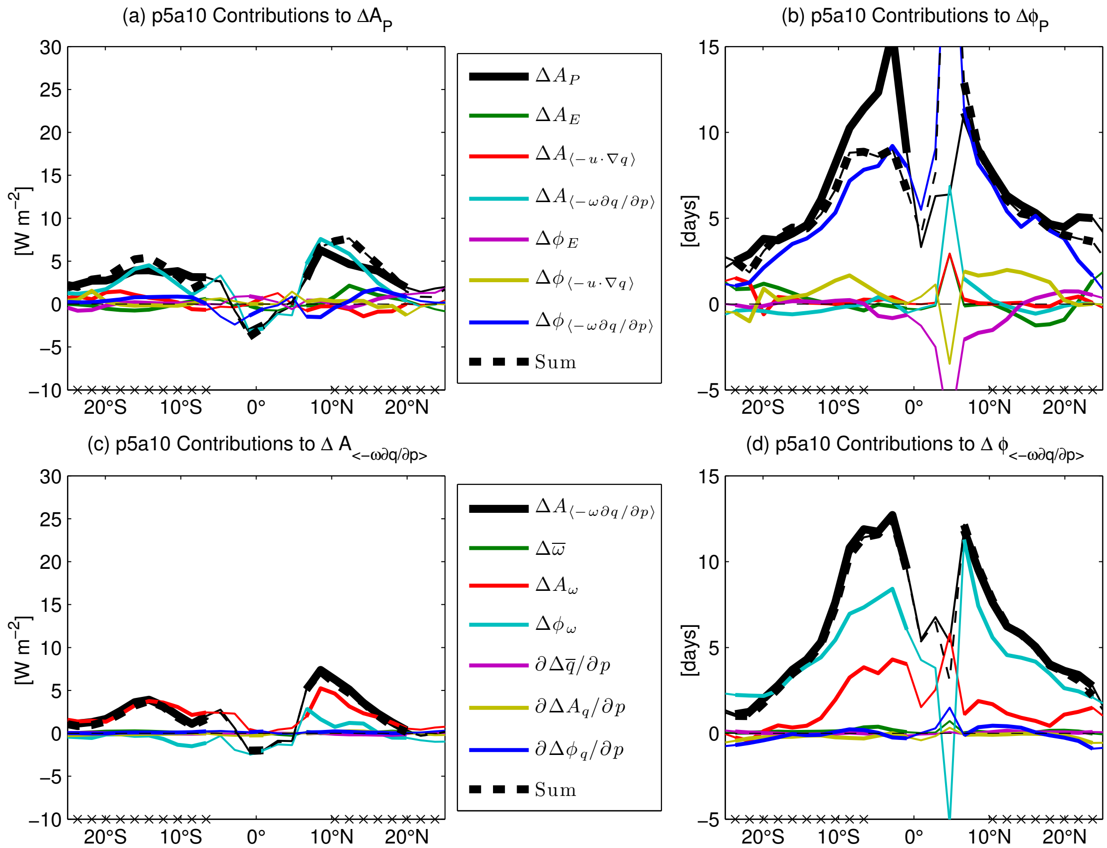

Figure 3.9: As in Figure 3.7, but for the p5a10 experiment. Contributions to (a) ΔA_P, (b) $\Delta\phi_P$, (c) $\Delta A_{\langle -\omega\frac{\partial q}{\partial p}\rangle}$, and (d) $\Delta\phi_{\langle -\omega\frac{\partial q}{\partial p}\rangle}$.

tion both have almost identical mean temperature increases in the tropical average (2.9 K for CMIP5 and 3 K for the UW simulation), I can determine the amplitude and phase change in precipitation in the CMIP5 models due to an annual mean warming by using the results of the UW simulation. Because I know the change in the amplitude of temperature in the CMIP5 models and the sensitivity of changes in the amplitude of precipitation to changes in the amplitude of SST (the slope of the black dots in Figure 3.8(d)), their product is the change of the amplitude of precipitation in the CMIP5 models due to ΔA_T. Similarly, I can repeat this for phase as well as for the cross-effects (the effect of $\Delta\phi_T$ on ΔA_P and ΔA_T on $\Delta\phi_P$).

I express the model mathematically as

$$\begin{bmatrix} \Delta A_P \\ \Delta \phi_P \end{bmatrix} = \begin{bmatrix} C_{A_P,A_{SST}} & C_{A_P,\phi_{SST}} & C_{A_P,\overline{SST}} \\ C_{\phi_P,A_{SST}} & C_{\phi_P,\phi_{SST}} & C_{\phi_P,\overline{SST}} \end{bmatrix} \begin{bmatrix} \Delta A_{SST} \\ \Delta \phi_{SST} \\ \Delta \overline{SST} \end{bmatrix}, \tag{3.8}$$

where, for example, $C_{A_P,A_{SST}}$ represents the change of the amplitude of precipitation due to the change in the amplitude of SST as derived from the AGCM simulations. The changes in the SST are taken from the CMIP5 models and when multiplied by the appropriate coefficients yield the calculated changes in the amplitude and phase of precipitation in the CMIP5 models.

There are some significant caveats to this method. I am using a model without an interactive ocean to interpret results from models with interactive oceans. This ignores any possibility that changes in the atmosphere may feed back on the seasonality of SST. It is possible that changes in the seasonality of SST are a consequence of changes in the seasonality of precipitation and not the other way around in the CMIP5 models. Additionally, there are differences between coupled and uncoupled versions of the same model even with the same SST. These differences suggest that the while useful, the AGCM is an imperfect tool to understand the GCM changes. Finally, I am not imposing the actual spatial pattern of annual mean or annual cycle changes of SST in the AGCM. Instead I impose a uniform change across the tropical oceans and calculate the results for the tropics as a whole.

I list the results in Table 3.3 for both ocean and land. Each entry in the table is the product of the change in SST multiplied by the appropriate coefficient in Equation 3.8. For ocean, around 90% of the contribution to ΔA_P comes from the annual mean increase of SST, with around 10% from the increase in ΔA_T and a small negative contribution due to the cross-effect of $\Delta \phi_T$. As a whole, these contributions outweigh the actual measured increase in ΔA_P by around 30%. Similarly, for $\Delta \phi_P$ the largest contribution (5.1 days) is from the annual mean SST increase, while

	Ocean		Land	
	Calc. A_P	Calc. ϕ_P	Calc. A_P	Calc. ϕ_P
$\Delta\overline{SST}_{CMIP5} = 2.9$ K	18.1 ± 0.6%	5.1 ± 0.2 d	6.3 ± 0.3%	1.6 ± 0.1 d
$\Delta A_{SST,CMIP5}$=4.2%	2.4 ± 0.3%	1.4 ± 0.2 d	0.8 ± 0.1%	0.8 ± 0.1 d
$\Delta\phi_{SST,CMIP5} = 1.1$ days	-0.1 ± 0.0%	1.0 ± 0.2 d	-0.3 ± 0.0%	0.4 ± 0.1 d
Total Calculated	20.4 ± 0.8%	7.4 ± 0.3 d	6.8 ± 0.3%	2.8 ± 0.1 d
Actual CMIP5	15.5 ± 1.1%	2.7 ± 0.6 d	8.2 ± 0.9%	3.5 ± 0.4 d

Table 3.3: Calculated changes in amplitude and phase in precipitation for both ocean and land given changes in the annual mean and annual cycle of SST in the CMIP5 models. I used the UW simulation to calculate the sensitivity of the amplitude and phase of precipitation to changes due to an annual mean SST increase and the sensitivity of the modified seasonality experiments to calculate the changes due to a phase or amplitude change of SST. Total calculated changes are the sum of the individual contributions. Actually CMIP5 changes are taken from Table 3.2. Confidence intervals represent one standard error of the multimodel mean CMIP5 projections.

ΔA_T contributes 1.4 days and $\Delta\phi_T$ contributes only 1.0 days. Even though phase changes in precipitation are sensitive to phase changes in temperature, the phase delay of SST in CMIP5 is only 1.1 days, resulting in a relatively weak contribution to the phase delay of precipitation. Again the total changes constructed by this empirical model are larger than the actual CMIP5 changes, here by over a factor of 2–3.

Over land the results are similar, though each term is smaller than over ocean. As a result the sum of the inferred changes for ΔA_P is 6.8%, very similar to the actual value for CMIP5 of 8.2%. For $\Delta\phi_P$, the sum of the contributions actually underestimates the total (2.8 days compared to 3.5 days). The better agreement over land compared to ocean suggests that coupling to a thermodynamically interactive lower boundary may be important. In the simulations, the land temperature is interactive, satisfying a consistent surface energy budget, while the ocean temperature is not. An interactive ocean mixed layer can respond locally to large-scale atmospheric influences in such a way as to mute or otherwise substantially alter the precipitation response compared to what would occur over an ocean surface with fixed SST (e.g., Chiang and Sobel (2002); Wu and Kirtman (2005, 2007); Emanuel and Sobel (2013)).

Much of this study has focused on precipitation changes over ocean. Nevertheless, Table 3.2 indicates that the delays in the phase of precipitation are not only larger but also more robust over tropical land than over tropical ocean – 34 of the 35 models project a phase delay over tropical land. Thus I now consider how the seasonality changes manifest over land in the idealized simulations and how they compare to changes in CMIP5 and those reported in the literature (Biasutti and Sobel, 2009; Seth et al., 2011, 2013).

The forced simulations produce similar changes in land monsoon regions to those of CMIP5. Specifically the UW simulation and the p5a10 simulation each show an amplification and phase delay in the annual cycle of precipitation in NH land monsoon regions, defined by averaging over land and over longitudes as in Seth et al. (2011).

Figures 3.10(a) and (b) show the CAM4 climatological precipitation (contour lines) and the percentage change in precipitation in the UW experiment (shading) for NH and SH monsoon regions, respectively. In both hemispheres the peak rainy season gets wetter, amplifying the annual cycle of precipitation. Additionally, an early season deficit and a late season excess of rain produce a phase delay. For the p5a10 simulation (Figure 3.10(c) and (d)), the amplitude increase is milder than in the UW simulation, but the phase delay is of similar strength. The structure of the changes in both simulations bear much similarity, especially at the beginning and the end of the monsoon season, despite the different nature of the imposed changes in SST between simulations.

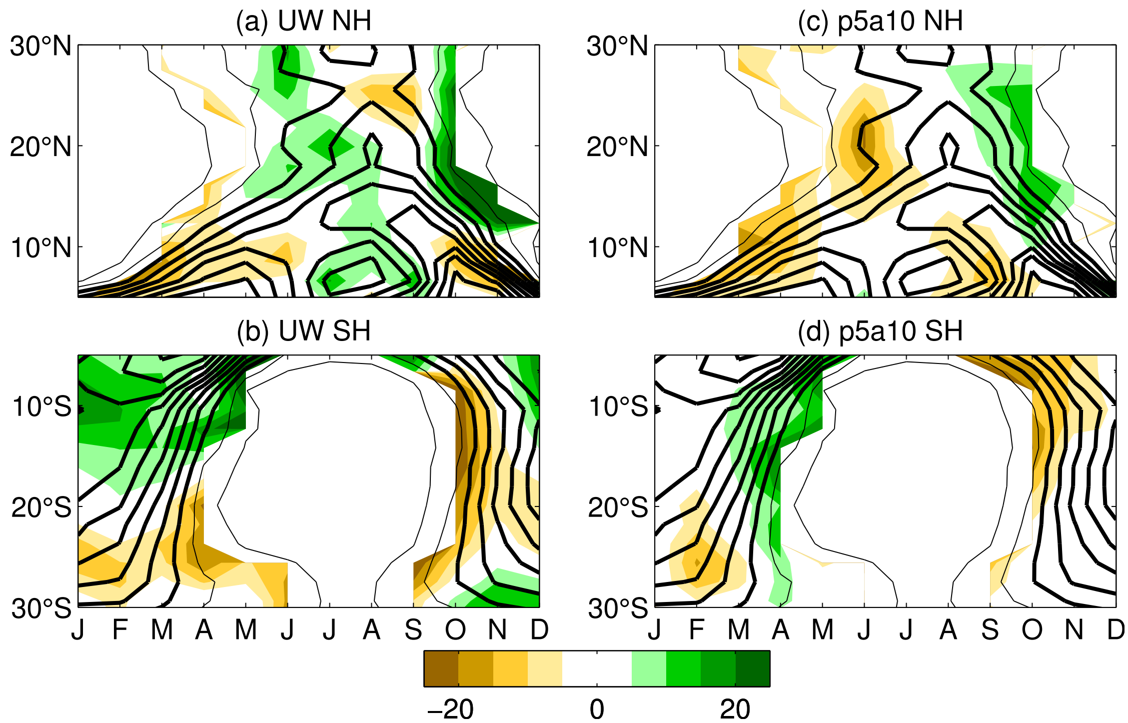

Figure 3.10: Precipitation in land monsoon regions as a function of season and latitude in the control run (contour lines) and the percentage change (shading) for the UW simulation (a, b) and for the p5a10 simulation (c, d). In computing precipitation for NH monsoons (a, c) and SH monsoons (b, d), ocean has been masked out. Contour lines are at 1 mm day^{-1} intervals with thick contours representing precipitation of at least 3 mm day^{-1}. The precipitation change is not shown for regions where the precipitation in the control run is less than 1 mm day^{-1}.

3.7 Conclusions

I have studied the annual mean and seasonal response of tropical surface temperature and precipitation in the CMIP5 models to additional radiative forcing specified by the rcp8.5 scenario. I found, in addition to annual mean increases of SST and oceanic precipitation, and consistent with past studies, that the amplitudes of the annual cycles of SST and oceanic precipitation increased by 4.2% and 15.5% and that the phases were delayed by 1.1 days and 2.7 days, respectively.

From an analysis of the CMIP5 moisture budget I corroborate the work of previous studies (Tan et al., 2008; Huang et al., 2013) that found that the coupled model response of the amplitude of P is the result of an increase in the annual mean vertical moisture gradient due to the Clausius-Clapeyron relation. This additional water vapor is vertically advected in the summer months by the ascending branch of the Hadley Cell. There is also a negative contribution to the amplitude of precipitation from a decrease in the amplitude of the annual cycle of vertical motion, consistent with a weakening of tropical circulation. I also find the delay in the phase of precipitation is mostly balanced by a delay in the phase of the tropical circulation, though other terms like an increase in the amplitude of evaporation also contribute.

To better understand the precipitation response, I performed simulations with an AGCM forced by changes in the annual mean and annual cycle of SST. Increasing the annual mean SST everywhere by 3 K in the UW simulation caused not only an increase in annual mean tropical precipitation, but also an amplification and a phase delay of the annual cycle of precipitation. I obtained seasonal precipitation changes of the same sign, albeit smaller, from the p5a10 simulation in which I left the mean value of SST unchanged, but amplified the annual cycle of SST by 10% and delayed it by 5 days. The changes in the CMIP5 models are better reproduced in the UW simulation than in the p5a10 simulation. A uniform SST warming produces amplitude changes in precipitation that are primarily balanced by an increase in the annual mean vertical gradient of moisture, just as in the coupled models. The p5a10 simulation, on the other hand, produces a weaker amplitude change (despite exaggerated forcing) that is due to an enhanced circulation rather than thermodynamic effects. Additionally, the magnitude and latitudinal structure of phase changes is more similar to the UW simulation than to the p5a10 simulation.

Because so many of the models have an amplification and delay in the annual cycle of precipitation, the mechanism responsible for this behavior is likely simple. The amplitude response can be explained by well-studied mechanisms: the increase in annual mean, vertical moisture gradient due to Clausius-Clapeyron and the slowdown in the circulation (Held and Soden, 2006; Vecchi et al., 2006) (though here the slowdown is in the annual cycle and the Hadley Cell, not the Walker Cell). The phase response of precipitation is associated with a phase delay in the circulation. While I can rule out the possibility that the phase delay is a simple Clausius-Clapeyron response, I do not yet have a full explanation of the mechanism behind the delay.

The simulations in which I varied the phase and amplitude of SST demonstrated that seasonal changes to SST force seasonal changes in tropical precipitation of the same sign, i.e., delayed SST causes delayed precipitation and amplified SST causes amplified precipitation. These changes are communicated effectively by seasonal changes to the tropical circulation. These effects are not limited to ocean, either. Land monsoon regions are sensitive to the seasonal characteristics of SST in the same way as the ocean. Land is also responsible for cross-effects: changes to the phase of SST affect the amplitude of precipitation and changes to the amplitude of SST affect the phase of precipitation.

These AGCM simulations help inform our understanding of the nature of the seasonal changes in the GCMs. Though the lack of atmosphere-ocean coupling, a realistic spatial pattern of SST changes, and identical atmospheric forcing agents in the AGCM preclude exact quantitative agreement with the GCMs, the AGCM simulations indicate that an annual mean SST change is sufficient to induce most of the amplitude increase and phase delay in the annual cycle of precipitation in the GCMs. An important corollary of this result is that the seasonal changes in SST alone are not wholly responsible for the seasonal changes in precipitation in the CMIP5 ensemble.

3.8 Appendix: Decomposition of Changes to the Moisture Budget

In this section I detail the procedure for expanding changes in the amplitude or phase of precipitation in terms of the amplitude or phase of evaporation, horizontal moisture advection, and vertical moisture advection. I begin by taking the Fourier transform of Equation 3.3 and neglecting the moisture storage term.

$$A_P e^{-i\phi_P} = A_E e^{-i\phi_E} + A_{\left\langle -\vec{u}\cdot\vec{\nabla}q \right\rangle} e^{-i\phi_{\left\langle -\vec{u}\cdot\vec{\nabla}q \right\rangle}} + A_{\left\langle -\omega\frac{\partial q}{\partial p} \right\rangle} e^{-i\phi_{\left\langle -\omega\frac{\partial q}{\partial p} \right\rangle}} \tag{3.9}$$

Solving this equation for the amplitude and phase of precipitation gives

$$\begin{aligned} A_P^2 =& A_E^2 + A_{\left\langle -\vec{u}\cdot\vec{\nabla}q \right\rangle}^2 + A_{\left\langle -\omega\frac{\partial q}{\partial p} \right\rangle}^2 + 2A_E A_{\left\langle -\vec{u}\cdot\vec{\nabla}q \right\rangle} \cos\left(\phi_E - \phi_{\left\langle -\vec{u}\cdot\vec{\nabla}q \right\rangle}\right) \\ &+ 2A_E A_{\left\langle -\omega\frac{\partial q}{\partial p} \right\rangle} \cos\left(\phi_E - \phi_{\left\langle -\omega\frac{\partial q}{\partial p} \right\rangle}\right) \\ &+ 2A_{\left\langle -\vec{u}\cdot\vec{\nabla}q \right\rangle} A_{\left\langle -\omega\frac{\partial q}{\partial p} \right\rangle} \cos\left(\phi_{\left\langle -\vec{u}\cdot\vec{\nabla}q \right\rangle} - \phi_{\left\langle -\omega\frac{\partial q}{\partial p} \right\rangle}\right) \end{aligned} \tag{3.10}$$

$$\tan\phi_P = \frac{A_E \sin\phi_E + A_{\left\langle -\vec{u}\cdot\vec{\nabla}q \right\rangle} \sin\phi_{\left\langle -\vec{u}\cdot\vec{\nabla}q \right\rangle} + A_{\left\langle -\omega\frac{\partial q}{\partial p} \right\rangle} \sin\phi_{\left\langle -\omega\frac{\partial q}{\partial p} \right\rangle}}{A_E \cos\phi_E + A_{\left\langle -\vec{u}\cdot\vec{\nabla}q \right\rangle} \cos\phi_{\left\langle -\vec{u}\cdot\vec{\nabla}q \right\rangle} + A_{\left\langle -\omega\frac{\partial q}{\partial p} \right\rangle} \cos\phi_{\left\langle -\omega\frac{\partial q}{\partial p} \right\rangle}}. \tag{3.11}$$

Applying a small perturbation to Equations 3.10 and 3.11 and neglecting 2nd order terms results in a linear combination of perturbations to the phases and amplitudes of the budget terms.

$$\Delta A_P = \frac{1}{A_P} \times$$

$$\begin{bmatrix} A_E + A_{\left\langle -\vec{u}\cdot\vec{\nabla}q \right\rangle} \cos\left(\phi_E - \phi_{\left\langle -\vec{u}\cdot\vec{\nabla}q \right\rangle}\right) + A_{\left\langle -\omega\frac{\partial q}{\partial p} \right\rangle} \cos\left(\phi_E - \phi_{\left\langle -\omega\frac{\partial q}{\partial p} \right\rangle}\right) \\ A_{\left\langle -\vec{u}\cdot\vec{\nabla}q \right\rangle} + A_E \cos\left(\phi_{\left\langle -\vec{u}\cdot\vec{\nabla}q \right\rangle} - \phi_E\right) + A_{\left\langle -\omega\frac{\partial q}{\partial p} \right\rangle} \cos\left(\phi_{\left\langle -\vec{u}\cdot\vec{\nabla}q \right\rangle} - \phi_{\left\langle -\omega\frac{\partial q}{\partial p} \right\rangle}\right) \\ A_{\left\langle -\omega\frac{\partial q}{\partial p} \right\rangle} + A_E \cos\left(\phi_{\left\langle -\omega\frac{\partial q}{\partial p} \right\rangle} - \phi_E\right) + A_{\left\langle -\vec{u}\cdot\vec{\nabla}q \right\rangle} \cos\left(\phi_{\left\langle -\omega\frac{\partial q}{\partial p} \right\rangle} - \phi_{\left\langle -\vec{u}\cdot\vec{\nabla}q \right\rangle}\right) \\ -A_E \left[A_{\left\langle -\vec{u}\cdot\vec{\nabla}q \right\rangle} \sin\left(\phi_E - \phi_{\left\langle -\vec{u}\cdot\vec{\nabla}q \right\rangle}\right) - A_{\left\langle -\omega\frac{\partial q}{\partial p} \right\rangle} \sin\left(\phi_E - \phi_{\left\langle -\omega\frac{\partial q}{\partial p} \right\rangle}\right)\right] \\ -A_{\left\langle -\vec{u}\cdot\vec{\nabla}q \right\rangle} \left[A_E \sin\left(\phi_{\left\langle -\vec{u}\cdot\vec{\nabla}q \right\rangle} - \phi_E\right) - A_{\left\langle -\omega\frac{\partial q}{\partial p} \right\rangle} \sin\left(\phi_{\left\langle -\vec{u}\cdot\vec{\nabla}q \right\rangle} - \phi_{\left\langle -\omega\frac{\partial q}{\partial p} \right\rangle}\right)\right] \\ -A_{\left\langle -\omega\frac{\partial q}{\partial p} \right\rangle} \left[A_E \sin\left(\phi_{\left\langle -\omega\frac{\partial q}{\partial p} \right\rangle} - \phi_E\right) - A_{\left\langle -\vec{u}\cdot\vec{\nabla}q \right\rangle} \sin\left(\phi_{\left\langle -\omega\frac{\partial q}{\partial p} \right\rangle} - \phi_{\left\langle -\vec{u}\cdot\vec{\nabla}q \right\rangle}\right)\right] \end{bmatrix}^\top \times$$

$$\begin{bmatrix} \Delta A_E \\ \Delta A_{\left\langle -\vec{u}\cdot\vec{\nabla}q \right\rangle} \\ \Delta A_{\left\langle -\omega\frac{\partial q}{\partial p} \right\rangle} \\ \Delta \phi_E \\ \Delta \phi_{\left\langle -\vec{u}\cdot\vec{\nabla}q \right\rangle} \\ \Delta \phi_{\left\langle -\omega\frac{\partial q}{\partial p} \right\rangle} \end{bmatrix} \tag{3.12}$$

$$
\Delta\phi_P = \frac{\cos^2\phi_P}{\left(A_E\cos\phi_E + A_{\left\langle -\vec{u}\cdot\vec{\nabla}q\right\rangle}\cos\phi_{\left\langle -\vec{u}\cdot\vec{\nabla}q\right\rangle} + A_{\left\langle -\omega\frac{\partial q}{\partial p}\right\rangle}\cos\phi_{\left\langle -\omega\frac{\partial q}{\partial p}\right\rangle}\right)^2}\times
$$

$$
\begin{bmatrix}
A_{\left\langle -\vec{u}\cdot\vec{\nabla}q\right\rangle}\sin\left(\phi_E - \phi_{\left\langle -\vec{u}\cdot\vec{\nabla}q\right\rangle}\right) + A_{\left\langle -\omega\frac{\partial q}{\partial p}\right\rangle}\sin\left(\phi_E - \phi_{\left\langle -\omega\frac{\partial q}{\partial p}\right\rangle}\right) \\
A_E\sin\left(\phi_{\left\langle -\vec{u}\cdot\vec{\nabla}q\right\rangle} - \phi_E\right) + A_{\left\langle -\omega\frac{\partial q}{\partial p}\right\rangle}\sin\left(\phi_{\left\langle -\vec{u}\cdot\vec{\nabla}q\right\rangle} - \phi_{\left\langle -\omega\frac{\partial q}{\partial p}\right\rangle}\right) \\
A_E\sin\left(\phi_{\left\langle -\omega\frac{\partial q}{\partial p}\right\rangle} - \phi_E\right) + A_{\left\langle -\vec{u}\cdot\vec{\nabla}q\right\rangle}\sin\left(\phi_{\left\langle -\omega\frac{\partial q}{\partial p}\right\rangle} - \phi_{\left\langle -\vec{u}\cdot\vec{\nabla}q\right\rangle}\right) \\
A_E^2 + A_E A_{\left\langle -\vec{u}\cdot\vec{\nabla}q\right\rangle}\cos\left(\phi_E - \phi_{\left\langle -\vec{u}\cdot\vec{\nabla}q\right\rangle}\right) + \\
A_E A_{\left\langle -\omega\frac{\partial q}{\partial p}\right\rangle}\cos\left(\phi_E - \phi_{\left\langle -\omega\frac{\partial q}{\partial p}\right\rangle}\right) \\
A^2_{\left\langle -\vec{u}\cdot\vec{\nabla}q\right\rangle} + A_{\left\langle -\vec{u}\cdot\vec{\nabla}q\right\rangle}A_E\cos\left(\phi_{\left\langle -\vec{u}\cdot\vec{\nabla}q\right\rangle} - \phi_E\right) + \\
A_{\left\langle -\vec{u}\cdot\vec{\nabla}q\right\rangle}A_{\left\langle -\omega\frac{\partial q}{\partial p}\right\rangle}\cos\left(\phi_{\left\langle -\vec{u}\cdot\vec{\nabla}q\right\rangle} - \phi_{\left\langle -\omega\frac{\partial q}{\partial p}\right\rangle}\right) \\
A^2_{\left\langle -\omega\frac{\partial q}{\partial p}\right\rangle} + A_{\left\langle -\omega\frac{\partial q}{\partial p}\right\rangle}A_E\cos\left(\phi_{\left\langle -\omega\frac{\partial q}{\partial p}\right\rangle} - \phi_E\right) + \\
A_{\left\langle -\omega\frac{\partial q}{\partial p}\right\rangle}A_{\left\langle -\vec{u}\cdot\vec{\nabla}q\right\rangle}\cos\left(\phi_{\left\langle -\omega\frac{\partial q}{\partial p}\right\rangle} - \phi_{\left\langle -\vec{u}\cdot\vec{\nabla}q\right\rangle}\right)
\end{bmatrix}^{\top} \times \tag{3.13}
$$

$$
\begin{bmatrix}
\Delta A_E \\
\Delta A_{\left\langle -\vec{u}\cdot\vec{\nabla}q\right\rangle} \\
\Delta A_{\left\langle -\omega\frac{\partial q}{\partial p}\right\rangle} \\
\Delta\phi_E \\
\Delta\phi_{\left\langle -\vec{u}\cdot\vec{\nabla}q\right\rangle} \\
\Delta\phi_{\left\langle -\omega\frac{\partial q}{\partial p}\right\rangle}
\end{bmatrix}
$$

3.9 Appendix: Decomposition of the Vertical Moisture Advection Term

Below I decompose $A_{\left\langle -\omega\frac{\partial q}{\partial p}\right\rangle}$ and $\phi_{\left\langle -\omega\frac{\partial q}{\partial p}\right\rangle}$ into changes in the annual mean, amplitude, and phase of ω and $\frac{\partial q}{\partial p}$. I begin by separating the annual mean and deviations from the annual mean

$$\left\langle \omega \frac{\partial q}{\partial p} \right\rangle = \left\langle (\overline{\omega} + \omega') \left(\frac{\partial \overline{q}}{\partial p} + \frac{\partial q'}{\partial p} \right) \right\rangle, \tag{3.14}$$

where the overline indicates an annual mean and the prime indicates a deviation from the annual mean. I expand around small changes to this expression

$$\begin{aligned} \Delta \left\langle \omega \frac{\partial q}{\partial p} \right\rangle = & \left\langle \Delta\overline{\omega} \frac{\partial \overline{q}}{\partial p} + \overline{\omega} \frac{\partial \Delta\overline{q}}{\partial p} + \Delta\overline{\omega} \frac{\partial q'}{\partial p} + \overline{\omega} \frac{\partial \Delta q'}{\partial p} \right\rangle + \\ & \left\langle \Delta\omega' \frac{\partial \overline{q}}{\partial p} + \omega' \frac{\partial \Delta\overline{q}}{\partial p} + \Delta\omega' \frac{\partial q'}{\partial p} + \omega' \frac{\partial \Delta q'}{\partial p} \right\rangle, \end{aligned} \tag{3.15}$$

where I have neglected second order terms, an assumption that I will show is valid momentarily. Next I take the Fourier transform of this equation, as indicated by curly braces:

$$\left\{ \Delta \left\langle \omega \frac{\partial q}{\partial p} \right\rangle \right\} = \left\langle \Delta\overline{\omega} \frac{\partial \{q'\}}{\partial p} \right\rangle + \left\langle \overline{\omega} \frac{\partial \{\Delta q'\}}{\partial p} \right\rangle + \left\langle \{\Delta\omega'\} \frac{\partial \overline{q}}{\partial p} \right\rangle + \left\langle \{\omega'\} \frac{\partial \Delta\overline{q}}{\partial p} \right\rangle. \tag{3.16}$$

I have neglected the first two and last two terms of Equation 3.15, the former because the annual mean does not project onto the annual cycle, and the latter because the product of the two terms, each of which has its maximal variance at the annual harmonic, has its maximum variance at the semi-annual harmonic. To determine the exact contribution of the phases and amplitudes of the terms in Equation 3.16 I perform a similar procedure as before to decompose the effects as a linear combination of perturbation terms. By taking the Fourier transform of

Equation 3.16, I obtain

$$\left(\Delta A_{\left\langle -\omega\frac{\partial q}{\partial p}\right\rangle} - iA_{\left\langle -\omega\frac{\partial q}{\partial p}\right\rangle}\Delta\phi_{\left\langle -\omega\frac{\partial q}{\partial p}\right\rangle}\right)e^{-i\phi_{\left\langle -\omega\frac{\partial q}{\partial p}\right\rangle}} = \tag{3.17}$$
$$\left(\Delta A_{\left\langle -\Delta\overline{\omega}\frac{\partial\{q'\}}{\partial p}\right\rangle} - iA_{\left\langle -\Delta\overline{\omega}\frac{\partial\{q'\}}{\partial p}\right\rangle}\Delta\phi_{\left\langle -\Delta\overline{\omega}\frac{\partial\{q'\}}{\partial p}\right\rangle}\right)e^{-i\phi_{\left\langle -\Delta\overline{\omega}\frac{\partial\{q'\}}{\partial p}\right\rangle}}$$
$$+\left(\Delta A_{\left\langle -\overline{\omega}\frac{\partial\{\Delta q'\}}{\partial p}\right\rangle} - iA_{\left\langle -\overline{\omega}\frac{\partial\{\Delta q'\}}{\partial p}\right\rangle}\Delta\phi_{\left\langle -\overline{\omega}\frac{\partial\{\Delta q'\}}{\partial p}\right\rangle}\right)e^{-i\phi_{\left\langle -\overline{\omega}\frac{\partial\{\Delta q'\}}{\partial p}\right\rangle}}$$
$$+\left(\Delta A_{\left\langle -\{\Delta\omega'\}\frac{\partial\overline{q}}{\partial p}\right\rangle} - iA_{\left\langle -\{\Delta\omega'\}\frac{\partial\overline{q}}{\partial p}\right\rangle}\Delta\phi_{\left\langle -\{\Delta\omega'\}\frac{\partial\overline{q}}{\partial p}\right\rangle}\right)e^{-i\phi_{\left\langle -\{\Delta\omega'\}\frac{\partial\overline{q}}{\partial p}\right\rangle}}$$
$$+\left(\Delta A_{\left\langle -\{\omega'\}\frac{\partial\Delta\overline{q}}{\partial p}\right\rangle} - iA_{\left\langle -\{\omega'\}\frac{\partial\Delta\overline{q}}{\partial p}\right\rangle}\Delta\phi_{\left\langle -\{\omega'\}\frac{\partial\Delta\overline{q}}{\partial p}\right\rangle}\right)e^{-i\phi_{\left\langle -\{\omega'\}\frac{\partial\Delta\overline{q}}{\partial p}\right\rangle}}$$

Where, for example, $\Delta A_{\left\langle -\Delta\overline{\omega}\frac{\partial\{q'\}}{\partial p}\right\rangle}$ represents the change in amplitude of $\left\langle -\Delta\overline{\omega}\frac{\partial\{q'\}}{\partial p}\right\rangle$ due to a change in the annual mean of ω. Because $\Delta\overline{\omega}$ in $\left\langle -\Delta\overline{\omega}\frac{\partial\{q'\}}{\partial p}\right\rangle$ is multiplied by the vertical moisture gradient at each level and vertically integrated, changes in $\overline{\omega}$ can alter the amplitude or phase of $\left\langle -\Delta\overline{\omega}\frac{\partial\{q'\}}{\partial p}\right\rangle$.

Solving Equation 3.17 for $\Delta A_{\left\langle -\omega\frac{\partial q}{\partial p}\right\rangle}$ and $\Delta\phi_{\left\langle -\omega\frac{\partial q}{\partial p}\right\rangle}$ separately yields the following:

$$\Delta A_{\left\langle -\omega\frac{\partial q}{\partial p}\right\rangle} = \begin{bmatrix} \cos\left(\phi_{\left\langle -\omega\frac{\partial q}{\partial p}\right\rangle} - \phi_{\left\langle -\Delta\overline{\omega}\frac{\partial\{q'\}}{\partial p}\right\rangle}\right) \\ \cos\left(\phi_{\left\langle -\omega\frac{\partial q}{\partial p}\right\rangle} - \phi_{\left\langle -\overline{\omega}\frac{\partial\{\Delta q'\}}{\partial p}\right\rangle}\right) \\ \cos\left(\phi_{\left\langle -\omega\frac{\partial q}{\partial p}\right\rangle} - \phi_{\left\langle -\{\Delta\omega'\}\frac{\partial\overline{q}}{\partial p}\right\rangle}\right) \\ \cos\left(\phi_{\left\langle -\omega\frac{\partial q}{\partial p}\right\rangle} - \phi_{\left\langle -\{\omega'\}\frac{\partial\Delta\overline{q}}{\partial p}\right\rangle}\right) \\ A_{\left\langle -\Delta\overline{\omega}\frac{\partial\{q'\}}{\partial p}\right\rangle}\sin\left(\phi_{\left\langle -\omega\frac{\partial q}{\partial p}\right\rangle} - \phi_{\left\langle -\Delta\overline{\omega}\frac{\partial\{q'\}}{\partial p}\right\rangle}\right) \\ A_{\left\langle -\overline{\omega}\frac{\partial\{\Delta q'\}}{\partial p}\right\rangle}\sin\left(\phi_{\left\langle -\omega\frac{\partial q}{\partial p}\right\rangle} - \phi_{\left\langle -\overline{\omega}\frac{\partial\{\Delta q'\}}{\partial p}\right\rangle}\right) \\ A_{\left\langle -\{\Delta\omega'\}\frac{\partial\overline{q}}{\partial p}\right\rangle}\sin\left(\phi_{\left\langle -\omega\frac{\partial q}{\partial p}\right\rangle} - \phi_{\left\langle -\{\Delta\omega'\}\frac{\partial\overline{q}}{\partial p}\right\rangle}\right) \\ A_{\left\langle -\{\omega'\}\frac{\partial\Delta\overline{q}}{\partial p}\right\rangle}\sin\left(\phi_{\left\langle -\omega\frac{\partial q}{\partial p}\right\rangle} - \phi_{\left\langle -\{\omega'\}\frac{\partial\Delta\overline{q}}{\partial p}\right\rangle}\right) \end{bmatrix}^{\top} \begin{bmatrix} \Delta A_{\left\langle -\Delta\overline{\omega}\frac{\partial\{q'\}}{\partial p}\right\rangle} \\ \Delta A_{\left\langle -\overline{\omega}\frac{\partial\{\Delta q'\}}{\partial p}\right\rangle} \\ \Delta A_{\left\langle -\{\Delta\omega'\}\frac{\partial\overline{q}}{\partial p}\right\rangle} \\ \Delta A_{\left\langle -\{\omega'\}\frac{\partial\Delta\overline{q}}{\partial p}\right\rangle} \\ \Delta\phi_{\left\langle -\Delta\overline{\omega}\frac{\partial\{q'\}}{\partial p}\right\rangle} \\ \Delta\phi_{\left\langle -\overline{\omega}\frac{\partial\{\Delta q'\}}{\partial p}\right\rangle} \\ \Delta\phi_{\left\langle -\{\Delta\omega'\}\frac{\partial\overline{q}}{\partial p}\right\rangle} \\ \Delta\phi_{\left\langle -\{\omega'\}\frac{\partial\Delta\overline{q}}{\partial p}\right\rangle} \end{bmatrix} \tag{3.18}$$

$$\Delta\phi_{\left\langle -\omega\frac{\partial q}{\partial p}\right\rangle} = \frac{1}{A_{\left\langle -\omega\frac{\partial q}{\partial p}\right\rangle}} \begin{bmatrix} \sin\left(\phi_{\left\langle -\Delta\overline{\omega}\frac{\partial\{q'\}}{\partial p}\right\rangle} - \phi_{\left\langle -\omega\frac{\partial q}{\partial p}\right\rangle}\right) \\ \sin\left(\phi_{\left\langle -\overline{\omega}\frac{\partial\{\Delta q'\}}{\partial p}\right\rangle} - \phi_{\left\langle -\omega\frac{\partial q}{\partial p}\right\rangle}\right) \\ \sin\left(\phi_{\left\langle -\{\Delta\omega'\}\frac{\partial\overline{q}}{\partial p}\right\rangle} - \phi_{\left\langle -\omega\frac{\partial q}{\partial p}\right\rangle}\right) \\ \sin\left(\phi_{\left\langle -\{\omega'\}\frac{\partial\Delta\overline{q}}{\partial p}\right\rangle} - \phi_{\left\langle -\omega\frac{\partial q}{\partial p}\right\rangle}\right) \\ A_{\left\langle -\Delta\overline{\omega}\frac{\partial\{q'\}}{\partial p}\right\rangle}\cos\left(\phi_{\left\langle -\Delta\overline{\omega}\frac{\partial\{q'\}}{\partial p}\right\rangle} - \phi_{\left\langle -\omega\frac{\partial q}{\partial p}\right\rangle}\right) \\ A_{\left\langle -\overline{\omega}\frac{\partial\{\Delta q'\}}{\partial p}\right\rangle}\cos\left(\phi_{\left\langle -\overline{\omega}\frac{\partial\{\Delta q'\}}{\partial p}\right\rangle} - \phi_{\left\langle -\omega\frac{\partial q}{\partial p}\right\rangle}\right) \\ A_{\left\langle -\{\Delta\omega'\}\frac{\partial\overline{q}}{\partial p}\right\rangle}\cos\left(\phi_{\left\langle -\{\Delta\omega'\}\frac{\partial\overline{q}}{\partial p}\right\rangle} - \phi_{\left\langle -\omega\frac{\partial q}{\partial p}\right\rangle}\right) \\ A_{\left\langle -\{\omega'\}\frac{\partial\Delta\overline{q}}{\partial p}\right\rangle}\cos\left(\phi_{\left\langle -\{\omega'\}\frac{\partial\Delta\overline{q}}{\partial p}\right\rangle} - \phi_{\left\langle -\omega\frac{\partial q}{\partial p}\right\rangle}\right) \end{bmatrix}^{\top} \begin{bmatrix} \Delta A_{\left\langle -\Delta\overline{\omega}\frac{\partial\{q'\}}{\partial p}\right\rangle} \\ \Delta A_{\left\langle -\overline{\omega}\frac{\partial\{\Delta q'\}}{\partial p}\right\rangle} \\ \Delta A_{\left\langle -\{\Delta\omega'\}\frac{\partial\overline{q}}{\partial p}\right\rangle} \\ \Delta A_{\left\langle -\{\omega'\}\frac{\partial\Delta\overline{q}}{\partial p}\right\rangle} \\ \Delta\phi_{\left\langle -\Delta\overline{\omega}\frac{\partial\{q'\}}{\partial p}\right\rangle} \\ \Delta\phi_{\left\langle -\overline{\omega}\frac{\partial\{\Delta q'\}}{\partial p}\right\rangle} \\ \Delta\phi_{\left\langle -\{\Delta\omega'\}\frac{\partial\overline{q}}{\partial p}\right\rangle} \\ \Delta\phi_{\left\langle -\{\omega'\}\frac{\partial\Delta\overline{q}}{\partial p}\right\rangle} \end{bmatrix} \tag{3.19}$$

Since I am interested in what effect the various changes of annual mean, amplitude, and phase of ω and $\partial q/\partial p$ have on $\left\langle -\omega\frac{\partial q}{\partial p}\right\rangle$, I further decompose the terms $A_{\left\langle -\overline{\omega}\frac{\partial\{\Delta q'\}}{\partial p}\right\rangle}$, $A_{\left\langle -\{\Delta\omega'\}\frac{\partial\overline{q}}{\partial p}\right\rangle}$, $\phi_{\left\langle -\overline{\omega}\frac{\partial\{\Delta q'\}}{\partial p}\right\rangle}$, and $\phi_{\left\langle -\{\Delta\omega'\}\frac{\partial\overline{q}}{\partial p}\right\rangle}$ each into separate terms relating to the change in amplitude or phase of $\partial q/\partial p$ or ω as follows:

$$\Delta A_{\left\langle -\overline{\omega}\frac{\partial\{\Delta q'\}}{\partial p}\right\rangle} = \Delta A_{\left\langle -\overline{\omega}\frac{\partial\{\Delta q'\}}{\partial p}\right\rangle;\Delta A_{\partial q/\partial p}} + \Delta A_{\left\langle -\overline{\omega}\frac{\partial\{\Delta q'\}}{\partial p}\right\rangle;\Delta\phi_{\partial q/\partial p}} \tag{3.20}$$

$$\Delta A_{\left\langle -\{\Delta\omega'\}\frac{\partial\overline{q}}{\partial p}\right\rangle} = \Delta A_{\left\langle -\{\Delta\omega'\}\frac{\partial\overline{q}}{\partial p}\right\rangle;\Delta A_{\omega}} + \Delta A_{\left\langle -\{\Delta\omega'\}\frac{\partial\overline{q}}{\partial p}\right\rangle;\Delta\phi_{\omega}} \tag{3.21}$$

$$\Delta\phi_{\left\langle -\overline{\omega}\frac{\partial\{\Delta q'\}}{\partial p}\right\rangle} = \Delta\phi_{\left\langle -\overline{\omega}\frac{\partial\{\Delta q'\}}{\partial p}\right\rangle;\Delta A_{\partial q/\partial p}} + \Delta\phi_{\left\langle -\overline{\omega}\frac{\partial\{\Delta q'\}}{\partial p}\right\rangle;\Delta\phi_{\partial q/\partial p}} \tag{3.22}$$

$$\Delta\phi_{\left\langle -\{\Delta\omega'\}\frac{\partial\overline{q}}{\partial p}\right\rangle} = \Delta\phi_{\left\langle -\{\Delta\omega'\}\frac{\partial\overline{q}}{\partial p}\right\rangle;\Delta A_{\omega}} + \Delta\phi_{\left\langle -\{\Delta\omega'\}\frac{\partial\overline{q}}{\partial p}\right\rangle;\Delta\phi_{\omega}}, \tag{3.23}$$

where, for example, $\Delta A_{\left\langle -\overline{\omega}\frac{\partial\{\Delta q'\}}{\partial p}\right\rangle;\Delta A_{\partial q/\partial p}}$ is the effect of a change in the amplitude of $\partial q/\partial p$ on $\Delta A_{\left\langle -\overline{\omega}\frac{\partial\{\Delta q'\}}{\partial p}\right\rangle}$. With this in mind I can write the effect that changes in various components changes of ω and q have on $A_{\left\langle -\omega\frac{\partial q}{\partial p}\right\rangle}$ and $\phi_{\left\langle -\omega\frac{\partial q}{\partial p}\right\rangle}$ as follows:

$$
\begin{bmatrix}
\Delta A_{\left\langle -\omega \frac{\partial q}{\partial p} \right\rangle ; \overline{\omega}} \\
\Delta A_{\left\langle -\omega \frac{\partial q}{\partial p} \right\rangle ; A_\omega} \\
\Delta A_{\left\langle -\omega \frac{\partial q}{\partial p} \right\rangle ; \phi_\omega} \\
\Delta A_{\left\langle -\omega \frac{\partial q}{\partial p} \right\rangle ; \partial \overline{q}/\partial p} \\
\Delta A_{\left\langle -\omega \frac{\partial q}{\partial p} \right\rangle ; A_{\partial q/\partial p}} \\
\Delta A_{\left\langle -\omega \frac{\partial q}{\partial p} \right\rangle ; \phi_{\partial q/\partial p}}
\end{bmatrix}
= \tag{3.24}
$$

$$
\begin{bmatrix}
\cos\left(\phi_{\left\langle -\omega \frac{\partial q}{\partial p} \right\rangle} - \phi_{\left\langle -\Delta\overline{\omega} \frac{\partial \{q'\}}{\partial p} \right\rangle}\right) \Delta A_{\left\langle -\Delta\overline{\omega} \frac{\partial \{q'\}}{\partial p} \right\rangle} + \\
A_{\left\langle -\Delta\overline{\omega} \frac{\partial \{q'\}}{\partial p} \right\rangle} \sin\left(\phi_{\left\langle -\omega \frac{\partial q}{\partial p} \right\rangle} - \phi_{\left\langle -\Delta\overline{\omega} \frac{\partial \{q'\}}{\partial p} \right\rangle}\right) \Delta \phi_{\left\langle -\Delta\overline{\omega} \frac{\partial \{q'\}}{\partial p} \right\rangle} \\
\cos\left(\phi_{\left\langle -\omega \frac{\partial q}{\partial p} \right\rangle} - \phi_{\left\langle -\{\Delta\omega'\} \frac{\partial \overline{q}}{\partial p} \right\rangle}\right) \Delta A_{\left\langle -\{\Delta\omega'\} \frac{\partial \overline{q}}{\partial p} \right\rangle ; \Delta A_\omega} + \\
A_{\left\langle -\{\Delta\omega'\} \frac{\partial \overline{q}}{\partial p} \right\rangle} \sin\left(\phi_{\left\langle -\omega \frac{\partial q}{\partial p} \right\rangle} - \phi_{\left\langle -\{\Delta\omega'\} \frac{\partial \overline{q}}{\partial p} \right\rangle}\right) \Delta \phi_{\left\langle -\{\Delta\omega'\} \frac{\partial \overline{q}}{\partial p} \right\rangle ; \Delta A_\omega} \\
\cos\left(\phi_{\left\langle -\omega \frac{\partial q}{\partial p} \right\rangle} - \phi_{\left\langle -\{\Delta\omega'\} \frac{\partial \overline{q}}{\partial p} \right\rangle}\right) \Delta A_{\left\langle -\{\Delta\omega'\} \frac{\partial \overline{q}}{\partial p} \right\rangle ; \Delta \phi_\omega} + \\
A_{\left\langle -\{\Delta\omega'\} \frac{\partial \overline{q}}{\partial p} \right\rangle} \sin\left(\phi_{\left\langle -\omega \frac{\partial q}{\partial p} \right\rangle} - \phi_{\left\langle -\{\Delta\omega'\} \frac{\partial \overline{q}}{\partial p} \right\rangle}\right) \Delta \phi_{\left\langle -\{\Delta\omega'\} \frac{\partial \overline{q}}{\partial p} \right\rangle ; \Delta \phi_\omega} \\
\cos\left(\phi_{\left\langle -\omega \frac{\partial q}{\partial p} \right\rangle} - \phi_{\left\langle -\{\omega'\} \frac{\partial \Delta\overline{q}}{\partial p} \right\rangle}\right) \Delta A_{\left\langle -\{\omega'\} \frac{\partial \Delta\overline{q}}{\partial p} \right\rangle} + \\
A_{\left\langle -\{\omega'\} \frac{\partial \Delta\overline{q}}{\partial p} \right\rangle} \sin\left(\phi_{\left\langle -\omega \frac{\partial q}{\partial p} \right\rangle} - \phi_{\left\langle -\{\omega'\} \frac{\partial \Delta\overline{q}}{\partial p} \right\rangle}\right) \Delta \phi_{\left\langle -\{\omega'\} \frac{\partial \Delta\overline{q}}{\partial p} \right\rangle} \\
\cos\left(\phi_{\left\langle -\omega \frac{\partial q}{\partial p} \right\rangle} - \phi_{\left\langle -\overline{\omega} \frac{\partial \{\Delta q'\}}{\partial p} \right\rangle}\right) \Delta A_{\left\langle -\overline{\omega} \frac{\partial \{\Delta q'\}}{\partial p} \right\rangle ; \Delta A_q} + \\
A_{\left\langle -\overline{\omega} \frac{\partial \{\Delta q'\}}{\partial p} \right\rangle} \sin\left(\phi_{\left\langle -\omega \frac{\partial q}{\partial p} \right\rangle} - \phi_{\left\langle -\overline{\omega} \frac{\partial \{\Delta q'\}}{\partial p} \right\rangle}\right) \Delta \phi_{\left\langle -\overline{\omega} \frac{\partial \{\Delta q'\}}{\partial p} \right\rangle ; \Delta A_q} \\
\cos\left(\phi_{\left\langle -\omega \frac{\partial q}{\partial p} \right\rangle} - \phi_{\left\langle -\overline{\omega} \frac{\partial \{\Delta q'\}}{\partial p} \right\rangle}\right) \Delta A_{\left\langle -\overline{\omega} \frac{\partial \{\Delta q'\}}{\partial p} \right\rangle ; \Delta \phi_q} + \\
A_{\left\langle -\overline{\omega} \frac{\partial \{\Delta q'\}}{\partial p} \right\rangle} \sin\left(\phi_{\left\langle -\omega \frac{\partial q}{\partial p} \right\rangle} - \phi_{\left\langle -\overline{\omega} \frac{\partial \{\Delta q'\}}{\partial p} \right\rangle}\right) \Delta \phi_{\left\langle -\overline{\omega} \frac{\partial \{\Delta q'\}}{\partial p} \right\rangle ; \Delta \phi_q}
\end{bmatrix}
$$

$$
\begin{bmatrix}
\Delta\phi_{\left\langle -\omega \frac{\partial q}{\partial p} \right\rangle ; \overline{\omega}} \\
\Delta\phi_{\left\langle -\omega \frac{\partial q}{\partial p} \right\rangle ; A_\omega} \\
\Delta\phi_{\left\langle -\omega \frac{\partial q}{\partial p} \right\rangle ; \phi_\omega} \\
\Delta\phi_{\left\langle -\omega \frac{\partial q}{\partial p} \right\rangle ; \partial\overline{q}/\partial p} \\
\Delta\phi_{\left\langle -\omega \frac{\partial q}{\partial p} \right\rangle ; A_{\partial q/\partial p}} \\
\Delta\phi_{\left\langle -\omega \frac{\partial q}{\partial p} \right\rangle ; \phi_{\partial q/\partial p}}
\end{bmatrix}
= \frac{1}{A_{\left\langle -\omega \frac{\partial q}{\partial p} \right\rangle}} \times \tag{3.25}
$$

$$
\begin{bmatrix}
\sin\left(\phi_{\left\langle -\Delta\overline{\omega} \frac{\partial\{q'\}}{\partial p} \right\rangle} - \phi_{\left\langle -\omega \frac{\partial q}{\partial p} \right\rangle}\right) \Delta A_{\left\langle -\Delta\overline{\omega} \frac{\partial\{q'\}}{\partial p} \right\rangle} + \\
A_{\left\langle -\Delta\overline{\omega} \frac{\partial\{q'\}}{\partial p} \right\rangle} \cos\left(\phi_{\left\langle -\Delta\overline{\omega} \frac{\partial\{q'\}}{\partial p} \right\rangle} - \phi_{\left\langle -\omega \frac{\partial q}{\partial p} \right\rangle}\right) \Delta\phi_{\left\langle -\Delta\overline{\omega} \frac{\partial\{q'\}}{\partial p} \right\rangle} \\
\sin\left(\phi_{\left\langle -\{\Delta\omega'\} \frac{\partial\overline{q}}{\partial p} \right\rangle} - \phi_{\left\langle -\omega \frac{\partial q}{\partial p} \right\rangle}\right) \Delta A_{\left\langle -\{\Delta\omega'\} \frac{\partial\overline{q}}{\partial p} \right\rangle ; \Delta A_\omega} + \\
A_{\left\langle -\{\Delta\omega'\} \frac{\partial\overline{q}}{\partial p} \right\rangle} \cos\left(\phi_{\left\langle -\{\Delta\omega'\} \frac{\partial\overline{q}}{\partial p} \right\rangle} - \phi_{\left\langle -\omega \frac{\partial q}{\partial p} \right\rangle}\right) \Delta\phi_{\left\langle -\{\Delta\omega'\} \frac{\partial\overline{q}}{\partial p} \right\rangle ; \Delta A_\omega} \\
\sin\left(\phi_{\left\langle -\{\Delta\omega'\} \frac{\partial\overline{q}}{\partial p} \right\rangle} - \phi_{\left\langle -\omega \frac{\partial q}{\partial p} \right\rangle}\right) \Delta A_{\left\langle -\{\Delta\omega'\} \frac{\partial\overline{q}}{\partial p} \right\rangle ; \Delta\phi_\omega} + \\
A_{\left\langle -\{\Delta\omega'\} \frac{\partial\overline{q}}{\partial p} \right\rangle} \cos\left(\phi_{\left\langle -\{\Delta\omega'\} \frac{\partial\overline{q}}{\partial p} \right\rangle} - \phi_{\left\langle -\omega \frac{\partial q}{\partial p} \right\rangle}\right) \Delta\phi_{\left\langle -\{\Delta\omega'\} \frac{\partial\overline{q}}{\partial p} \right\rangle ; \Delta\phi_\omega} \\
\sin\left(\phi_{\left\langle -\{\omega'\} \frac{\partial\Delta\overline{q}}{\partial p} \right\rangle} - \phi_{\left\langle -\omega \frac{\partial q}{\partial p} \right\rangle}\right) \Delta A_{\left\langle -\{\omega'\} \frac{\partial\Delta\overline{q}}{\partial p} \right\rangle} + \\
A_{\left\langle -\{\omega'\} \frac{\partial\Delta\overline{q}}{\partial p} \right\rangle} \cos\left(\phi_{\left\langle -\{\omega'\} \frac{\partial\Delta\overline{q}}{\partial p} \right\rangle} - \phi_{\left\langle -\omega \frac{\partial q}{\partial p} \right\rangle}\right) \Delta\phi_{\left\langle -\{\omega'\} \frac{\partial\Delta\overline{q}}{\partial p} \right\rangle} \\
\sin\left(\phi_{\left\langle -\overline{\omega} \frac{\partial\{\Delta q'\}}{\partial p} \right\rangle} - \phi_{\left\langle -\omega \frac{\partial q}{\partial p} \right\rangle}\right) \Delta A_{\left\langle -\overline{\omega} \frac{\partial\{\Delta q'\}}{\partial p} \right\rangle ; \Delta A_q} + \\
A_{\left\langle -\overline{\omega} \frac{\partial\{\Delta q'\}}{\partial p} \right\rangle} \cos\left(\phi_{\left\langle -\overline{\omega} \frac{\partial\{\Delta q'\}}{\partial p} \right\rangle} - \phi_{\left\langle -\omega \frac{\partial q}{\partial p} \right\rangle}\right) \Delta\phi_{\left\langle -\overline{\omega} \frac{\partial\{\Delta q'\}}{\partial p} \right\rangle ; \Delta A_q} \\
\sin\left(\phi_{\left\langle -\overline{\omega} \frac{\partial\{\Delta q'\}}{\partial p} \right\rangle} - \phi_{\left\langle -\omega \frac{\partial q}{\partial p} \right\rangle}\right) \Delta A_{\left\langle -\overline{\omega} \frac{\partial\{\Delta q'\}}{\partial p} \right\rangle ; \Delta\phi_q} + \\
A_{\left\langle -\overline{\omega} \frac{\partial\{\Delta q'\}}{\partial p} \right\rangle} \cos\left(\phi_{\left\langle -\overline{\omega} \frac{\partial\{\Delta q'\}}{\partial p} \right\rangle} - \phi_{\left\langle -\omega \frac{\partial q}{\partial p} \right\rangle}\right) \Delta\phi_{\left\langle -\overline{\omega} \frac{\partial\{\Delta q'\}}{\partial p} \right\rangle ; \Delta\phi_q}
\end{bmatrix}
$$

Chapter 4

Idealized Simulations of Projected Changes in the Tropical Annual Cycle

4.1 Introduction

Over recent years our understanding of the tropical climate and how it may change in a world with increased greenhouse gases has greatly improved thanks in large part to global climate models (GCMs). These models have increased our confidence in many projected tropical changes including the pattern of surface temperature change (Xie et al., 2010; Byrne and O'Gorman, 2013), increased precipitation in convective regions and a reduction in the subtropics (Chou and Neelin, 2004; Held and Soden, 2006), a weakening of the annual mean tropical circulation (Betts and Ridgway, 1989; Knutson and Manabe, 1995; Sugi et al., 2002; Held and Soden, 2006; Vecchi and Soden, 2007), and a widening of the tropical belt (Seidel et al., 2008). However, there is still uncertainty surrounding projected seasonality changes in the tropics. This chapter aims to improve our understanding by investigating the seasonal changes and potential mechanisms in several numerical models.

These models, each detailed in the following sections of the chapter, range in complexity from fully-coupled GCMs to semi-empirical models that can be described with just two equations. Each provides clues and insights into the processes that may be at work and are also useful for ruling out certain phenomena as mechanisms for the seasonal changes.

First I study how the seasonality changes in CMIP5 coupled model simulations with idealized greenhouse forcings. Unlike the "historical" and "rcp8.5" scenarios which attempt to simulate past and future anthropogenic and natural forcings, the simulations I focus on are intended to be used as tools for understanding various processes affecting the climate and its sensitivity. In addition to a control scenario with pre-industrial atmospheric conditions, these simulations include an "abrupt4xCO_2" simulation in which CO_2 levels are instantaneously quadrupled and a "1%to4xCO_2" simulation in which the atmospheric CO_2 concentration increases at 1% per year until quadrupling at year 140. When compared to the 1% simulation, the abrupt simulation helps determine the causes of different climate changes.

Motivated by some of the land-ocean discrepancy in seasonality in the CMIP5 models, I then formulate a semi-empirical model in which the annual cycle of precipitation is a function of the annual cycles of surface temperatures over land and ocean and the annual mean precipitation over land and ocean. By applying the model on CMIP5 output from the 20th century, I find scaling parameters which I apply to 21st century CMIP5 output. This model is helpful for testing whether the same processes are occurring in all of the CMIP5 simulations. While an oversimplification for precipitation, it is useful for finding links between changes and understanding the relative importance of land and ocean effects.

Next I study the seasonality changes in tropical precipitation and circulation using a zonally-symmetric aquaplanet with prescribed sea surface temperature and sea ice cover. This model is more complicated than the semi-empirical model, but the simulation is simpler than the CMIP5 GCMs and allows me to test the effect that land, (or land-ocean interaction) has on the annual cycle of tropical precipitation.

Finally I perform simulations with the dynamical core of a dry atmospheric model to which I have added an annual cycle. This model reproduces many aspects of the real climate, including a Hadley cell-like circulation in the tropics. Because it is computationally inexpensive to run and simple to manipulate, it is useful for testing the effects of atmospheric changes on the annual cycle.

4.2 CMIP5 Simulations with Idealized Forcing

4.2.1 Description of Seasonal Changes

I begin by looking at the changes in the annual cycle of precipitation in the CMIP5 simulations with idealized forcing. In order to capture the most information about the annual cycle in a concise manner I perform an EOF analysis of precipitation between 45°S and 45°N, chosen because at this latitude the projected changes in the amplitude of surface temperature reverse sign in the CMIP3 simulations (see Chapters 2 and 3 for further details about the method). I analyze ocean and land separately, because if combined the loading pattern can shift its weight from ocean to land, which have different climatological phasing for many variables. To study the time-dependence of the changes, I perform the EOF analysis for each year individually, yielding values for phase and amplitude for every year of the simulation. Finally I normalize by the control simulation, for which the EOF is calculated in the same manner and then averaged over the last 140 years. The EOF patterns for all of the variables discussed below can be found in Section 4.7.

I begin by studying the amplitude of ocean precipitation for three CMIP5 simu-

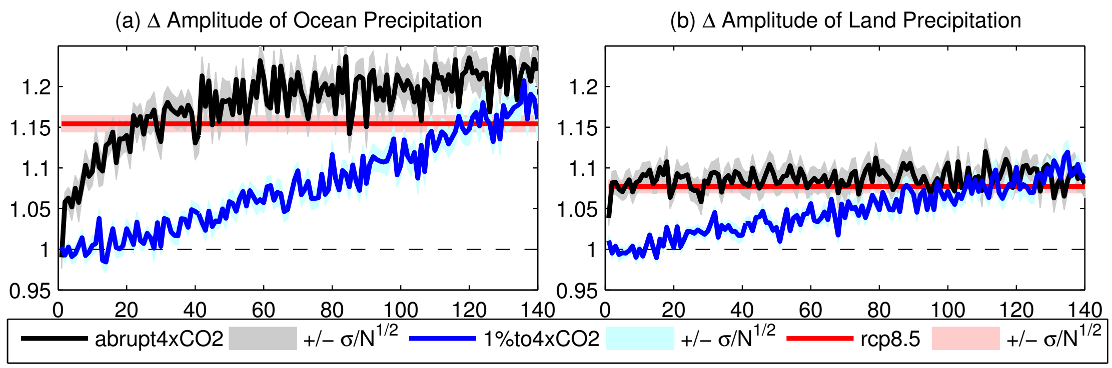

Figure 4.1: The time series of the change in the amplitude of precipitation over ocean (a) and land (b) for the abrupt4xCO_2 (black line) and the 1%to4xCO_2 (blue line) simulations normalized by dividing by the amplitude of precipitation in the piControl simulation. Also included for reference is the change in the rcp8.5 simulation relative to the historical simulation (red line) for the last two decades of the 21st and 20th centuries (time dependence has been removed). The lines are the multimodel median and the shading represents one standard error among the CMIP5 models. The amplitude is calculated from the sinusoidal fit to the first principal component on a yearly basis for ocean and land separately.

lations, the two with idealized forcings described above and the rcp8.5 21st century simulation in Figure 4.1(a). By year 140 of the abrupt and 1% simulations, the amplitude has increased by around 20%, compared to around 15% in the rcp8.5 simulation (averaged over 2080–2099 with the CO_2 equivalent concentration increasing to around 1100 ppmv). The time scale of the response is very different between these simulations, though. In the abrupt case, the amplitude of precipitation increases quickly over the first two decades and then slows to a gradual increase over the rest of the record. By contrast, the rate of increase in the 1% case is small at first but gradually increases.

The time scales of each response is set by the rate of increase of annual mean temperature, depicted in Figure 4.2 and consistent with the UW experiment. Because an increase in annual mean temperature increases the vertical gradient of water vapor in the tropics as a thermodynamic consequence of the Clausius-Clapeyron relation, the upwelling branch of the Hadley Cell produces precipitation from this

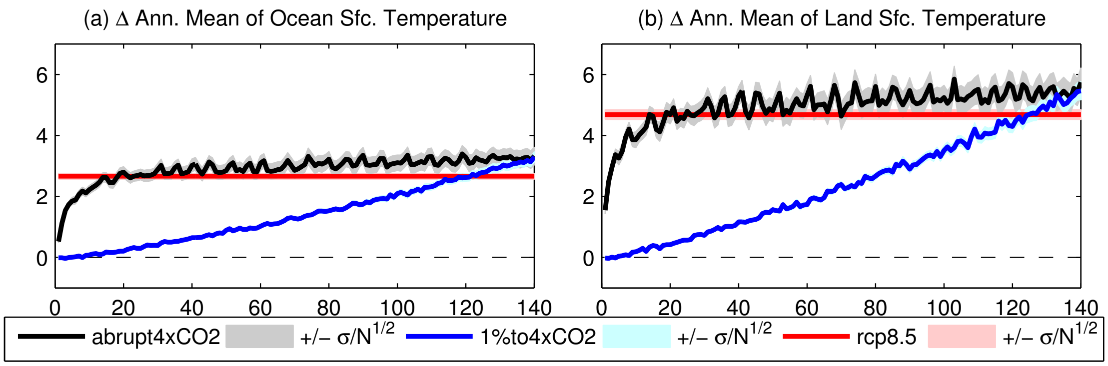

Figure 4.2: As in Figure 4.1, but for the annual mean surface temperature change. Variability in the abrupt simulation is a result of taking the multimodel median, rather than mean.

additional moisture. Since the upwelling branch is located in the summer hemisphere, precipitation increases in the summer and decreases in the winter resulting in an increase in the amplitude of precipitation.

The behavior over land is different. Figure 4.1(b) shows that even in the very first year of the abrupt simulation, the amplitude of precipitation is 4% larger than in the control simulation and reaches an equilibrium value of a 10% increase after only a few years. This suggests that the annual mean temperature rise is not the primary mechanism for increasing the amplitude of land precipitation since it operates on a much slower time scale.

The time series of the amplitude of surface temperature has a similar behavior to that of land precipitation. Figure 4.3 shows that the amplitudes of both land and ocean surface temperature immediately increase in the abrupt simulation and the values reached in the first few years are equivalent to the values reached at year 140 in the 1% simulation. The immediacy of the amplitude responses of land precipitation and surface temperature over both ocean and land suggests that the changes are linked in some way. For example, in the p5a10 AGCM simulation I found that an amplitude increase of SST caused an amplitude increase in precipitation. The nature of the link will be discussed in more detail below.

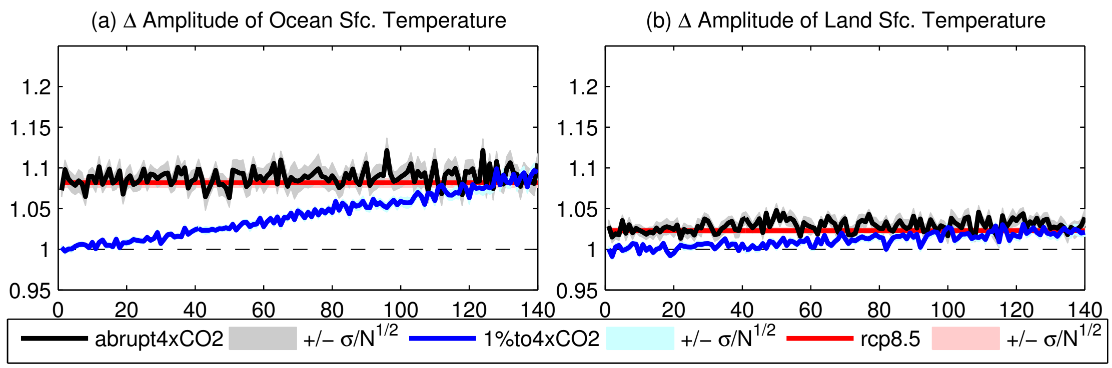

Figure 4.3: As in Figure 4.1, but for the amplitude of surface temperature.

Next I look at the changes in the timing of the annual cycle of precipitation in Figure 4.4. As in the rcp8.5 scenario over both ocean and land, there is a phase delay in both the 1% and abrupt simulation but with different time scales. The delay in the 1% run develops at a roughly linear rate, consistent with the annual mean increase in surface temperature (and many other variables). By contrast the delay in the abrupt simulation increases rapidly, but not quite as rapidly as the increase in the amplitude of SST, eventually reaching 4 days.

Despite the changes in the seasonality of many other variables, in both the abrupt and 1% simulations, the models do not have any phase delay in the seasonal cycle of SST (Figure 4.5(a)). This is surprising given a multiday phase delay in the CMIP3 models (Biasutti and Sobel, 2009; Dwyer et al., 2012) and a 1 day delay in the CMIP5 rcp8.5 scenario (Dwyer et al., 2014). Figure 4.5(a) shows less than a half day phase delay in the rcp8.5 scenario. The discrepancy is due to the EOF analysis here being performed equatorward of 45°, while previously it was performed equatorward of 25°. That the CMIP5 simulations with idealized forcing shows no SST phase delay suggests that this term is not driving seasonality changes in other variables in either these simulations or the CMIP3 suite.

Unlike for ocean, there is a phase delay in surface temperature over land. Figure 4.5(b) shows that this 2 day delay occurs nearly instantaneously in the abrupt

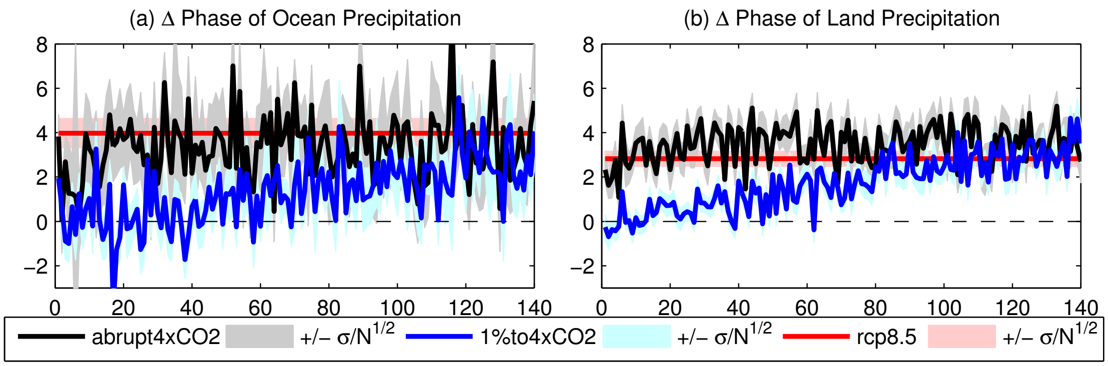

Figure 4.4: As in Figure 4.1, but for the phase of precipitation. Units of phase are in days relative to the control simulation with positive values indicating a delay.

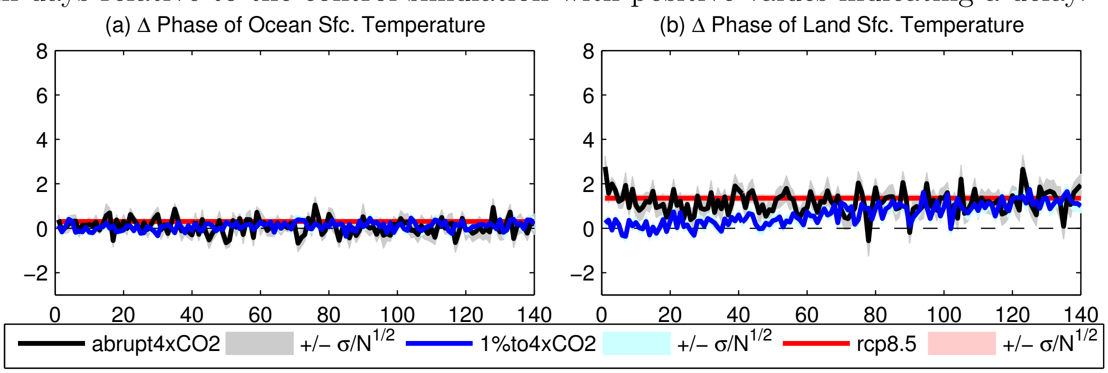

Figure 4.5: As in Figure 4.4, but for the phase of surface temperature.

simulation, suggesting a link with nearly instantaneous changes in the phases and amplitudes of other variables in this simulation. In fact the phase delay in the first few years is actually larger than the steady state value of the delay, a detail which will be addressed further in Section 4.6.

Finally I look at the seasonality changes of vertical motion (see Figure 4.25 for the loading pattern). In all three CMIP5 simulations over both ocean and land, the amplitude of the vertical velocity decreases as illustrated in Figure 4.6. In the abrupt run, the amplitude of vertical velocity actually increases in the first few years of the simulation, before a period of rapid weakening that transitions to a gradual weakening over the next 140 years. The CMIP5 simulations also show a delay in the phase of vertical velocity (Figure 4.7). The delay, about 2–3 days over

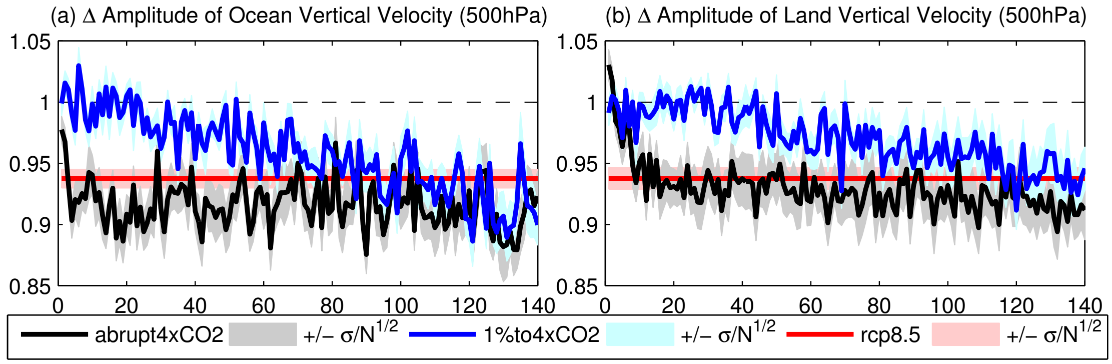

Figure 4.6: As in Figure 4.1, but for the amplitude of the annual cycle of vertical velocity at 500 hPa.

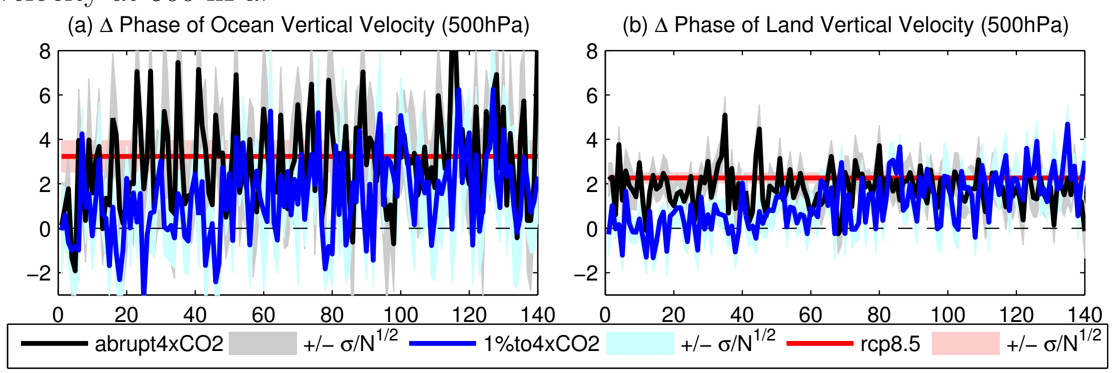

Figure 4.7: As in Figure 4.6, but for phase.

both ocean and land, occurs quickly in the abrupt simulation, especially over land. While a relatively noisy quantity, it does not appear to increase instantaneously over ocean, similar in time scale to the phase delay of precipitation.

4.2.2 Surface Wind Mechanism for Surface Temperature

One potential mechanism for the projected changes in the seasonality of surface temperature is forcing by the surface wind. Sobel and Camargo (2011) investigated the relationship between these terms in the CMIP3 models and found an amplitude increase in the surface wind speed and SST in the CMIP3 models. The authors proposed that these seasonal wind changes were driving corresponding changes in

SST via the surface latent heat flux, often approximated as:

$$E = L\rho_a C|\vec{v}|\left[q^*(T) - q_a\right], \tag{4.1}$$

where L is the latent heat of vaporization, ρ_a is the surface air density, C is the air-sea exchange coefficient, $|\vec{v}|$ is the surface wind speed, $q^*(T)$ is the saturation specific humidity as a function of surface temperature, and q_a is the specific humidity of the air at the surface. Both the surface wind speed and surface temperature enter the equation, providing a pathway for interaction (Sobel and Camargo, 2011). I extend that work by studying these terms in the abrupt, 1%, and rcp8.5 simulations and analyzing their projected phase changes. I also look at their relationship over land, for which evaporative cooling is limited by water availability.

In all of the CMIP5 runs the amplitude of surface wind increases as shown in Figure 4.8(a). In the abrupt simulation, this increase happens very quickly, in line with similarly rapid increases in the amplitude of SST (Figure 4.3(a)), suggesting a link between these terms. If E, $q^*(T) - q_a$, and the other surface flux terms did not change, the increase in amplitude of both the surface wind speed and surface temperature terms would be consistent. Since the wind speed and surface temperature terms are six months out of phase (maximum wind speed increase occurs during winter, while the maximum surface temperature increase occurs during summer), amplitude increases in both terms satisfies their inverse relationship in Equation 4.1.

The precise nature of the relationship between the surface wind speed and SST is more complicated, though, as E and $q^*(T) - q_a$ are not constant. Further complicating the picture, is that E is only one of several terms that make up the total surface heat flux and on seasonal time scales, T also enters the surface energy balance through its tendency. As shown in Figure 4.19(a) and 4.20(a), the amplitudes of both evaporation and surface flux, respectively, increases in all CMIP5 simulations. The increase of the amplitude of surface flux is consistent with the results of Chapter 2, where it was linked to the increase of the amplitude of SST. However,

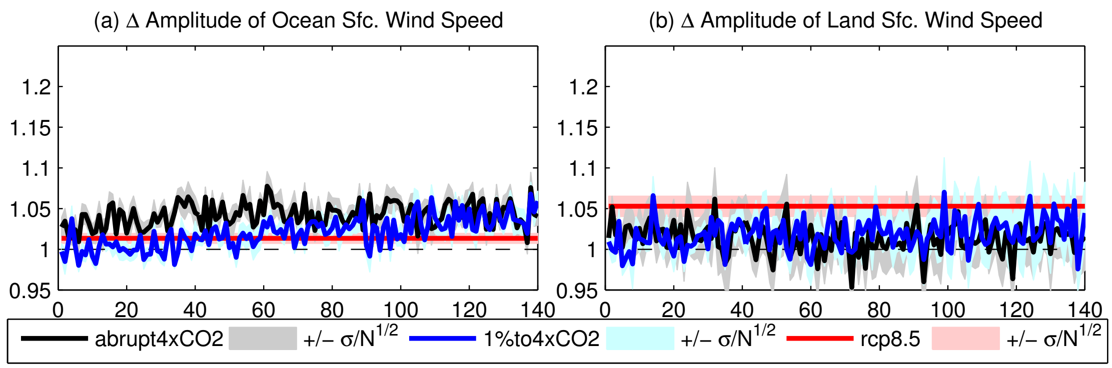

Figure 4.8: As in Figure 4.1, but for the amplitude of the surface wind speed.

the rate of increase in the amplitude of surface flux is slower than that of SST in the abrupt simulation. While the exact relationship between the terms is complicated, the similar timing and appearance in four different suites of model comparisons strongly suggests a link between the amplitude of the surface wind and surface temperature over ocean.

There are also increases in the amplitude of surface wind speed over land. For the abrupt and 1% runs, these are smaller than over ocean (a 1–2% increase compared with a 4–5% increase), perhaps accounting for the smaller increase in the amplitude of surface temperature over land compared to ocean. (Though the rcp8.5 simulation has a larger amplitude increase in surface wind speed over land than it does over ocean). The seasonality of the surface energy balance and its component terms is different over land than ocean as Figure 4.19(b) shows little change in the amplitude of the surface latent heat flux and Figure 4.20(b) shows a decrease in the amplitude of the total surface flux over land. Evaporation is also limited by water availability over land. Despite these potential complications, the amplitude of surface wind speed and surface temperature over land both increase nearly instantaneously in the abrupt run suggesting that the terms may be linked in the same way as they may be over ocean.

I also study the phase of the annual cycle of the surface wind speed and surface

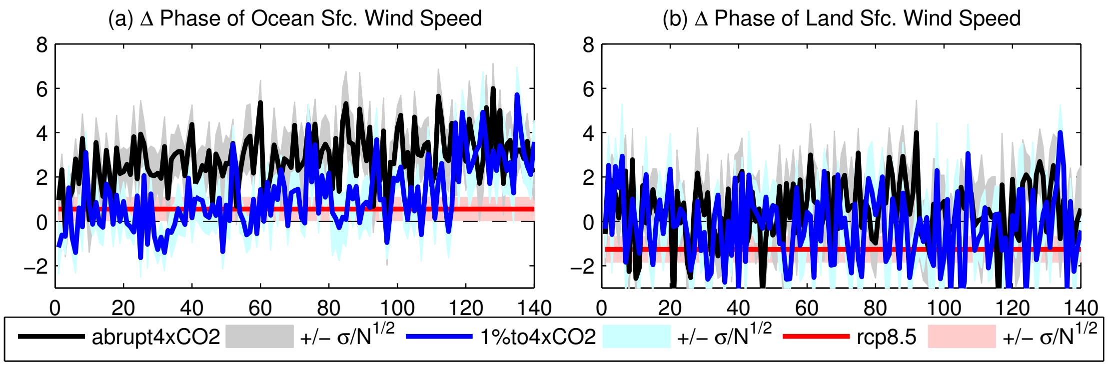

Figure 4.9: As in Figure 4.1, but for the phase of the surface wind speed.

fluxes in the CMIP5 runs with idealized forcings. Figure 4.9(a) shows a 2–3 day phase delay in the surface wind speed over ocean. In the abrupt run, the phase delay increases rapidly before increasing slowly over the rest of the run. These phase delays are larger than those in the rcp8.5 simulation, which has a phase delay of less than 1 day. Over land (Figure 4.9(b)), there is no evidence of a phase delay in the surface wind speed, and in fact the rcp8.5 run shows a phase advance. These results suggest that the proposed wind-surface temperature mechanism for amplitude is not operating for phase. If they were we would expect to see phase delays for both over ocean and land. Instead, there is a delay in surface wind speed over ocean and not land while there is a phase delay in surface temperature over land and not ocean.

Sobel and Camargo (2011) relate the seasonal changes in the amplitude of surface wind speed to changes in the tropical circulation. Many studies have found that the 21st century coupled models project an expansion in the latitudinal extent and a weakening in the strength of the Hadley Cell (Frierson et al., 2007; Johanson and Fu, 2009; Lu et al., 2007). The poleward expansion of the cell is an especially robust result as these changes are evident in observations and 20th century models. This expansion primarily occurs in the winter hemisphere (Gastineau et al., 2008; Kang et al., 2013), and it extends the reach of the subtropical east-

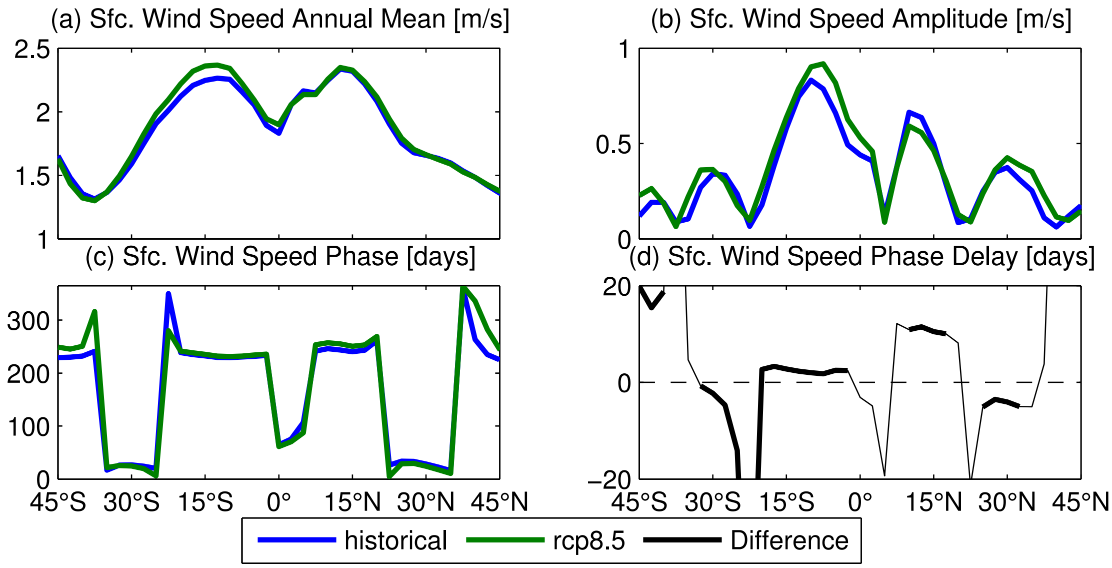

Figure 4.10: Projected zonal-mean surface wind speed changes in the CMIP5 historical and rcp8.5 scenarios for the annual mean (a), amplitude (b), phase relative to insolation (c), and the change in phase between simulations (d). For the phase change, positive values indicate a delay and thick lines indicate where the annual cycle for both the 20th and 21st century simulations makes up at least 50% of the total variance. Seasonal characteristics were calculated from the multimodel mean.

erly winds. Figure 4.10(b) shows the effect of this expansion on the amplitude of surface wind speed, most clearly between 30°–40° in both hemispheres. The weakening of the tropical circulation is also widely projected in models, especially for the Walker Cell (Vecchi et al., 2006; Vecchi and Soden, 2007) and is larger in the summer hemisphere, weakening the summer easterlies (Sobel and Camargo, 2011). These changes are also illustrated in Figure 4.10(b) and show amplitude increasing throughout the tropics except around 15°N.

It is also possible that the SST is driving the surface wind, rather than the other way around (Lindzen and Nigam, 1987; Wallace et al., 1989). However, this seems less likely since there would be no obvious driver leading to immediate seasonality changes in surface temperature in the abrupt simulation. Rather, it appears more probable that the seasonality changes in SST are driven by those of surface wind speed via the latent heat flux equation, with the surface wind changes being a consequence of changes in the extent and strength of the Hadley Circulation. Understanding the nature of the changes in the Hadley Cell in the 20th and 21st century models is an active body of research with hypothesized mechanisms including increased tropospheric static stability (Lu et al., 2007), increased tropopause height (Lorenz and DeWeaver, 2007), a poleward shift in the latitude of the onset of baroclinic instability (Frierson et al., 2007), a poleward shift of baroclinic eddies (Chen and Held, 2007), stratospheric ozone decreases (Son et al., 2008), and an increase in the eddy length scale (Kidston et al., 2010).

Further supporting this direction of causality is that the seasonality changes all happen so rapidly in the abrupt simulation. In a similar experiment with instantaneous CO_2 increases, Wu et al. (2011) and Wu et al. (2012) found a very rapid adjustment of the atmospheric circulation, beginning in the stratosphere and propagating into the troposphere, resulting in a poleward shift of the eddy-driven jets within four months. This rapid adjustment is an attractive mechanism to ultimately explain the amplitude changes in the Hadley circulation, surface wind speed, and surface temperature.

4.3 Semi-empirical Model

The CMIP5 simulations indicate substantial changes to the annual cycle of tropical variables. But these model results show different responses for some variables over land and ocean. For surface temperature there is a phase delay and weak amplitude increase over land, but no phase change and a strong amplitude increase over ocean. The amplitude of ocean precipitation increases at the rate of the annual mean temperature increase, but the amplitude of land precipitation increases instantaneously and by a smaller total amount.

Because of the different climatological phase and amplitude of land and ocean surface temperatures, behavior that depends on their interaction might react in an unexpected manner due to changes in only one domain. For example, in an atmospheric model with a prescribed delay in the phase of SST, the amplitude of precipitation increases and when the model is give an amplitude increase in SST, the phase of precipitation delays. Dwyer et al. (2014) attribute these effects to precipitation responding to a mixing of sinusoids of insolation and SST (Stine et al., 2009). Similarly, past AGCM suggested that while the annual cycle of ocean precipitation is primarily due to the effects of SST and the annual cycle of land precipitation is primarily due to insolation directly, cross effects are non-negligible (Biasutti et al., 2003, 2004). These results provide motivation for a simple model that assumes that the evolution of the seasonality pattern of precipitation over either ocean or land can be described as a linear combination of surface temperature over ocean and land:

$$P_o(t) = a_o\overline{P_o}T_o(t) + b_o(1-x)\overline{P_l}T_l(t) \tag{4.2}$$

$$P_l(t) = a_l\overline{P_o}T_o(t) + b_l(1-x)\overline{P_l}T_l(t), \tag{4.3}$$

where $P(t)$ and $T(t)$ represent the leading principal components of precipitation and surface temperature, the subscripts o and l restrict the domain to ocean or land, $\overline{P}$ is the annual mean precipitation (included so as to appropriately weight the relative influences of ocean and land precipitation not related to the annual cycle), and a and b are scaling coefficients that weight the influence of each term. I use the principal component time series for P and T because it captures a leading amount of the variability associated with the annual cycle throughout the tropics. The PCs are plotted in Figure 4.23(c) for both ocean and land, and show the former with a smaller amplitude and larger lag from insolation compared to the latter.

I use the 20th century CMIP5 historical data to find the a and b parameters, using a least-squares regression. Then I apply those parameters to the 21st century rcp8.5 data and compare the changes in seasonality in this model with those in the CMIP5 simulations to ensure that the model works. Finally I measure the contributions of each term to both the phase and the amplitude of land and ocean precipitation by keeping all but one component of the model fixed at historical values and permitting the remaining variable to take on its 21st century value.

Values of a_o ranged from 0.12 to 0.33, while b_o ranged from -0.05 to 0.07 for the different CMIP5 simulations. Negative values of the scaling parameters do not make physical sense as they imply that land interaction delays the ocean precipitation; I consider these models separately. Over land, there are no negative scaling parameters and a_l ranges from 0.02 to 0.07 while b_l ranges from 0.04 to 0.10. That $b_l > a_l$ while $b_o < a_o$ reflects the greater role of the local compared to the remote influence – over land, land surface temperature is more important than SST, while the reverse is true over ocean.

I plot the changes to the amplitude of ocean precipitation in the rcp8.5 scenario as well as the changes estimated by the simple model in Figure 4.11(a), above the horizontal, dividing line. The semi-empirical model is able to capture the amplitude increase for each simulation, though models with $b_o > 0$ underestimate the amplitude increase, while models with $b_o < 0$ overestimate it. The main cause of the changes in the CMIP models, the Clausius-Clapeyron-induced increase in the annual mean moisture, is not directly represented. Instead the semi-empirical model gives an amplitude increase due to an increase in annual mean ocean precipitation and an increase in the amplitude of SST. The latter term is not the main driver of the amplitude increase in ocean precipitation but might be providing a contribution in the coupled models. Next I plot the changes in the phase of ocean precipitation in Figure 4.11(b). Here the semi-empirical model fails to capture the rcp8.5 phase delay as only 17 of 35 models yield a positive delay compared to 29 for CMIP5.

The land results are more promising. For precipitation amplitude over land

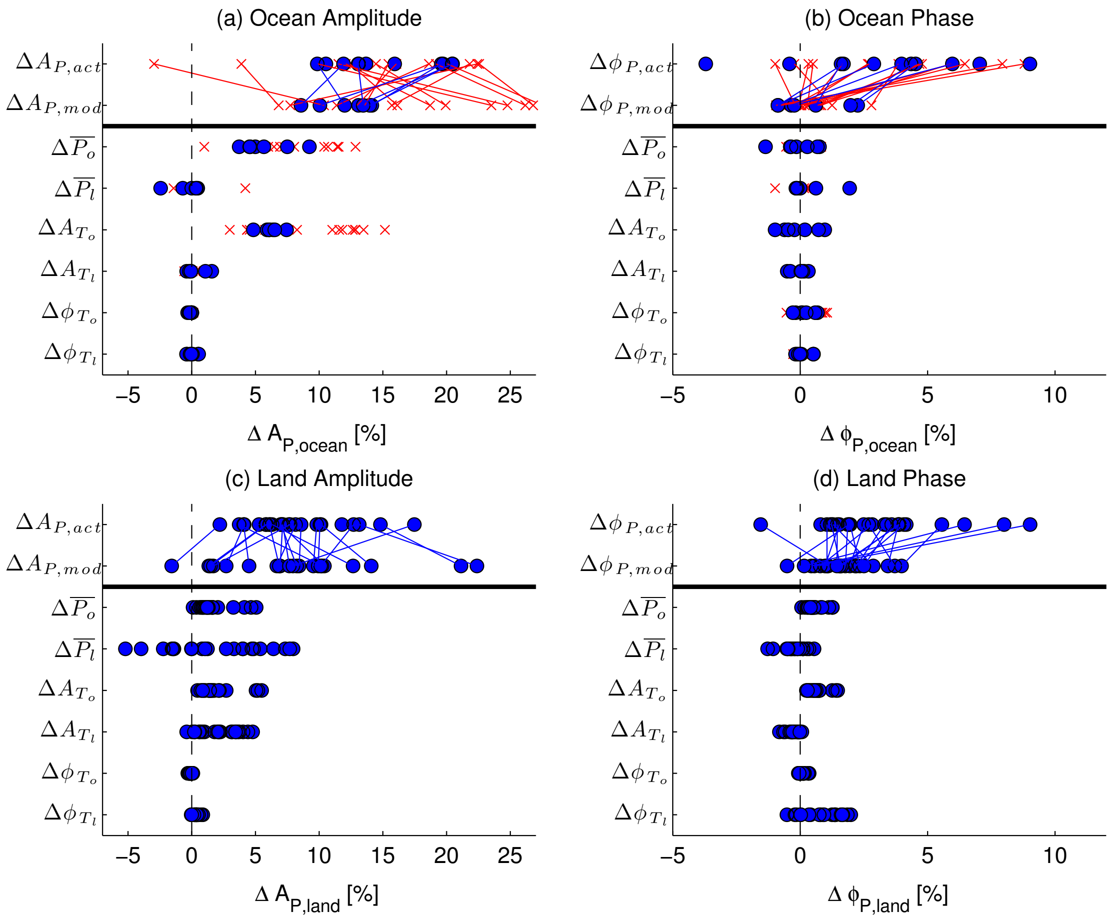

Figure 4.11: Via the model described in Section 4.3, changes in the amplitude of ocean precipitation (a), phase of ocean precipitation (b), amplitude of land precipitation (c), and phase of land precipitation (d) as well as contributions to those changes for various terms over the tropics. Individual models are marked with a circle (or an $\times$ if $b < 0$ in Equations 4.2 or 4.3). The top two rows of each subfigure indicate the actual rcp8.5 changes, and the changes expressed by the model with lines connecting the same models. Data below the dividing line shows the contributions of various terms to the quantity in question.

(Figure 4.11(c)), most simulations in the semi-empirical model give an amplitude increase. Looking at the individual components, the positive contributions come from three terms: an increase in the annual mean ocean precipitation and amplitude increases in SST and land surface temperature. The semi-empirical model is perhaps most informative for the phase delay in land precipitation (Figure 4.11(d)), which the model is able to capture with only a slight underestimation. Several terms contribute including a direct effect from the phase delay in land surface temperature. Changes in the other two terms (annual mean ocean precipitation and the amplitude of SST) operate more indirectly. In the context of this model, both of these terms result in land precipitation responding more to the ocean, rather than land influence. Because the climatological annual cycle of SST is lagged more than the annual cycle of land surface temperature, weighting the ocean term more leads to a phase delay in land precipitation.

While this model is a very simplified representation of precipitation, it links certain processes to changes in the seasonality of precipitation. It suggests that part of the increase in the amplitude of oceanic precipitation might be due in part to an amplitude increase in SST (similar to the results of the p5a10 AGCM simulation with an increased amplitude of SST). Over land, it suggests that both the amplitude of SST and land surface temperature are contributing. Finally for land precipitation, it suggests that that the phase delay is not only responding directly to a phase delay in land surface temperature, but also becoming more oceanic in character, suggesting that to capture the full phase delay of land precipitation, it is necessary to consider effects of both land and ocean surface temperature.

4.4 Aquaplanet Simulations

In the previous section I described a model that allowed changes in surface temperature over land to influence ocean precipitation and changes over ocean to influence land. I found that in the context of a simple model the interaction between the annual cycles of SST and land surface temperature, two sinusoids with different phasing, could give rise to changes in the timing of precipitation. This happened most clearly for the phase delay of precipitation over land. Here I test whether allowing for land-ocean interactions is necessary to produce seasonal changes in precipitation by performing simulations with an aquaplanet, a global climate model with no land or other zonal asymmetries in the boundary conditions.

I performed the aquaplanet simulations using the the atmospheric component (CAM4) of the National Center for Atmospheric Research (NCAR) Community Climate Systems Model, version 4 (CCSM4) (Gent et al., 2011) at the standard resolution ($1.9^{\circ}\times 2.5^{\circ}$), more fully described in Section 3.2. For simplicity, I ran the simulation with prescribed SST, which I calculated from the zonal mean of SST in the CAM4 control simulation described in Chapter 3. While a more idealized SST distribution would make for an even simpler simulation, my choice preserves a realistic seasonal cycle in SST, while maintaining an Earth-like latitudinal distribution of sea ice. The SST for each month of the year is plotted in Figure 4.12. I run the aquaplanet experiments for 10 years each.

The annual mean tropical precipitation in the aquaplanet control simulation is larger than that in the CAM control simulation, perhaps due to more available energy at the surface as a result of a decreased surface albedo. Comparing the thin and thick blue lines in Figure 4.13(a) shows that precipitation in the aquaplanet has a single local maximum around 5°N, while the CAM control experiment has two local maxima around 7°N and 5°S.While the maximum zonal mean precipitation in the aquaplanet is not greater than that in the CAM control simulation, the annual mean is larger from 5°S–5°N and north of 10°N.

The amplitude of the annual cycle of precipitation in the aquaplanet is also different than that in the CAM control (Figure 4.13(b)). In the CAM control

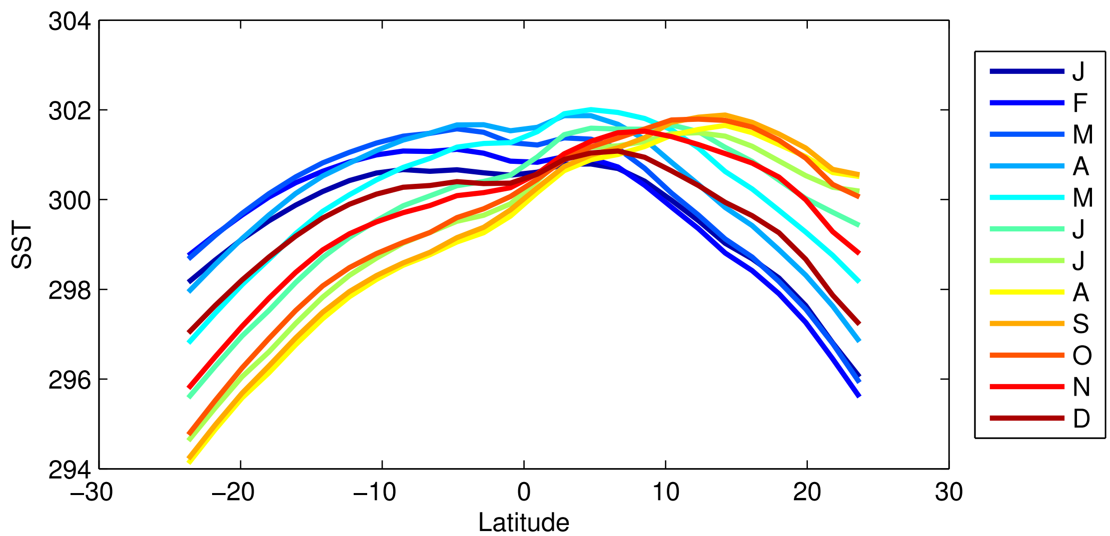

Figure 4.12: The prescribed zonal-mean SST (units of K) for different months of the year in the aquaplanet control simulation.

simulation the amplitude has two broad, off-equatorial peaks and maximizes around 2.5 mm day^{-1}, while the aquaplanet has four distinct local maxima and an absolute maximum of around 4 mm day^{-1}. This structure occurs because the aquaplanet has a double ITCZ for several months of the year that shifts meridionally with the seasonal cycle and has different phasing than that of the CAM control simulation (Figure 4.13(c)).

I also performed simulations in which I uniformly increased the SST by 3K at all locations for all months of the year, analogous to the UW+3K experiments described in Chapter 3. As in that experiment, the annual mean precipitation increases throughout the tropics, here by 0.4 mm/day on average (compare the blue and green thick lines in Figure 4.13(a)). Additionally the amplitude of the annual cycle of precipitation increases. Figure 4.13(b) shows that this occurs throughout the entire tropics. This increase is expected based on the mechanism identified in Chapter 3, that an annual mean increase in the vertical gradient of water vapor coupled with the seasonally shifting upwelling branch of the Hadley Cell results in

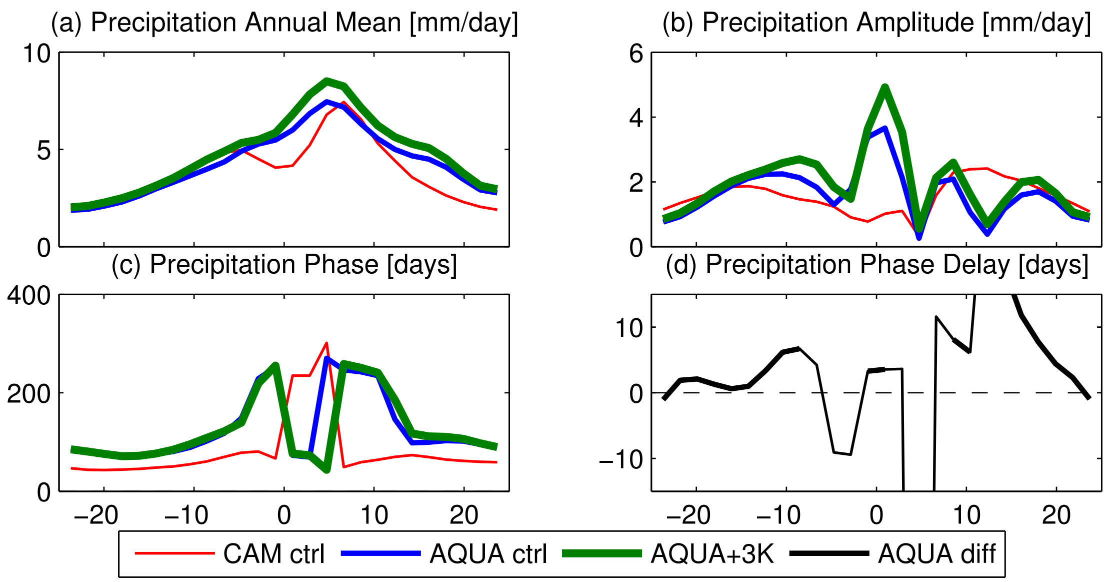

Figure 4.13: The annual mean (a), amplitude (b), phase relative to insolation (c), and phase delay (d) of precipitation in different simulations with prescribed SST. The thin, red line in (a), (b), and (c) show values for the CAM control experiments described in Chapter 3, while the thick, blue line represents the aquaplanet control simulation and the thick, green line represents the aquaplanet experiment with a uniform SST warming of 3K. The phase delay in (d) is the change in phase between the aquaplanet control and the aquaplanet experiment with 3K warming with the thick line indicating where the annual cycle represents at least 50% of the total variance.

an increase of summer precipitation and a slight decrease of winter precipitation. Land or zonal asymmetries are not necessary for that mechanism to work. The amplitude of tropical precipitation increases by 26.7% in the AQUA+3K experiment, compared with 18.1% in UW+3K experiment, as calculated via EOF analysis.

There are also changes in the phase of precipitation in the aqua+3K. Figure 4.13(d) shows a phase delay wherever the annual cycle of precipitation is strong in the tropics. Calculated by EOF analysis, the phase delay is 6.8 days in the aqua+3K simulation, compared with 5.1 days in the UW simulation with the same SST forcing. That the precipitation phase delay occurs without any seasonal changes in SST in the aquaplanet indicates that land is not necessary to produce this phenomenon. However, it does not rule out the possibility that land-ocean interactions play a larger role in producing a precipitation phase delay in more Earth-like simulations for two reasons. One is that the semi-empirical model identified land-ocean interaction as playing a key role for the phase of land precipitation, not ocean precipitation. The second is that the annual cycle of tropical precipitation is very different in the aquaplanet simulation than in the CAM control simulation or in the actual climate.

4.5 Dry Dynamical Model Results

The final model I study in this chapter is the spectral version of the dynamical core of the Geophysical Fluid Dynamics Laboratory (GFDL) Flexible Modeling System (FMS) with T42 resolution (Held and Suarez, 1994). This model is simpler than an AGCM or aquaplanet allowing for easy testing of parameter dependencies. This atmospheric model relaxes temperature toward a radiative equilibrium temperature, given by the following equation at the lowest model level,

$$T_s^e(\phi) = \overline{T}_s^e + \Delta_h \cos^2 \phi, \tag{4.4}$$

where $\overline{T}_s^e = 280K$ is the global mean surface temperature, $\Delta_h = 60\text{K}$ is the equator-to-pole temperature difference, and ϕ is latitude (there is no topography or other zonal asymmetries in the boundary or forcing). The radiative equilibrium temperature in the troposphere is given by:

$$T^e(\phi, p) = T_t^e \left[1 + d_0(\phi) \left(\frac{p}{p_0} \right)^{\alpha} \right]^{1/4}, \tag{4.5}$$

where $T_t^e = 200\text{K}$ is the skin temperature at the top of the atmosphere and the equilibrium temperature in the stratosphere, p is pressure, p_0 is the surface pressure, and $\alpha = 3.5$ controls the lapse rate and is the ratio of the pressure scale height to the pressure scale height of infrared absorbers, and

$$d_0(\phi) = \left(\frac{T_s^e(\phi)}{T_t^e}\right)^4 - 1. \tag{4.6}$$

Further description of the details of this model are contained in Schneider (2004). The model has been modified to better represent the tropical circulation by adding a dry convection scheme that mimics the effect of latent heat release (Schneider and Walker, 2006). The convection scheme relaxes temperatures towards profiles with a specified convective lapse rate of $\Gamma = \gamma\Gamma_d$, where γ is a rescaling parameter and $\Gamma_d = g/c_p = 9.8$ K km^{-1} is the dry adiabatic lapse rate. I add an idealized seasonal cycle to the equilibrium temperature of the form:

$$T^e(\phi, p, t) = T^e(\phi, p)\left(-A_T \sin\phi \cos(\omega t - \phi_T)\right), \tag{4.7}$$

where $A_T = 20$K, $\phi_T = 0$ days, and $\omega = 2\pi$ year^{-1} are the amplitude, phase, and angular frequency, respectively, and $\sin\phi$ gives the amplitude a monotonic increase with latitude and no annual cycle directly at the equator.

I run each model simulation including the control simulation for 20 years, sufficient time for the model to equilibrate (verified by the lack of hemispheric asymmetry in the results). Before discussing the model results, I verify that the climatology of the model is realistic by plotting the zonally-averaged amplitude and phase of the annual cycle and the annual mean of the control run in Figure 4.14 for the (imposed) equilibrium temperature, the actual temperature, zonal wind U, meridional wind V, and vertical velocity ω.

While I imposed an amplitude of 20K for T_{eq}, the amplitude of T is less than half as strong. The model simulates a realistic climatology, with two zonal jets that shift meridionally following the annual cycle of insolation. In this configuration,

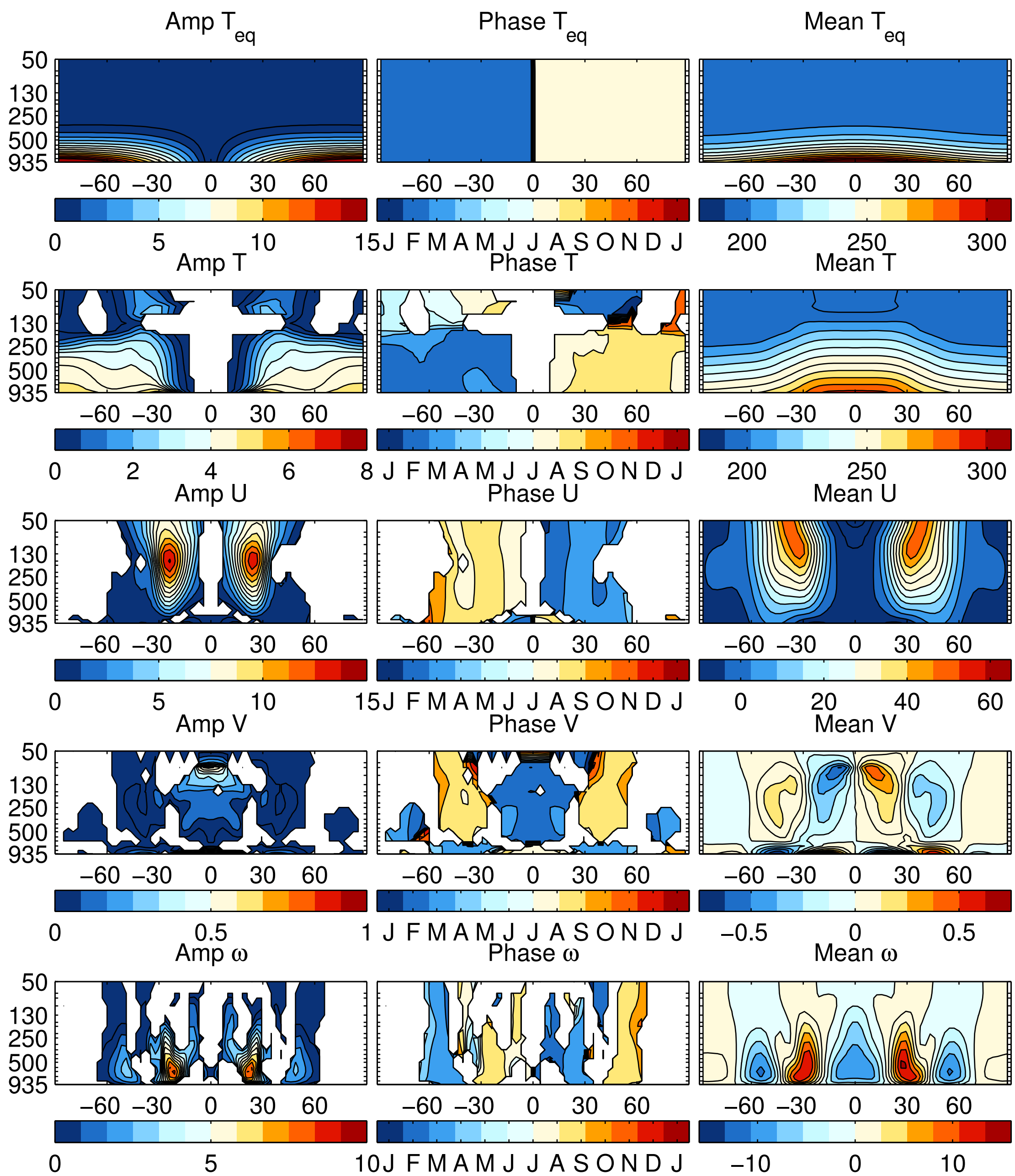

Figure 4.14: The amplitude (left column), phase (middle column), and annual mean (right column) of the dry dynamical model's control simulation for (top to bottom): equilibrium temperature (K), temperature (K), zonal wind(m/s), meridional wind (m/s), and vertical velocity (Pa/s). The color for the phase plots indicates the month that the annual cycle attains its maximum value. For amplitude and phase, only locations for which the annual cycle makes up at least 80% of the total variance are plotted.

the model is also able to capture a Hadley Cell-like circulation in both the annual mean and throughout the annual cycle. The strongest amplitude of V occurs right on the equator around 100 hPa, where the wind shifts from northerly to southerly when insolation maximizes in the Southern and Northern hemispheres, respectively. The annual mean vertical velocity is strongest upwards in the deep tropics, flanked by subsidence regions in the subtropics in each hemisphere. But the strongest amplitude of vertical velocity maximizes in the lower troposphere around 20°, where the annual mean vertical velocity is zero. Air in this region is ascending during the summer and subsiding during the winter.

I use EOF analysis to study changes in the annual cycle with the dry dynamical model as in previous studies (Kutzbach, 1967; Biasutti and Sobel, 2009; Dwyer et al., 2012, 2014). The EOF spatial loading patterns in Figure 4.15 reflect those calculated by Fourier Transform in Figure 4.14. For example, T_{eq}, T, U, and ω all have an anti-symmetric spatial structure across the equator and their leading PCs (Figure 4.15) capture the annual cycle as they are sinusoids with periods of one year. V is symmetric about the equator, reflecting a sign change over the seasonal cycle as the convecting region of the Hadley Cell shifts back and forth across the equator. In these simulations, the origin of the seasonal forcing comes from the imposed seasonal cycle of T_{eq} since there is no direct solar absorption in the atmosphere or land or ocean surface. The variables reflect this forcing homogeneity as T, U, V, and ω are all in phase with each other and have a slight phase lag compared to T_{eq}.

I change various parameters in this model in similar ways as are projected to change in the CMIP models and study the seasonal response. These changes include an increase in the annual mean surface temperature $\overline{T}_s^e$, a reduced pole-to-equator temperature gradient Δ_h, a uniform atmospheric warming T^e, and an increased upper-tropospheric, tropical warming. Somewhat surprisingly the model

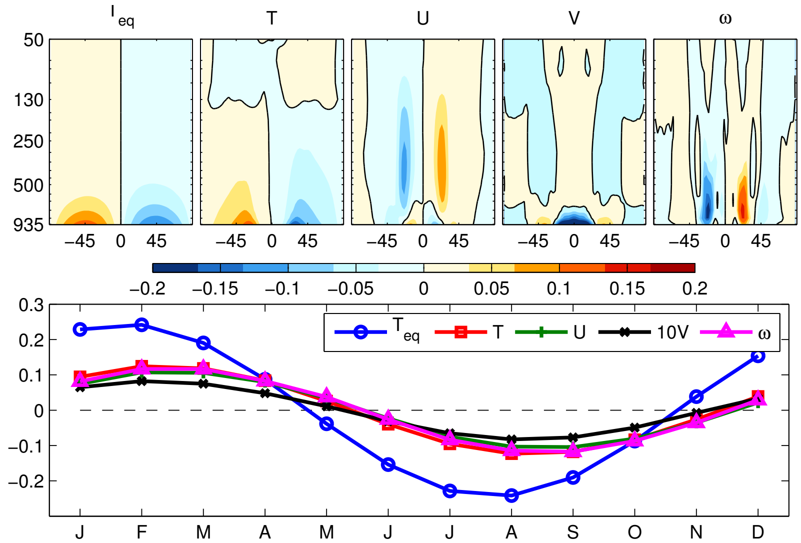

Figure 4.15: The leading empirical orthogonal functions (top) and principal components (bottom) for different variables in the dry dynamical model's control simulation. All variables are plotted on the same scale, but have different units (K for T_eq and T, m/s for U and V, and Pa/s for ω). Note that V is multiplied by a factor of 10.

simulates an amplitude increase and a phase advance in the annual cycle of vertical motions for all of these changes. Only one parameter whose dependence I tested, the atmospheric stability, produced seasonality changes of the sign projected by the coupled models. Because the temperature of the tropical troposphere can be approximately represented by a moist adiabat (Xu and Emanuel, 1989), surface warming leads to greater warming aloft in the tropics resulting in an increase in atmospheric stability.

All of the 21st century rcp8.5 CMIP5 simulations agree with this result. Figure 4.16 shows the lapse rate, defined as $\Gamma = -dT/dz$ and calculated by averaging data at each level between 45°S and 45°N and performing a least-squares regression on temperature and geopotential height over seven levels from 850 hPa to 250 hPa. The multimodel mean decrease in the lapse rate is 0.41 K/km, with all of the models agreeing on the sign of the change, ranging from 0.23 K/km to 0.63 K/km,

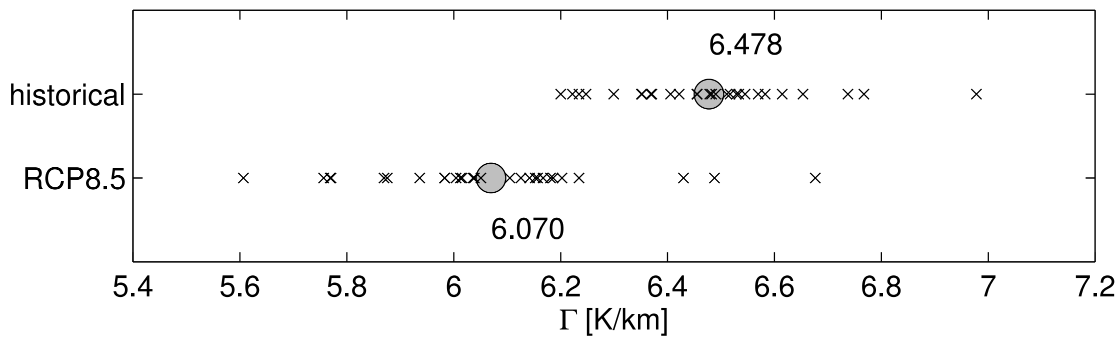

Figure 4.16: The lapse rate in CMIP5 runs calculated over 45°S–45°N and 850 hPa–250 hPa, as described in the text. Individual models are depicted with a $\times$, and the multimodel mean is plotted with a large gray circle and its value is given in the figure.

resulting in a more stable tropical atmosphere.

By modifying γ, the parameter that controls the lapse rate, I can change the stability of the atmosphere in the simulations. Smaller values of γ simulate greater latent heat release for convecting parcels and consequently warm the upper troposphere more, resulting in a stabler troposphere. The value of γ in the control simulation is 0.6. (By comparison $\Gamma/\Gamma_d = 0.661$ in the historical CMIP5 simulation). I tested the sensitivity of the seasonal cycle by running 14 simulations of twenty years each with γ varying from 0.5 to 0.7. The results, where the phase and amplitude of key variables is calculated from the leading principal component, are shown in Figure 4.17.

The seasonal cycle of most variables is sensitive to the atmospheric stability. In particular, the variables with EOF loading patterns that best represent the tropical circulation, V and ω, have a monotonic amplitude decrease as a function of decreasing γ (increasing stability). As γ decreases over a range of roughly 2 K/km, A_V and A_ω decrease by 40 percentage points. The other variables are less sensitive, with A_T and A_U showing no change for $\gamma > 0.6$ and a modest decrease for $0.5 \leq \gamma \leq 0.6$.

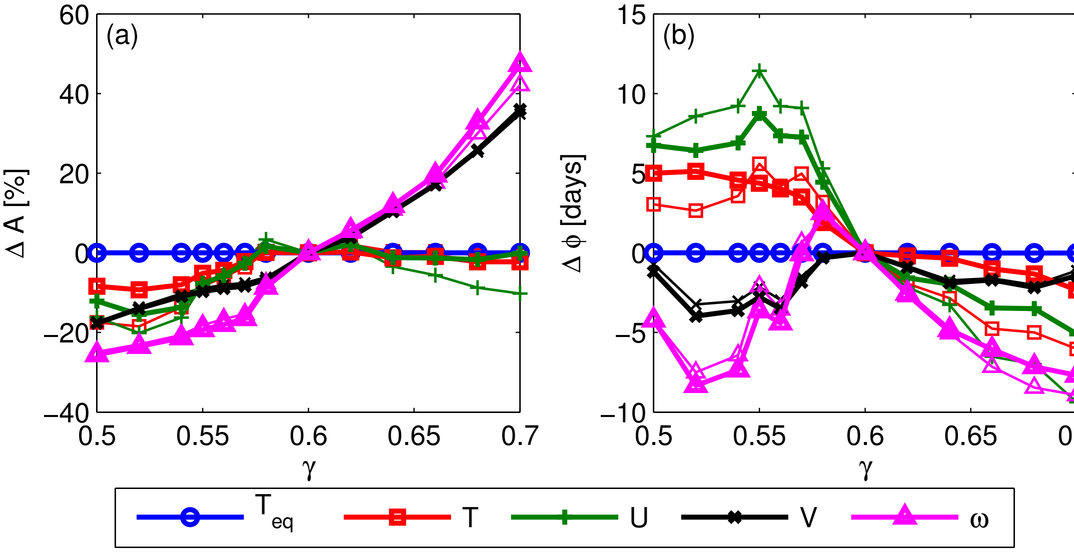

Figure 4.17: Changes in the amplitude (a) and phase (b) of the annual cycle as a function of changing the lapse rate scaling parameter γ, in the dry, dynamical simulations. Changes in the annual cycle of the equilibrium temperature, temperature, zonal wind, meridional wind, and vertical velocity are plotted with different colors and markers. Thin lines represent an EOF analysis in which the domain was constrained equatorward of 30°, while thick lines are for an EOF with no latitudinal bounds.

The behavior of ϕ_V and ϕ_ω (Figure 4.17(b)) is more complex. For $0.58 \leq \gamma \leq 0.7$, ω and to a lesser extent V have a phase delay for decreasing γ. Over this range, ϕ_ω delays by around 10 days, while ϕ_V delays by a couple days. For $0.50 \leq \gamma \leq 0.58$, these variables begin to advance and display non-monotonic behavior. ϕ_T and ϕ_U respond in a more straightforward manner, with delaying phase for decreasing γ over most of the parameter range, leveling off for small values of γ. The results here are mostly insensitive to whether the EOF analysis is performed over the tropics only or without any restriction on the latitudinal domain, as indicated by the similarity of the thick and thin lines in Figure 4.17.

Over the values corresponding to γ in the historical and rcp8.5 simulation (0.65 and 0.61, respectively), the dry dynamical model has an amplitude decrease in V and ω of about 10% and a phase delay of 5 days for ω and 2 days for V. These results

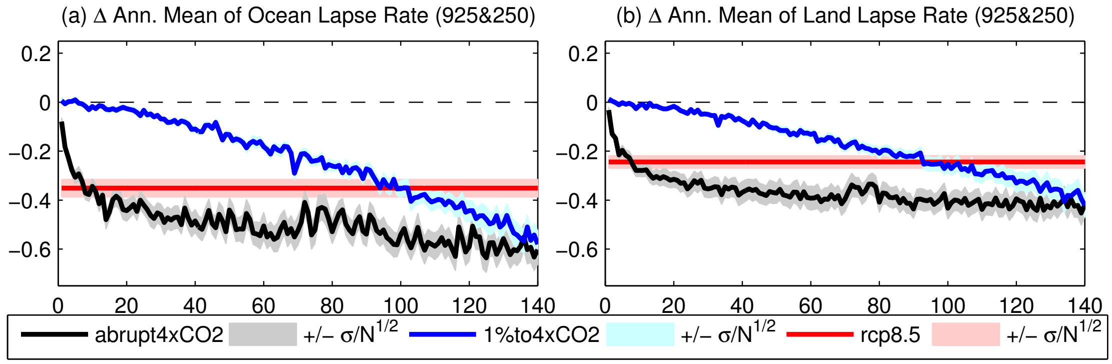

Figure 4.18: As in Figure 4.2, for the annual mean lapse rate in units of K/km calculated at 925 hPa and 250 hPa as described in the text.

compare favorably with the rcp8.5 changes in V ($\Delta A = -2.3\%$, $\Delta\phi = 1.6$ days) and ω ($\Delta A = -6.1\%$, $\Delta\phi = 3.5$ days), suggesting that changes in the atmospheric stability could potentially be affecting the seasonality of the tropical circulation in the CMIP5 models too, though the potential mechanism is unclear.

Next I test whether changes in lapse rate might be driving changes in seasonality in the CMIP5 abrupt simulation. In that simulation, some of the seasonality changes in temperature, precipitation, and vertical motion occur nearly instantly. If changes in stability are responsible for these changes in the abrupt simulation, they must also happen nearly instantaneously.

I examine the atmospheric stability via the lapse rate $\Gamma = -\Delta T/\Delta Z$, calculated at two levels (925 hPa and 250 hPa) for simplicity and plotted in Figure 4.18. In both the abrupt and 1% runs, the lapse rate decreases by around 0.5 K/km over ocean and 0.4 K/km over land, exceeding the changes in the rcp8.5 simulation. But the time scale of the changes in stability echo that of the annual mean surface temperature, far slower than the seasonality changes in the other variables. Since the seasonality changes in precipitation (excluding amplitude over ocean) do not continue to change after a decade or two, changes in atmospheric stability cannot explain those of precipitation in these simulations.

4.6 Summary and Discussion

In this chapter, I use models of varying complexity to gain a better understanding of projected seasonality changes due to increased greenhouse gases in tropical surface temperature, tropical precipitation, and vertical motion. These models project a phase delay in each of these quantities over both ocean and land, an amplitude increase for precipitation and SST, and an amplitude decrease for vertical motion.

Each of the models provides insight into some aspects of these projected changes. The CMIP5 simulations with an instantaneous CO_2 increase establish temporal order and provide links between different variables. The semi-empirical model suggests that, among other things, the phase delay in land precipitation is partly a result of ocean influencing land precipitation to a greater degree. The aquaplanet runs show that the phase delay over ocean can occur even without land. Finally, the dry, dynamical model suggests that the projected changes in the seasonality of vertical motions can result from increased atmospheric stability. Below I use the results of all of these models and previous work to relate the seasonality changes in the different variables.

The amplitude of the annual cycle of vertical motion is projected to decrease over both land and ocean. Previous work has found a weakening in the annual mean (Knutson and Manabe, 1995; Vecchi and Soden, 2007) that has been attributed to a faster increase in lower-tropospheric water vapor (7%/K) compared to precipitation (2%/K) (Held and Soden, 2006), which is perhaps limited by a slow increase in surface radiation (Hartmann and Larson, 2002; Larson and Hartmann, 2003). A weaker annual mean is consistent with a weaker annual cycle because both the speed of updrafts and subsidence weakens (Bony et al., 2013). In the abrupt simulation with instantaneously quadrupled CO_2, the circulation abruptly decreases faster over ocean than over land, where it actually increases for the first few years of the simulation before decreasing.

The amplitude of precipitation over ocean increases as a thermodynamic consequence of tropical mean temperature increase (Dwyer et al., 2014). An enhanced moisture gradient leads to increased precipitation when coupled with the seasonally shifting Hadley Cell. This effect would be even larger if not for the decrease in the amplitude of vertical motion, which partially compensates for this thermodynamic effect.

Unlike ocean, the amplitude of precipitation over land increases instantly in response to an abrupt CO_2 increase. One possible cause is a dynamic increase in the amplitude of precipitation over land, but this does not explain the behavior throughout the run since the amplitude of vertical velocity decreases after the initial increase. Another possibility is the thermodynamic effect of an annual mean water vapor increase as occurs over ocean, but this effect occurs slowly and cannot explain the amplitude increase in the first few years. While neither mechanism can explain the behavior entirely on its own, a combination of the two would account for both the instantaneous increase and the steady state behavior in the amplitude of land precipitation. Further support for this idea comes from Figure S1 of Bony et al. (2013), which slows changes in annual mean precipitation decomposed into thermodynamic and dynamic components in land convective regimes in the abrupt simulation. Initially the thermodynamic component is negative but increases with time, while the dynamic component is positive, but decreases with time. The combination of these two terms yields an increase in precipitation with relatively little time dependence.

The amplitude of the annual cycle of surface wind speed increases over both ocean and land. These changes are a consequence of at least two factors – weaker summer subtropical easterlies (Sobel and Camargo, 2011) and an expansion of the Hadley Cell, primarily in the winter, which extends the region of subtropical easterlies poleward (Gastineau et al., 2008). This increase in the amplitude of surface winds may be responsible for increasing the amplitude of surface temperature. The terms are linked via the surface latent heat flux and are of the right sign to account for one another if various other terms do not change (latent heat, air-sea humidity difference, and the other surface flux terms). But these other terms do change, complicating the relationship. Still, the nearly instantaneous increase in amplitude of both of these terms in the abrupt simulation suggests that they are linked in some complex manner.

The CMIP models project a phase delay to most tropical fields, with the notable exception of SST. It is unclear what is responsible for these delays. Results from a dry, dynamical model show that an increase in the atmospheric stability causes a phase delay of the tropical circulation. But stability increases at a slower rate than the phase of vertical velocity in the abrupt simulation, suggesting it is not forcing the phase delay in the CMIP models. Whatever the cause is, it must be robust since it occurs in an atmospheric model when the surface temperature is uniformly increased (Dwyer et al., 2014) and even in an aquaplanet with zonally symmetrical boundary conditions. The result of the phase delay in vertical motions is a phase delay in precipitation over both ocean and land. (Land precipitation may also be responding to factors which make it more oceanic in character). The delay in vertical motion also results in a phase delay in the annual cycle of surface wind speed.

The phase of surface temperature has a delay over land, but no delay over ocean in the CMIP5 models, while the phase of the surface wind has a delay over ocean, but no delay over land, suggesting that the surface wind speed changes are not driving the phase of surface temperature in the same way as for amplitude. One potential clue to the phase delay of surface temperature over land is that the delay in the first few years of the simulation is larger than its steady state value. Another variable with similar behavior is the amplitude of vertical velocity over land, which initially increases before decreasing. This behavior is likely due to an increase of mass convergence because of the much greater warming over land than ocean in the first few years (Bony et al., 2013). If this mass convergence persists throughout the simulation (as might be expected based on the greater temperature rise over land throughout the entire simulation), land may be becoming more oceanic in its phase character (i.e., delayed). Further work is needed to test this effect.

4.7 Appendix

Included here are several figures showing the time series of the changes in the amplitudes of surface latent heat flux (Figure 4.19) and total surface flux (Figure 4.20) as well as changes in the phases of surface latent heat flux (Figure 4.21) and total surface flux (Figure 4.22). Also included are the leading EOF and PC for surface temperature (Figure 4.23), precipitation (Figure 4.24), vertical velocity at 500 hPa (Figure 4.25), surface wind speed (Figure 4.26), surface latent heat flux (Figure 4.27), and total surface flux (Figure 4.28).

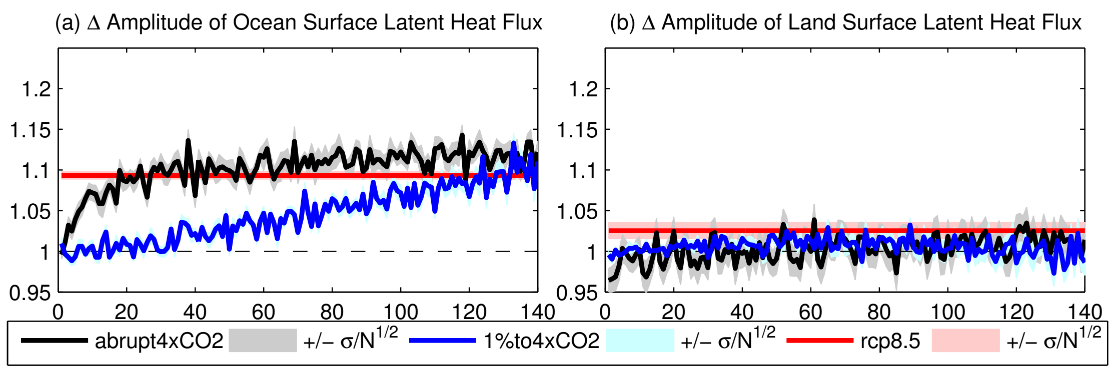

Figure 4.19: As in Figure 4.8, but for the amplitude of the surface latent heat flux.

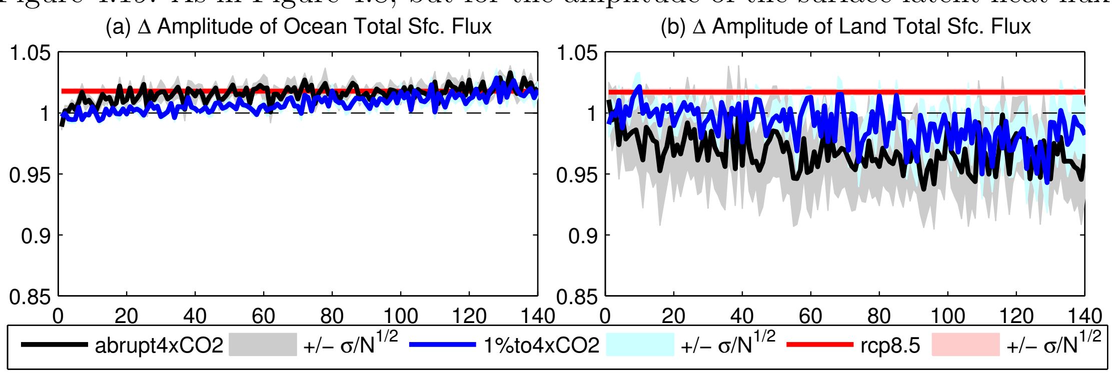

Figure 4.20: As in Figure 4.8, but for the amplitude of the total surface flux (shortwave and longwave radiation and latent and sensible heat flux).

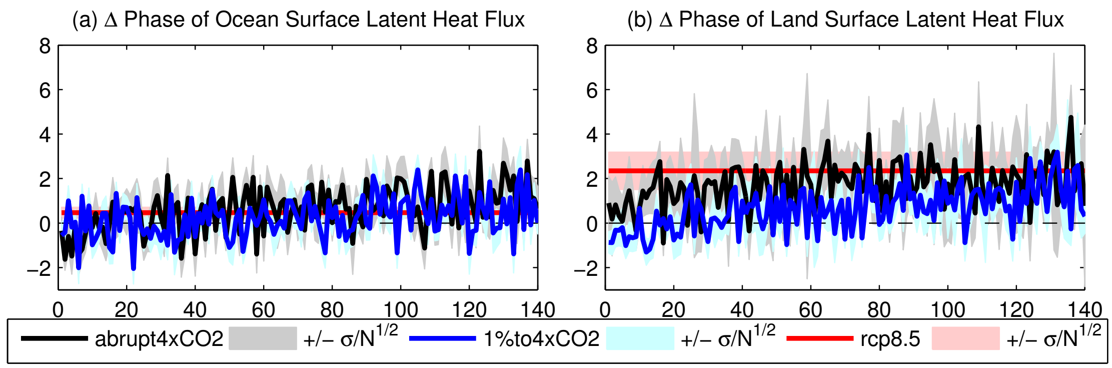

Figure 4.21: As in Figure 4.9, but for the phase of the latent heat flux).

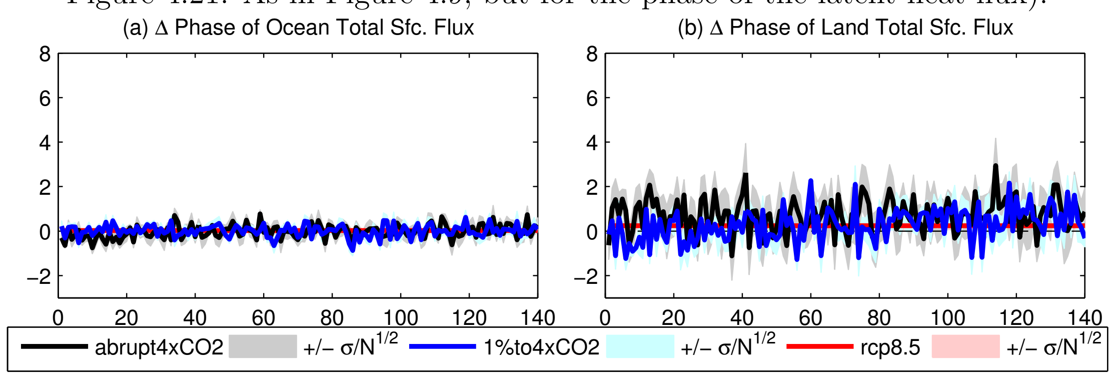

Figure 4.22: As in Figure 4.9, but for the phase of the total surface flux (shortwave and longwave radiation and latent and sensible heat flux).

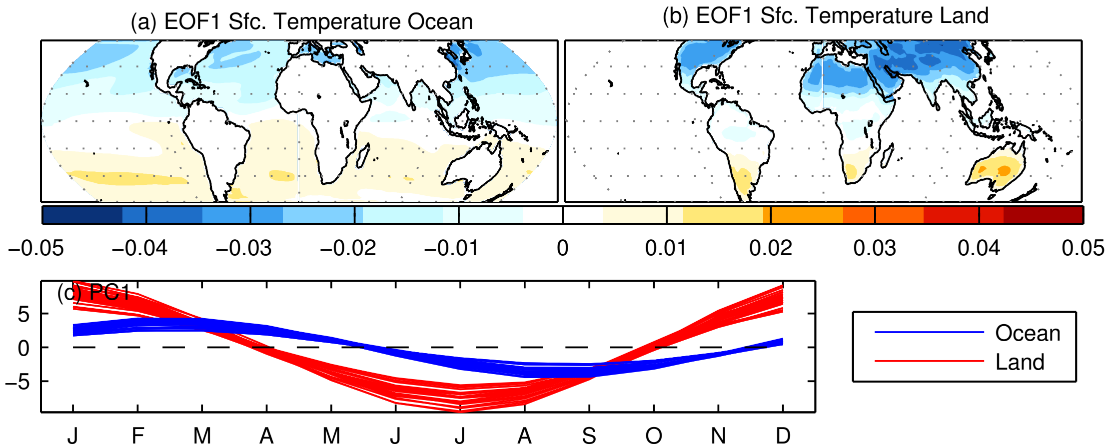

Figure 4.23: The leading EOFs for ocean (a) and land (b) and their corresponding PCs (c) for surface temperature in the pre-industrial control simulations described in Section 4.2.

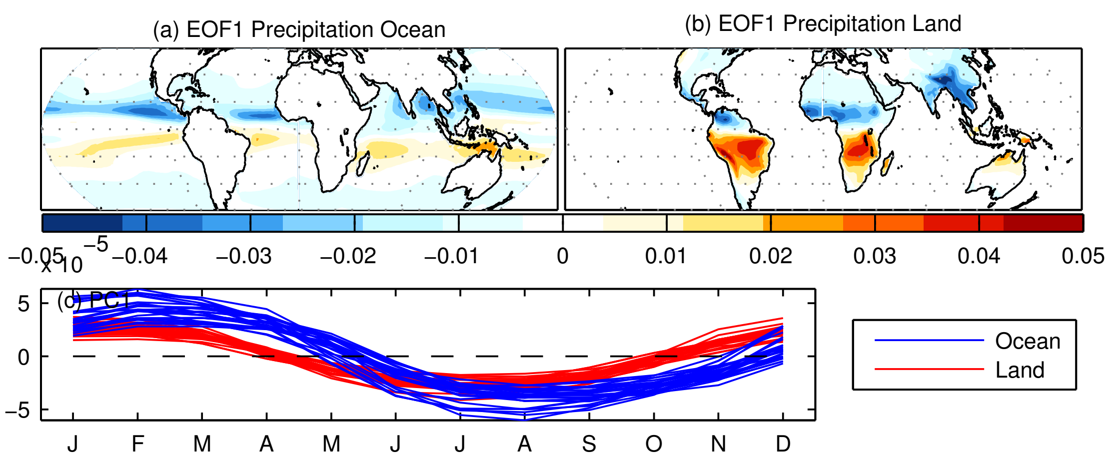

Figure 4.24: As in Figure 4.23 but for precipitation.

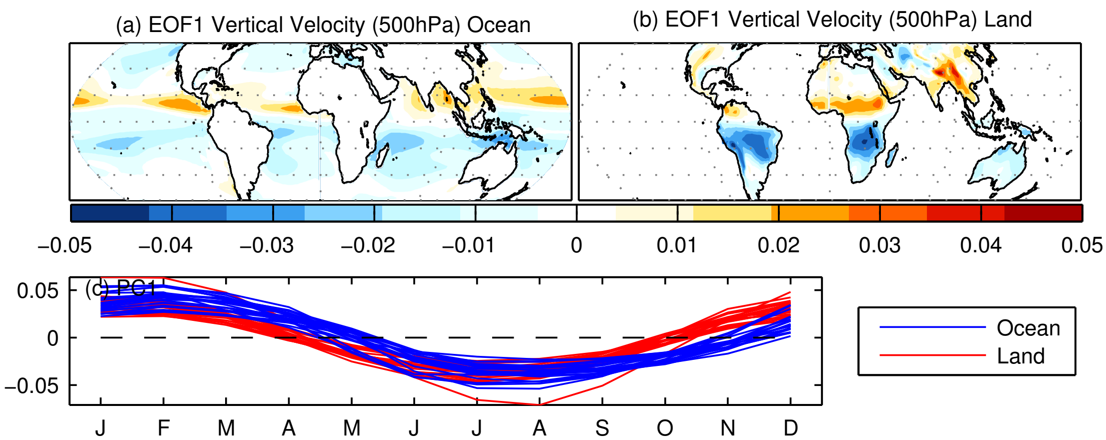

Figure 4.25: As in Figure 4.23 but for vertical velocity at 500 hPa.

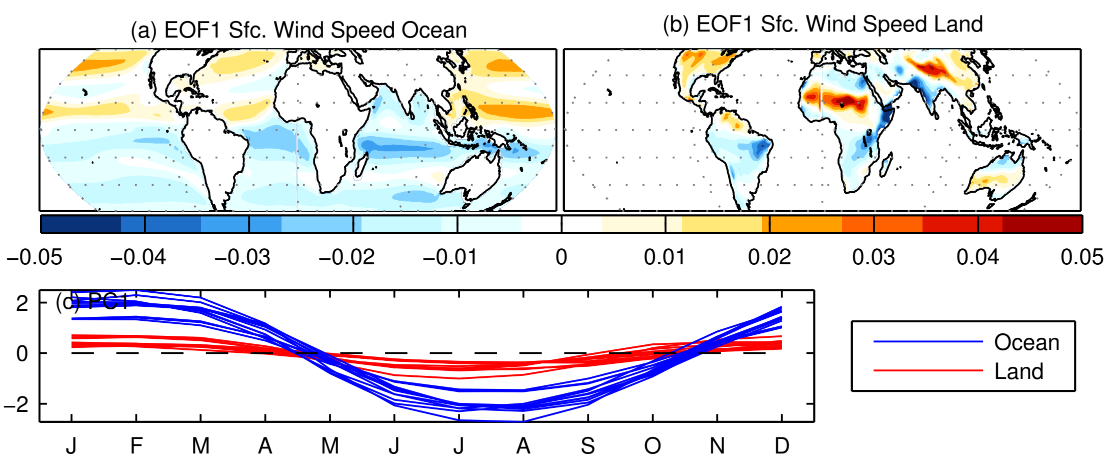

Figure 4.26: As in Figure 4.23 but for surface wind speed.

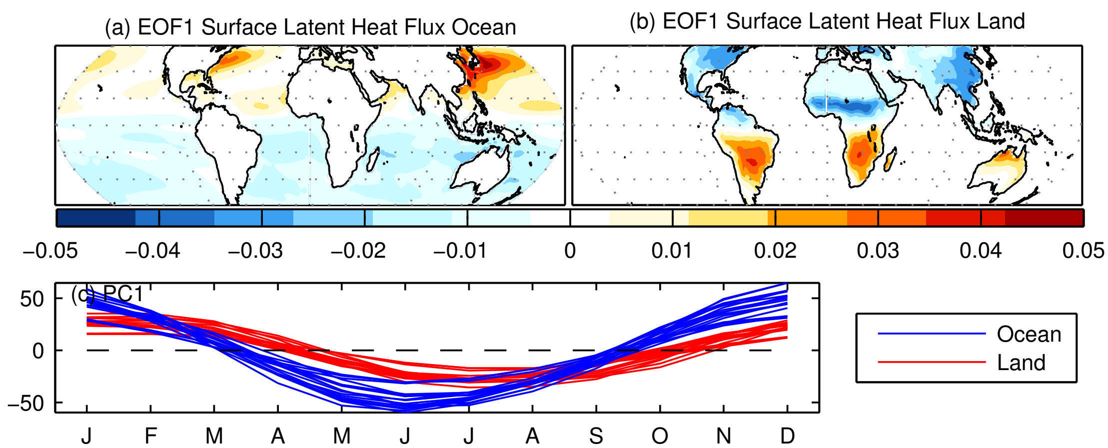

Figure 4.27: As in Figure 4.23 but for surface latent heat flux.

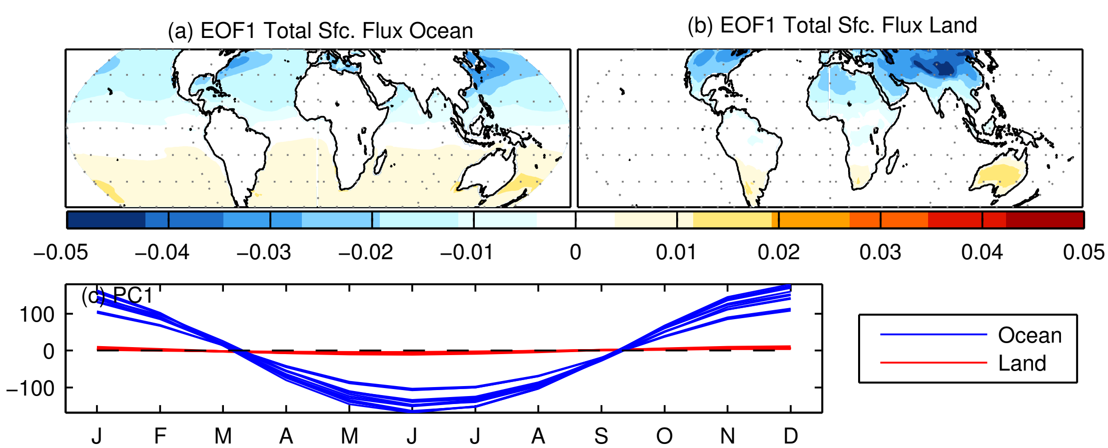

Figure 4.28: As in Figure 4.23 but for total surface flux.

Chapter 5

Conclusion

In this thesis I have focused on describing and understanding projected changes in the annual cycle of key atmospheric variables due to increases in greenhouse gases and other anthropogenic effects on the atmosphere. These changes, a delay in the phase and decrease in the amplitude of surface temperature at high latitudes, a delay in the phase and increase in the amplitude of surface temperature and precipitation at low latitudes, and a delay in the phase and decrease in the amplitude of the tropical circulation, are projected in response to greenhouse gas increases by nearly all of the global climate models in the most recent model intercomparison suites (CMIP3 and CMIP5). In the previous chapters I detailed these changes, studied their relationship and analyzed the processes at work.

In Chapter 2, I focused on the projected changes in surface temperature near the poles and in the tropics, two regions with a different character of seasonality changes. In the high latitudes, every climate model projects an amplitude decrease and a phase delay in the annual cycle of surface temperature. These changes are a consequence of melting sea ice in response to global warming (Manabe and Stouffer, 1980; Mann and Park, 1996; Biasutti and Sobel, 2009). Melting sea ice thins and removes the insulating buffer at the surface, better coupling the atmosphere and ocean. As a result the large heat capacity of the mixed layer ocean is less isolated from the atmosphere and the surface temperature's response to insolation is damped and sluggish. At low latitudes the models also project a phase delay, and an amplitude increase, rather than a decrease. Such changes cannot be mainly a result of changes in heat capacity (otherwise there could not be a delay and an amplitude increase) but I find that they are linked to changes in the annual cycle of surface flux, partly based on a strong spatial correlation of subtropical ocean grid points with phase delays in both annual cycles and amplitude increase in both annual cycles.

Next in Chapter 3, I study the projected amplitude increase and phase delay in the annual cycle of tropical precipitation and its potential link to changes in the annual mean and annual cycle of temperature. I begin by corroborating previous studies that found a hemispheric seasonal asymmetry in precipitation in the CMIP models (Chou et al., 2007; Chou and Tu, 2008; Tan et al., 2008; Chou and Lan, 2011; Huang et al., 2013). These models identified the cause as an annual mean increase in the vertical gradient of water vapor imprinted onto the seasonal cycle by the ascending branch of the Hadley Cell, located in the summer hemisphere. I verify this mechanism by Fourier transforming the moisture budget. My analysis shows a decrease in the annual cycle of vertical motion, a dynamical effect that partially compensates the thermodynamically-driven amplitude increase in precipitation. The cause of the phase delay in precipitation is not as clear as the amplitude increase, but the moisture budget analysis links it to a delay in the phase of the annual cycle of vertical motion. I study this behavior by performing two sets of atmospheric model simulations with prescribed ocean surface temperature. In the first simulation, I increase the annual mean SST by 3 K at all locations for all months of the year, while in the second set I leave the annual mean SST unchanged but apply a phase shift and/or an amplification to the annual cycle of SST. The

CMIP results much better resemble the "uniform warming" simulation than the simulation with a delayed phase and increased amplitude of SST. Interestingly, even without any phase delay in SST, the uniform warming simulation produces a phase delay in precipitation. The modified seasonality simulations are also informative as they show that a delayed annual cycle of SST produces a delayed annual cycle of precipitation and a stronger annual cycle of SST produces a stronger annual cycle of precipitation. Furthermore there are cross effects in these simulations – a delayed annual cycle of SST leads to a weaker annual cycle of precipitation while a stronger annual cycle of SST leads to a delayed annual cycle of precipitation.

Finally in Chapter 4, I analyze the results of four simulations of varying complexity to better understand the mechanisms and links between the projected changes in seasonality in tropical precipitation, circulation and temperature. These simulations include CMIP5 models with idealized forcings, a semi-empirical model to study land-ocean interactive effects, an aquaplanet simulation, and a dry, dynamic model. Each model provides different insights about the links between and potential mechanisms leading to the seasonality changes, especially when studied in the context of previous results. The results suggest that the amplitude decrease in vertical motion is a manifestation of the annual mean decrease on seasonal time scales (Bony et al., 2013). This dynamical change weakens, but does not overcome the thermodynamically-driven amplitude increase in precipitation, especially over ocean. Over land, an increase in low-level convergence due to relatively greater warming increases the amplitude of precipitation on a very fast time scale. A weaker amplitude of tropical circulation coupled with an expansion of the winter Hadley Cell (Gastineau et al., 2008; Kang et al., 2013) increase the amplitude of the annual cycle of surface wind speed. This term enters the surface latent heat flux equation and likely leads to the increase in the annual cycle of surface temperature (Sobel and Camargo, 2011). The mechanism responsible for the phase delays is not yet fully understood, but it results in a phase delay in the annual cycle of vertical motions. As tropical precipitation is strongly tied to the circulation, this delay is directly communicated to precipitation, especially over ocean. Over land, precipitation may be responding more to the remote influence of SST than to the local influence of land temperature, leading to a delay since SST has a larger lag from insolation than land surface temperature. In the most recent model intercomparison suites (CMIP5), the phase delay of SST is much smaller than in an earlier suite (CMIP3) and does not seem to be driving changes in any variable. In CMIP5, there is still a delay in land surface temperature, which may be partly attributable to increase low-level convergence, making the land more oceanic in character.

While the focus of this work is on the annual cycle, the research is linked to many other problems in climate dynamics. The projected seasonality changes in surface temperature at high latitudes offer clues to the processes involved in Arctic Amplification. The projected weaker annual cycle of the tropical circulation is the seasonal manifestation of the weaker annual mean tropical circulation found in previous work, but affects the Hadley Cell and not just the Walker Cell. While the driving force behind the weaker circulation is an open question, this work shows that the changes occur on seasonal time scales too. Finally, the phase delays in tropical precipitation, vertical motion, and land temperature illustrate the interdependencies of tropical variables, though the proximate cause of the delays is not yet fully understood.

This work also prompts a number of questions motivating future work. These include detailing the exact connection between the projected increase in the amplitude of surface wind speed and the amplitude of surface temperature, whether and how changes in the land-sea temperature contrast could be delaying the phase of land variables, and a determination of the cause of the phase delay in the annual cycle of vertical motion.

There is evidence for a connection between the increases in the amplitudes of surface wind speed and surface temperature. Previous work has suggested that the two affect each other via the surface energy balance, most likely through the latent heat term (Sobel and Camargo, 2011; Dwyer et al., 2012). Both surface wind speed and temperature increase nearly instantaneously in the abrupt simulation. To fully understand the connection, though, it seems likely that a full surface energy balance decomposition must be performed. This will involve taking the Fourier transform of all of the surface flux terms and looking at their balance with the heat storage term. If the driving force comes from the latent heat term, it can then be decomposed into thermodynamic and dynamic components. I suspect that the dynamic (wind-driven) aspect component is driving the changes, though other effects like cloud radiative forcing cannot be completely ruled out.

This work suggested that one possible cause of the phase delay in land surface temperature and land precipitation was a greater oceanic influence over land. Because the annual cycle of ocean temperature has a greater phase lag from insolation than land temperature, a more oceanic influence over land would lead to a phase delay. The delay in these variables happens instantaneously in the abrupt simulation, suggesting the driving mechanism must operate very rapidly. I proposed that this was due to rapid changes in the circulation brought about by the greater warming over land than ocean, which occurs in year one of the abrupt simulation and continues throughout the length of the run. Two different mechanisms are possible for the circulation changes. One, described in Lindzen and Nigam (1987), suggests that surface temperature contrasts create surface pressure gradients which drive low-level convergence. In the other, the surface temperature changes are quickly communicated vertically via convection and the entire tropical troposphere adjusts to smooth out the temperature anomalies (Sobel et al., 2001). The actual mechanism at work could be tested by looking to see if there is convergence above the boundary layer in the first few years of the abrupt simulation. If that is the case, then the weak temperature gradient mechanism is operating, rather than the low-level convergence mechanism.

Finally, one possible mechanism for the delay in the circulation (which drives the delay in precipitation) could be related to forcing by eddy momentum fluxes. (Though this does not seem to be the case in the dry-dynamical model). Recent work has underscored the important role these eddies play in affecting the Hadley Cell, especially the summer (non-angular momentum conserving) cell (Walker and Schneider, 2006; Caballero, 2007; Schneider and Bordoni, 2008; Sobel and Schneider, 2009; Bordoni and Schneider, 2009). As many of the mechanisms proposed to understand the expansion of the Hadley Cell under global warming involve extratropical eddies in some way (Lu et al., 2007; Lorenz and DeWeaver, 2007; Frierson et al., 2007; Chen and Held, 2007; Son et al., 2008; Kidston et al., 2010), they may also affect the timing of the tropical circulation.

Bibliography

Betts, A. K. and W. Ridgway, 1989: Climatic equilibrium of the atmospheric convective boundary layer over a tropical ocean. *Journal of the Atmospheric Sciences*, **46 (17)**, 2621–2641, doi:10.1175/1520-0469(1989)046⟨2621:CEOTAC⟩2.0.CO;2.

Biasutti, M., 2013: Forced Sahel rainfall trends in the CMIP5 archive. *Journal of Geophysical Research: Atmospheres*, **118 (4)**, 1613–1623, doi:10.1002/jgrd.50206.

Biasutti, M., D. S. Battisti, and E. S. Sarachik, 2003: The annual cycle over the tropical Atlantic, South America, and Africa. *Journal of Climate*, **16 (15)**, 2491–2508, doi:10.1175/1520-0442(2003)016⟨2491:TACOTT⟩2.0.CO;2.

Biasutti, M., D. S. Battisti, and E. S. Sarachik, 2004: Mechanisms controlling the annual cycle of precipitation in the tropical Atlantic sector in an atmospheric GCM. *Journal of Climate*, **17 (24)**, 4708–4723, doi:10.1175/JCLI-3235.1.

Biasutti, M. and A. Sobel, 2009: Delayed Sahel rainfall and global seasonal cycle in a warmer climate. *Geophysical Research Letters*, **36**, doi:10.1029/2009GL041303.

Bony, S., G. Bellon, D. Klocke, S. Sherwood, S. Fermepin, and S. Denvil, 2013: Robust direct effect of carbon dioxide on tropical circulation and regional precipitation. *Nature Geoscience*, **6 (6)**, 447–451, doi:10.1038/ngeo1799.

Bordoni, S. and T. Schneider, 2009: Regime transitions of steady and time-dependent Hadley circulations: Comparison of axisymmetric and eddy-permitting simulations. *Journal of the Atmospheric Sciences*, **67 (5)**, 1643–1654, doi:10.1175/2009JAS3294.1.

Broccoli, A. J., K. A. Dahl, and R. J. Stouffer, 2006: Response of the ITCZ to Northern Hemisphere cooling. *Geophysical Research Letters*, **33 (1)**, L01 702, doi:10.1029/2005GL024546.

Brooks, C. E. P., 1917: Continentality and temperature. *Quarterly Journal of the Royal Meteorological Society*, **43 (182)**, 159–174, doi:10.1002/qj.49704318204.

Brooks, C. E. P., 1918: Continentality and temperature—second paper: The effect of latitude on the influence of continentality on temperature. *Quarterly Journal of the Royal Meteorological Society*, **44 (188)**, 253–270, doi:10.1002/qj.49704418802.

Brunt, D., 1924: Climatic continentality and oceanity. *The Geographical Journal*, **64 (1)**, 43–49, doi:10.2307/1781368.

Byrne, M. P. and P. A. O'Gorman, 2013: Land–ocean warming contrast over a wide range of climates: Convective quasi-equilibrium theory and idealized simulations. *Journal of Climate*, **26 (12)**, 4000–4016, doi:10.1175/JCLI-D-12-00262.1.

Caballero, R., 2007: Role of eddies in the interannual variability of Hadley cell strength. *Geophysical Research Letters*, **34 (22)**, L22 705, doi:10.1029/2007GL030971.

Carson, J. and H. Moses, 1963: The annual and diurnal heat-exchange cycles in upper layers of soil. *Journal of Applied Meteorology*, **2 (3)**, 397–406, doi:10.1175/1520-0450(1963)002⟨0397:TAADHE⟩2.0.CO;2.

Cess, R. D., et al., 1990: Intercomparison and interpretation of climate feedback processes in 19 atmospheric general circulation models. *Journal of Geophysical Research: Atmospheres*, **95 (D10)**, 16 601–16 615, doi:10.1029/JD095iD10p16601.

Chen, G. and I. M. Held, 2007: Phase speed spectra and the recent poleward shift of Southern Hemisphere surface westerlies. *Geophysical Research Letters*, **34 (21)**, L21 805, doi:10.1029/2007GL031200.

Chiang, J., Y. Kushnir, and A. Giannini, 2002: Deconstructing Atlantic Intertropical Convergence Zone variability: Influence of the local cross-equatorial sea surface temperature gradient and remote forcing from the eastern equatorial Pacific. *Journal of Geophysical Research: Atmospheres*, **107 (D1)**, 4004, doi:10.1029/2000JD000307.

Chiang, J. C. H. and C. M. Bitz, 2005: Influence of high latitude ice cover on the marine Intertropical Convergence Zone. *Climate Dynamics*, **25 (5)**, 477–496, doi:10.1007/s00382-005-0040-5.

Chiang, J. C. H. and A. H. Sobel, 2002: Tropical tropospheric temperature variations caused by ENSO and their influence on the remote tropical climate. *Journal of Climate*, **15 (18)**, 2616–2631, doi:10.1175/1520-0442(2002)015⟨2616:TTTVCB⟩2.0.CO;2.

Chmielewski, F.-M. and T. Rötzer, 2001: Response of tree phenology to climate change across Europe. *Agricultural and Forest Meteorology*, **108 (2)**, 101–112, doi:10.1016/S0168-1923(01)00233-7.

Chou, C., J. C. H. Chiang, C.-W. Lan, C.-H. Chung, Y.-C. Liao, and C.-J. Lee, 2013: Increase in the range between wet and dry season precipitation. *Nature Geoscience*, **6 (4)**, 263–267, doi:10.1038/ngeo1744.

Chou, C. and C.-W. Lan, 2011: Changes in the annual range of precipitation under global warming. *Journal of Climate*, **25 (1)**, 222–235, doi:10.1175/JCLI-D-11-00097.1.

Chou, C. and J. D. Neelin, 2004: Mechanisms of global warming impacts on regional tropical precipitation. *Journal of Climate*, **17 (13)**, 2688–2701, doi:10.1175/1520-0442(2004)017⟨2688:MOGWIO⟩2.0.CO;2.

Chou, C. and J.-Y. Tu, 2008: Hemispherical asymmetry of tropical precipitation in ECHAM5/MPI-OM during El Niño and under global warming. *Journal of Climate*, **21 (6)**, 1309–1332, doi:10.1175/2007JCLI1928.1.

Chou, C., J.-Y. Tu, and P.-H. Tan, 2007: Asymmetry of tropical precipitation change under global warming. *Geophysical Research Letters*, **34 (17)**, L17 708, doi:10.1029/2007GL030327.

Deser, C., R. Tomas, M. Alexander, and D. Lawrence, 2010: The seasonal atmospheric response to projected Arctic sea ice loss in the late twenty-first century. *Journal of Climate*, **23 (2)**, 333–351, doi:10.1175/2009JCLI3053.1.

Dima, I. and J. Wallace, 2003: On the seasonality of the Hadley cell. *Journal of the Atmospheric Sciences*, **60 (12)**, 1522–1527, doi:10.1175/1520-0469(2003)060⟨1522:OTSOTH⟩2.0.CO;2.

Donohoe, A. and D. S. Battisti, 2013: The seasonal cycle of atmospheric heating and temperature. *Journal of Climate*, **26 (14)**, 4962–4980, doi:10.1175/JCLI-D-12-00713.1.

Donohoe, A., J. Marshall, D. Ferreira, K. Armour, and D. McGee, 2014: The interannual variability of tropical precipitation and interhemispheric energy transport. *Journal of Climate*, **27 (9)**, 3377–3392, doi:10.1175/JCLI-D-13-00499.1.

Dwyer, J. G., M. Biasutti, and A. H. Sobel, 2012: Projected changes in the seasonal cycle of surface temperature. *Journal of Climate*, **25 (18)**, 6359–6374, doi:10.1175/JCLI-D-11-00741.1.

Dwyer, J. G., M. Biasutti, and A. H. Sobel, 2014: The effect of greenhouse gas–induced changes in SST on the annual cycle of zonal mean tropical precipitation. *Journal of Climate*, **27 (12)**, 4544–4565, doi:10.1175/JCLI-D-13-00216.1.

Edwards, M. and A. J. Richardson, 2004: Impact of climate change on marine pelagic phenology and trophic mismatch. *Nature*, **430 (7002)**, 881–884, doi:10.1038/nature02808.

Eicken, H., 2008: From the microscopic, to the macroscopic, to the regional scale: Growth, microstructure and properties of sea ice. *Sea Ice: An Introduction to its Physics, Chemistry, Biology and Geology*, D. N. Thomas and G. S. Dieckmann, Eds., Blackwell Science Ltd, Oxford, UK, chap. 2, 22–81, doi:10.1002/9780470757161.ch2.

Emanuel, K. and A. Sobel, 2013: Response of tropical sea surface temperature, precipitation, and tropical cyclone-related variables to changes in global and local forcing. *Journal of Advances in Modeling Earth Systems*, **5 (2)**, 447–458, doi:10.1002/jame.20032.

Fang, M. and K. K. Tung, 1999: Time-dependent nonlinear Hadley circulation. *Journal of the Atmospheric Sciences*, **56 (12)**, 1797–1807, doi:10.1175/1520-0469(1999)056⟨1797:TDNHC⟩2.0.CO;2.

Fitter, A. H. and R. S. R. Fitter, 2002: Rapid changes in flowering time in British plants. *Science*, **296 (5573)**, 1689–1691, doi:10.1126/science.1071617.

Frierson, D. M. W. and Y.-T. Hwang, 2011: Extratropical influence on ITCZ shifts in slab ocean simulations of global warming. *Journal of Climate*, **25 (2)**, 720–733, doi:10.1175/JCLI-D-11-00116.1.

Frierson, D. M. W., J. Lu, and G. Chen, 2007: Width of the Hadley cell in simple and comprehensive general circulation models. *Geophysical Research Letters*, **34 (18)**, L18 804, doi:10.1029/2007GL031115.

Fu, R., R. E. Dickinson, M. Chen, and H. Wang, 2001: How do tropical sea surface temperatures influence the seasonal distribution of precipitation in the equatorial Amazon? *Journal of Climate*, **14 (20)**, 4003–4026, doi:10.1175/1520-0442(2001)014⟨4003:HDTSST⟩2.0.CO;2.

Fu, X. and B. Wang, 2004: Differences of boreal summer intraseasonal oscillations simulated in an atmosphere–ocean coupled model and an atmosphere-only model. *Journal of Climate*, **17 (6)**, 1263–1271, doi:10.1175/1520-0442(2004)017⟨1263:DOBSIO⟩2.0.CO;2.

Gastineau, G., H. Le Treut, and L. Li, 2008: Hadley circulation changes under global warming conditions indicated by coupled climate models. *Tellus A*, **60 (5)**, 863–884, doi:10.1111/j.1600-0870.2008.00344.x.

Gent, P. R., et al., 2011: The Community Climate System Model Version 4. *Journal of Climate*, **24 (19)**, 4973–4991, doi:10.1175/2011JCLI4083.1.

Gorczyński, L., 1920: Sur le calcul du degrédu continentalisme et son application dans la climatologie. *Geografiska Annaler*, **2**, 324–331, doi:10.2307/519539.

Hadley, G., 1735: Concerning the cause of the general trade-winds. *Philosophical Transactions*, **39 (436-444)**, 58–62, doi:10.1098/rstl.1735.0014.

Hartmann, D. L. and K. Larson, 2002: An important constraint on tropical cloud

- climate feedback. *Geophysical Research Letters*, **29 (20)**, 1951, doi:10.1029/2002GL015835.

Hela, I., 1953: Regional distribution of the continentality in the climate of the oceans. *Geophysica*, **4 (2)**.

Held, I. and B. Soden, 2006: Robust responses of the hydrological cycle to global warming. *Journal of Climate*, **19 (21)**, 5686–5699, doi:10.1175/JCLI3990.1.

Held, I. M. and M. J. Suarez, 1994: A proposal for the intercomparison of the dynamical cores of atmospheric general circulation models. *Bulletin of the American Meteorological Society*, **75 (10)**, 1825–1830, doi:10.1175/1520-0477(1994)075⟨1825:APFTIO⟩2.0.CO;2.

Huang, P., S.-P. Xie, K. Hu, G. Huang, and R. Huang, 2013: Patterns of the seasonal response of tropical rainfall to global warming. *Nature Geoscience*, **6 (5)**, 357–361, doi:10.1038/ngeo1792.

Hurrell, J. W., J. J. Hack, D. Shea, J. M. Caron, and J. Rosinski, 2008: A new sea surface temperature and sea ice boundary dataset for the community atmosphere model. *Journal of Climate*, **21 (19)**, 5145–5153, doi:10.1175/2008JCLI2292.1.

Johanson, C. M. and Q. Fu, 2009: Hadley cell widening: Model simulations versus observations. *Journal of Climate*, **22 (10)**, 2713–2725, doi:10.1175/2008JCLI2620.1.

Kang, S. M., C. Deser, and L. M. Polvani, 2013: Uncertainty in climate change projections of the hadley circulation: The role of internal variability. *Journal of Climate*, **26 (19)**, 7541–7554, doi:10.1175/JCLI-D-12-00788.1.

Kang, S. M., D. M. W. Frierson, and I. M. Held, 2009: The tropical response to extratropical thermal forcing in an idealized GCM: The importance of radiative feedbacks and convective parameterization. *Journal of the Atmospheric Sciences*, **66 (9)**, 2812–2827, doi:10.1175/2009JAS2924.1.

Kang, S. M., I. M. Held, D. M. W. Frierson, and M. Zhao, 2008: The response of the ITCZ to extratropical thermal forcing: Idealized slab-ocean experiments with a GCM. *Journal of Climate*, **21 (14)**, 3521–3532, doi:10.1175/2007JCLI2146.1.

Keeling, C., 1958: The concentration and isotopic abundances of atmospheric carbon dioxide in rural areas. *Geochimica et Cosmochimica Acta*, **13**, 322–334, doi:10.1016/0016-7037(58)90033-4.

Kidston, J., S. M. Dean, J. A. Renwick, and G. K. Vallis, 2010: A robust increase in the eddy length scale in the simulation of future climates. *Geophysical Research Letters*, **37 (3)**, L03 806, doi:10.1029/2009GL041615.

Kitoh, A. and O. Arakawa, 1999: On overestimation of tropical precipitation by an atmospheric GCM with prescribed SST. *Geophysical Research Letters*, **26 (19)**, 2965–2968, doi:10.1029/1999GL900616.

Knutson, T. and S. Manabe, 1995: Time-mean response over the tropical Pacific to increased CO2 in a coupled ocean-atmosphere model. *Journal of Climate*, **8 (9)**, 2181–2199, doi:10.1175/1520-0442(1995)008⟨2181:TMROTT⟩2.0.CO;2.

Kumar, A., et al., 2010: Contribution of sea ice loss to Arctic amplification. *Geophysical Research Letters*, **37 (21)**, L21 701, doi:10.1029/2010GL045022.

Kutzbach, J., 1967: Empirical eigenvectors of sea-level pressure, surface temperature and precipitation complexes over North America. *Journal of Applied Meteorology*, **6 (5)**, 791–802, doi:10.1175/1520-0450(1967)006⟨0791:EEOSLP⟩2.0.CO;2.

Larson, K. and D. L. Hartmann, 2003: Interactions among cloud, water vapor, radiation, and large-scale circulation in the tropical climate. part I: Sensitivity to uniform sea surface temperature changes. *Journal of Climate*, **16 (10)**, 1425–1440, doi:10.1175/1520-0442(2003)016⟨1425:IACWVR⟩2.0.CO;2.

Lea, D. W., D. K. Pak, L. C. Peterson, and K. A. Hughen, 2003: Synchroneity of tropical and high-latitude Atlantic temperatures over the last glacial termination. *Science*, **301 (5638)**, 1361–1364, doi:10.1126/science.1088470.

Li, T. and S. G. H. Philander, 1997: On the seasonal cycle of the equatorial Atlantic Ocean. *Journal of Climate*, **10 (4)**, 813–817, doi:10.1175/1520-0442(1997)010⟨0813:OTSCOT⟩2.0.CO;2.

Lin, J.-L., 2007: The double-ITCZ problem in IPCC AR4 coupled GCMs: Ocean–atmosphere feedback analysis. *Journal of Climate*, **20 (18)**, 4497–4525, doi:10.1175/JCLI4272.1.

Lindzen, R. S. and A. V. Hou, 1988: Hadley circulations for zonally averaged heating centered off the equator. *Journal of the Atmospheric Sciences*, **45 (17)**, 2416–2427, doi:10.1175/1520-0469(1988)045⟨2416:HCFZAH⟩2.0.CO;2.

Lindzen, R. S. and S. Nigam, 1987: On the role of sea surface temperature gradients in forcing low-level winds and convergence in the tropics. *Journal of the Atmospheric Sciences*, **44 (17)**, 2418–2436, doi:10.1175/1520-0469(1987)044⟨2418:OTROSS⟩2.0.CO;2.

Liu, C., R. P. Allan, and G. J. Huffman, 2012: Co-variation of temperature and precipitation in CMIP5 models and satellite observations. *Geophysical Research Letters*, **39 (13)**, L13 803, doi:10.1029/2012GL052093.

Loon, H. V., 1967: The half-yearly oscillations in middle and high southern latitudes and the coreless winter. *Journal of the Atmospheric Sciences*, **24**, 472–486, doi:10.1175/1520-0469(1967)024⟨0472:THYOIM⟩2.0.CO;2.

Lorenz, D. J. and E. T. DeWeaver, 2007: Tropopause height and zonal wind response to global warming in the IPCC scenario integrations. *Journal of Geophysical Research: Atmospheres*, **112 (D10)**, D10 119, doi:10.1029/2006JD008087.

Lu, J., G. A. Vecchi, and T. Reichler, 2007: Expansion of the Hadley cell under global warming. *Geophysical Research Letters*, **34 (6)**, L06 805, doi:10.1029/2006GL028443.

Machida, T., T. Nakazawa, Y. Fujii, S. Aoki, and O. Watanabe, 1995: Increase in the atmospheric nitrous oxide concentration during the last 250 years. *Geophysical Research Letters*, **22 (21)**, 2921–2924, doi:10.1029/95GL02822.

Manabe, S., M. Spelman, and R. Stouffer, 1992: Transient responses of a coupled ocean-atmosphere model to gradual changes of atmospheric CO2. Part II: Seasonal response. *Journal of Climate*, **5 (2)**, 105–126, doi:10.1175/1520-0442(1992)005⟨0105:TROACO⟩2.0.CO;2.

Manabe, S. and R. Stouffer, 1980: Sensitivity of a global climate model to an increase of CO2 concentration in the atmosphere. *Journal of Geophysical Research: Oceans*, **85 (C10)**, 5529–5554, doi:10.1029/JC085iC10p05529.

Mann, M. and J. Park, 1996: Greenhouse warming and changes in the seasonal cycle of temperature: Model versus observations. *Geophysical Research Letters*, **23 (10)**, 1111–1114, doi:10.1029/96GL01066.

McKinnon, K. A., A. R. Stine, and P. Huybers, 2013: The spatial structure of the annual cycle in surface temperature: Amplitude, phase, and Lagrangian history. *Journal of Climate*, **26 (20)**, 7852–7862, doi:10.1175/JCLI-D-13-00021.1.

Meehl, G. A., C. Covey, K. E. Taylor, T. Delworth, R. J. Stouffer, M. Latif, B. McAvaney, and J. F. B. Mitchell, 2007: The WCRP CMIP3 multimodel dataset: A new era in climate change research. *Bulletin of the American Meteorological Society*, **88 (9)**, 1383–1394, doi:10.1175/BAMS-88-9-1383.

Merlis, T. M., T. Schneider, S. Bordoni, and I. Eisenman, 2012: The tropical precipitation response to orbital precession. *Journal of Climate*, **26 (6)**, 2010–2021, doi:10.1175/JCLI-D-12-00186.1.

Pahnke, K., J. P. Sachs, L. Keigwin, A. Timmermann, and S.-P. Xie, 2007: Eastern tropical Pacific hydrologic changes during the past 27,000 years from D/H ratios in alkenones. *Paleoceanography*, **22 (4)**, PA4214, doi:10.1029/2007PA001468.

Philip, S. and G. V. Oldenborgh, 2006: Shifts in ENSO coupling processes under global warming. *Geophysical Research Letters*, **33**, doi:10.1029/2006GL026196.

Prescott, J. A. and J. A. Collins, 1951: The lag of temperature behind solar radiation. *Quarterly Journal of the Royal Meteorological Society*, **77 (331)**, 121–126, doi:10.1002/qj.49707733112.

Regonda, S. K., B. Rajagopalan, M. Clark, and J. Pitlick, 2005: Seasonal cycle shifts in hydroclimatology over the western United States. *Journal of Climate*, **18 (2)**, 372–384, doi:10.1175/JCLI-3272.1.

Robock, A., K. Y. Vinnikov, G. Srinivasan, J. K. Entin, S. E. Hollinger, N. A. Speranskaya, S. Liu, and A. Namkhai, 2000: The global soil moisture data bank. *Bulletin of the American Meteorological Society*, **81 (6)**, 1281–1299, doi:10.1175/1520-0477(2000)081⟨1281:TGSMDB⟩2.3.CO;2.

Roy, D. B. and T. H. Sparks, 2000: Phenology of British butterflies and climate change. *Global Change Biology*, **6 (4)**, 407–416, doi:10.1046/j.1365-2486.2000.00322.x.

Sachs, J. P., D. Sachse, R. H. Smittenberg, Z. Zhang, D. S. Battisti, and S. Golubic, 2009: Southward movement of the Pacific intertropical convergence zone AD1400-1850. *Nature Geoscience*, **2 (7)**, 519–525, doi:10.1038/ngeo554.

Schneider, T., 2004: The tropopause and the thermal stratification in the extratropics of a dry atmosphere. *Journal of the Atmospheric Sciences*, **61 (12)**, 1317–1340, doi:10.1175/1520-0469(2004)061⟨1317:TTATTS⟩2.0.CO;2.

Schneider, T. and S. Bordoni, 2008: Eddy-mediated regime transitions in the seasonal cycle of a Hadley circulation and implications for monsoon dynamics. *Journal of the Atmospheric Sciences*, **65 (3)**, 915–934, doi:10.1175/2007JAS2415.1.

Schneider, T. and C. C. Walker, 2006: Self-organization of atmospheric macroturbulence into critical states of weak nonlinear eddy–eddy interactions. *Journal of the Atmospheric Sciences*, **63 (6)**, 1569–1586, doi:10.1175/JAS3699.1.

Screen, J. and I. Simmonds, 2010: Increasing fall-winter energy loss from the Arctic Ocean and its role in Arctic temperature amplification. *Geophysical Research Letters*, **37**, doi:10.1029/2010GL044136.

Seager, R. and N. Henderson, 2013: Diagnostic computation of moisture budgets in the ERA-Interim reanalysis with reference to analysis of CMIP-archived atmospheric model data. *Journal of Climate*, **26 (20)**, 7876–7901, doi:10.1175/JCLI-D-13-00018.1.

Seidel, D. J., Q. Fu, W. J. Randel, and T. J. Reichler, 2008: Widening of the tropical belt in a changing climate. *Nature Geoscience*, **1 (1)**, 21–24, doi:10.1038/ngeo.2007.38.

Serreze, M., A. Barrett, J. Stroeve, D. Kindig, and M. Holland, 2009: The emergence of surface-based Arctic amplification. *The Cryosphere*, **3 (1)**, 11–19, doi:10.5194/tc-3-11-2009.

Serreze, M. and J. Francis, 2006: The Arctic amplification debate. *Climatic Change*, **76 (3)**, 241–264, doi:10.1007/s10584-005-9017-y.

Seth, A., S. Rauscher, M. Rojas, A. Giannini, and S. Camargo, 2011: Enhanced spring convective barrier for monsoons in a warmer world? *Climatic Change*, **104 (2)**, 403–414, doi:10.1007/s10584-010-9973-8.

Seth, A., S. A. Rauscher, M. Biasutti, A. Giannini, S. J. Camargo, and M. Rojas, 2013: CMIP5 projected changes in the annual cycle of precipitation in monsoon regions. *Journal of Climate*, doi:10.1175/JCLI-D-12-00726.1.

Shukla, J. and M. Fennessy, 1994: Simulation and predictability of monsoons. Proceedings of the international conference on monsoon variability and prediction. Tech. rep., WCRP-84, World Climate Research Program, Geneva, Switzerland. 567-575.

Simpson, G. C., D. W. Barker, L. C. W. Bonacina, H. R. Mill, G. S. L. Clowes, and D. Brunt, 1924: Climatic continentality and oceanity: Discussion. *The Geographical Journal*, **64 (1)**, 49–56, doi:10.2307/1781369.

Sobel, A. and S. Camargo, 2011: Projected future seasonal changes in tropical summer climate. *Journal of Climate*, **24**, 473–487, doi:10.1175/2010JCLI3748.1.

Sobel, A., J. Nilsson, and L. Polvani, 2001: The weak temperature gradient approximation and balanced tropical moisture waves. *Journal of the Atmospheric Sciences*, **58 (23)**, 3650–3665.

Sobel, A. and T. Schneider, 2009: Single-layer axisymmetric model for a Hadley circulation with parameterized eddy momentum forcing. *Journal of Advances in Modeling Earth Systems*, **1 (3)**, 10, doi:10.3894/JAMES.2009.1.10.

Solomon, S., D. Qin, M. Manning, Z. Chen, M. Marquis, K. Averyt, M. Tignor, and H. Miller, (Eds.) , 2007: *Contribution of Working Group I to the Fourth Assessment Report of the Intergovernmental Panel on Climate Change*. Cambridge University Press, Cambridge, United Kingdom and New York, NY, USA.

Son, S. W., et al., 2008: The impact of stratospheric ozone recovery on the Southern Hemisphere westerly jet. *Science*, **320 (5882)**, 1486–1489, doi:10.1029/2010JD014271.

Spitaler, R., 1922: Klimatische kontinentalität und ozeanität. *Petermanns Geographische Mitteilungen*.

Stewart, I., D. Cayan, and M. Dettinger, 2005: Changes toward earlier streamflow timing across western North America. *Journal of Climate*, **18 (8)**, 1136–1155, doi:10.1175/JCLI3321.1.

Stine, A. R. and P. Huybers, 2012: Changes in the seasonal cycle of temperature and atmospheric circulation. *Journal of Climate*, **25 (21)**, 7362–7380, doi:10.1175/JCLI-D-11-00470.1.

Stine, A. R., P. Huybers, and I. Y. Fung, 2009: Changes in the phase of the annual cycle of surface temperature. *Nature*, **457 (7228)**, 435–440, doi:10.1038/nature07675.

Stocker, T., et al., (Eds.) , 2013: *IPCC, 2013: Climate Change 2013: The Physical Science Basis. Contribution of Working Group I to the Fifth Assessment Report of the Intergovernmental Panel on Climate Change*. Cambridge University Press, Cambridge, United Kingdom and New York, NY, USA, 1535 pp.

Stroeve, J., M. Holland, W. Meier, T. Scambos, and M. Serreze, 2007: Arctic sea ice decline: Faster than forecast. *Geophysical Research Letters*, **34 (9)**, L09 501, doi:10.1029/2007GL029703.

Sugi, M., A. Noda, and N. Sato, 2002: Influence of the global warming on tropical cyclone climatology : An experiment with the JMA global model. *Journal of the Meteorological Society of Japan. Ser. II*, **80 (2)**, 249–272, doi:10.2151/jmsj.80.249.

Tan, P.-H., C. Chou, and J.-Y. Tu, 2008: Mechanisms of global warming impacts on robustness of tropical precipitation asymmetry. *Journal of Climate*, **21 (21)**, 5585–5602, doi:10.1175/2008JCLI2154.1.

Taylor, K. E., R. J. Stouffer, and G. A. Meehl, 2011: An overview of CMIP5 and the experiment design. *Bulletin of the American Meteorological Society*, **93 (4)**, 485–498, doi:10.1175/BAMS-D-11-00094.1.

Thompson, R., 1995: Complex demodulation and the estimation of the changing continentality of Europe's climate. *International Journal of Climatology*, **15 (2)**, 175–185, doi:10.1002/joc.3370150204.

Thomson, D., 1995: The seasons, global temperature, and precession. *Science*, **268 (5207)**, 59, doi:10.1126/science.268.5207.59.

Trenberth, K., 1983: What are the seasons?. *Bulletin of the American Meteorological Society*, **64**, 1276–1277, doi:10.1175/1520-0477(1983)064⟨1276:WATS⟩2.0.CO;2.

Trenberth, K. E., D. P. Stepaniak, and J. M. Caron, 2000: The global monsoon as seen through the divergent atmospheric circulation. *Journal of Climate*, **13 (22)**, 3969–3993, doi:10.1175/1520-0442(2000)013⟨3969:TGMAST⟩2.0.CO;2.

Uppala, S., et al., 2005: The ERA-40 re-analysis. *Quarterly Journal of the Royal Meteorological Society*, **131 (612)**, 2961–3012, doi:10.1256/qj.04.176.

Van den Dool, H. and G. Können, 1981: Strong variations in the delay of the annual cycle in the air temperature near the coast. *Proceedings of the First International Conference on Meteorology and Air/Sea Interaction of the Coastal Zone*.

Van Loon, A. F., E. Tijdeman, N. Wanders, H. A. J. Van Lanen, A. J. Teuling, and R. Uijlenhoet, 2014: How climate seasonality modifies drought duration and deficit. *Journal of Geophysical Research: Atmospheres*, **119 (8)**, 4640–4656, doi: 10.1002/2013JD020383.

Vecchi, G. A. and B. J. Soden, 2007: Global warming and the weakening of the tropical circulation. *Journal of Climate*, **20 (17)**, 4316–4340, doi:10.1175/JCLI4258.1.

Vecchi, G. A., B. J. Soden, A. T. Wittenberg, I. M. Held, A. Leetmaa, and M. J. Harrison, 2006: Weakening of tropical Pacific atmospheric circulation due to anthropogenic forcing. *Nature*, **441 (7089)**, 73–76, doi:10.1038/nature04744.

Visser, M. E. and C. Both, 2005: Shifts in phenology due to global climate change: the need for a yardstick. *Proceedings of the Royal Society B: Biological Sciences*, **272 (1581)**, 2561–2569, doi:10.1098/rspb.2005.3356.

Visser, M. E. and L. J. M. Holleman, 2001: Warmer springs disrupt the synchrony of oak and winter moth phenology. *Proceedings of the Royal Society of London. Series B: Biological Sciences*, **268 (1464)**, 289–294, doi:10.1098/rspb.2000.1363.

Walker, C. C. and T. Schneider, 2006: Eddy influences on Hadley circulations: Simulations with an idealized GCM. *Journal of the Atmospheric Sciences*, **63 (12)**, 3333–3350, doi:10.1175/JAS3821.1.

Wallace, C. and T. Osborn, 2002: Recent and future modulation of the annual cycle. *Climate Research*, **22 (1)**, 1–11, doi:10.3354/cr022001.

Wallace, J. M., T. P. Mitchell, and C. Deser, 1989: The influence of sea-surface temperature on surface wind in the eastern equatorial Pacific: Seasonal and interannual variability. *Journal of Climate*, **2 (12)**, 1492–1499, doi:10.1175/1520-0442(1989)002⟨1492:TIOSST⟩2.0.CO;2.

Ward, R. D., 1906: The classification of climates: I. *Bulletin of the American Geographical Society*, **38 (7)**, 401–412, doi:10.2307/198943.

Webster, P., 1987: The elementary monsoon. *Monsoons*, J. Fein and P. Stephens, Eds., John Wiley & Sons, Ltd, chap. 1, 3–32.

Wu, R. and B. Kirtman, 2005: Roles of Indian and Pacific Ocean air–sea coupling in tropical atmospheric variability. *Climate Dynamics*, **25 (2-3)**, 155–170, doi:10.1007/s00382-005-0003-x.

Wu, R. and B. Kirtman, 2007: Regimes of seasonal air–sea interaction and implications for performance of forced simulations. *Climate Dynamics*, **29 (4)**, 393–410, doi:10.1007/s00382-007-0246-9.

Wu, Y., R. Seager, T. A. Shaw, M. Ting, and N. Naik, 2012: Atmospheric circulation response to an instantaneous doubling of carbon dioxide. part II: Atmospheric transient adjustment and its dynamics. *Journal of Climate*, **26 (3)**, 918–935, doi:10.1175/JCLI-D-12-00104.1.

Wu, Y., R. Seager, M. Ting, N. Naik, and T. A. Shaw, 2011: Atmospheric circulation response to an instantaneous doubling of carbon dioxide. Part I: Model experiments and transient thermal response in the troposphere. *Journal of Climate*, **25 (8)**, 2862–2879, doi:10.1175/JCLI-D-11-00284.1.

Xie, S.-P., C. Deser, G. A. Vecchi, J. Ma, H. Teng, and A. T. Wittenberg, 2010: Global warming pattern formation: Sea surface temperature and rainfall. *Journal of Climate*, **23 (4)**, 966–986, doi:10.1175/2009JCLI3329.1.

Xu, K.-M. and K. A. Emanuel, 1989: Is the tropical atmosphere conditionally unstable? *Monthly Weather Review*, **117 (7)**, 1471–1479, doi:10.1175/1520-0493(1989)117⟨1471:ITTACU⟩2.0.CO;2.